A COMPUTATIONAL STUDY OF INTERFACIAL PHENOMENA IN DISSOCIATIVE WATER CONFINED BY NANOSTRUCTURED SILICA

by

THIRUVILLAMALAI SUNDARESHWARAN MAHADEVAN

A dissertation submitted to the

Graduate School – New Brunswick

Rutgers, The State University of New Jersey

In partial fulfillment of the requirements

For the degree of

Doctor of Philosophy

Graduate Program in Materials Science and Engineering

Written under the direction of

Professor Stephen H. Garofalini

And approved by

_____

_____

_____

_____

New Brunswick, New Jersey

January 2008

ABSTRACT OF THE DISSERTATION

A Computational Study of Interfacial Phenomena in Dissociative Water Confined by Silica Nanolayers.

By

THIRUVILLAMALAI SUNDARESHWARAN MAHADEVAN

Dissertation Director:

Professor Stephen H. Garofalini

Molecular Dynamics (MD) Simulation techniques were used to build a dissociative model for water that accurately represents the structure, vibration spectrum and thermal expansion curves over a wide range of temperatures and pressure. The structural changes and interaction of this water model when confined by nano layers of silica were observed. Hydronium formation was observed and the structure and diffusion properties between confined water, bulk water, and water far from the silica interface were compared.

The water model was based on a pair potential and atomic water which allows for dissociation of water and its interaction with silica to form silanols. An interaction parameter representing the O-H distance ($\xi_{r\text{-}OH}$) was adjusted based on temperature and pressure as a strong correlation was observed between changes in the OH distance and the structure, density and energies of simulated water. The properties of water were close to the experimentally observed physical properties of water.

An atomic model for vitreous silica was also built based on the same potential and using the same parameters for oxygen-oxygen interactions in silica as that of water. The cross species interactions (Si-H and Si-O) were determined to accurately predict the structure of vitreous silica and low energy structures of interacting silicic acid – water clusters.

Based on the above potentials, a 3nm water film was placed between layers of vitreous silica and MD simulations of the above system were carried out for seven temperatures. The structure of water far away from the interface was closer to that of bulk water and the structure of the penetrated water had features of bulk water at higher temperature and pressure. The self diffusion coefficient of the penetrated water molecules was observed to an order of magnitude lower than that of bulk water. The confined water was also observed to respond differently to changes in temperature as compared to bulk water thus changing the averaged properties of water and exhibiting variation in phase behavior.

PREFACE

This thesis is organized into a sequence of chapters describing the background , development of interaction potential and results and discussions. The gist of the results and discussions are appended as three manuscripts one of which has already been published as a paper and the other two are ready for submission. The appended manuscripts are as follows :

I. "Dissociative Water Potential for Molecular Dynamics Simulations", T.S.Mahadevan and S.H.Garofalini, J.Phys. Chem. B **111**(30) 8919-8927 (2007).

II. "Water induced relaxation of silica surfaces with a long range dissociative water potential" , T.S.Mahadevan and S.H.Garofalini, Accepted with slight modifications in Journal of Physical Chemistry.

III. "Water confined in Silica Nano layers: A Molecular Dynamics Study", T.S.Mahadevan and S.H.Garofalini, Manuscript to be submitted for publication.

I have been the principle writer of all the manuscripts with guidance from Dr.Garofalini. I have conducted the computer simulations, interpreted and analysed results and drawn conclusions for all the papers with the guidance of Dr.Garofalini.

Chapter 1 contains the background information and literature survey for this work and also describes some of the experimental techniques adopted for measuring the properties of materials that we have undertaken. Chapter 2 is a brief on simulation

techniques with particular emphasis on molecular dynamics techniques and algorithms that have been used in this study. Chapter 3 discusses the way we developed the potentials and some more details on interpreting the various aspects of the potential. Chapter 4 gives the summary of the appended manuscripts and additional results that are not included in any of the manuscripts. Chapter 5 gives the conclusions and some of the ideas on areas that can be investigated based on this work.

New Jersey 2007 T.S.Mahadevan

ACKNOWLEDGEMENTS

I express my gratitude to Dr.Stephen Garofalini for his guidance and mentorship that lead to this project. The discussions that I had with him during the course of this project have been very useful in the completion of this project and I sincerely appreciate all his ideas and the motivation that he has provided. He has been the driving force for the completion of this project and has enlightened me about problem solving methods and approaches in relation to the project and has been an inspiration for me to take up scientific research.

I thank my thesis committee members Dr.George H. Sigel, Dr.Lisa Klein and Dr.Alberto Cuitino for their guidance in writing and review of this thesis. Dr.Sigel has also provided me ample encouragement and advice during the course of my association with him.

I also thank the Department of Materials science and engineering in general and Dr.Holly Crawford and graduate director Dr.Lisa Klein in particular for providing a part of the funding during the course of this project. Dr. Crawford and Dr. Jack Wenzel of the department have been my mentors during my stint as a Teaching Assistant and have thus helped me understand computational methods.

This work is dedicated to my wife Bhagawathy and my parents and I thank them and my extended family and friends for providing inspiration, encouragement and affection.

TABLE OF CONTENTS

1. INTRODUCTION

Water and silica are two of the most abundant chemicals on the earth's crust [1] and the understanding their role in technological, biological and geological processes is an important undertaking by scientists. This current study is focused primarily in building an atomic model for water that is capable of dissociation and reproduce interactions with silica.

Water as a unique chemical has posed a spectrum of problems for scientists and engineers. Among the earliest scientific studies of water relevant to today's world was in 1781, when Priestly synthesized water and shortly afterwards Lavoisier decomposed it into oxygen and hydrogen. By the late 1800's, anomalous properties of water were being observed and in 1933 Bernal and Fowler came up with an interaction potential for water. With the advent of x-ray techniques in 1930's the research on water was intensified and by the 50's computational studies of water were being undertaken [2].

Some important milestone works that served the advancement of computational studies of water were as follows [3] :

- Monte Carlo sampling scheme by Metropolis, Rosenbluth and Teller in 1953.
- The first molecular dynamics simulation by Alder Wainwright around 1957.
- Barker and Watts and Rahman and Stillinger's first computer simulation of water in 1969 and 1971 respectively.
- Derivation of a pair potential for water from ab-initio calculations by Clementi et al. in 1976.

Most of today's water models are based on pair potentials and sometimes a combination of intra-molecular potentials and three body potentials, where the charge

distribution on the water molecule is modeled by point charges either on the nuclei or on the extra sites in the plane of the molecule. The goal of most simulations of water is to understand the evolution of properties of water over a large range of thermodynamics conditions and the basis for the anomalous properties. However, to understand the interactions of water in different ambient conditions, the robustness and transferability of the water model is also essential. Consequently, most of the currently used water models are designed to reproduce the properties over a limited range of thermodynamic conditions or to suit specific needs.

1.1 A brief on water.

Traditionally, in molecular simulations, one of the basis of evaluating the accuracy of a model has been the capacity of the model to predict the observable properties. Keeping in mind the primary objective of this thesis as being the study of the interaction of water in silica nanopores, reproduction by the model of the physical properties of water, like the structure at ambient conditions, equation of state, thermal expansivity and diffusivity were considered important for use in silica-water systems. Thus, a look at some of the relevant experimental methods and physical properties of water would be useful at this point.

1.1.1 Molecular Structure.

Water molecules belong to the symmetry group of C_{2v} with two mirror planes and a two fold rotation axis [4]. Since the hydrogen atoms are about 16 times lighter than the oxygen there is an ease in their rotation and relative movements. A rough definition of the electronic structure would be as a molecule containing four sp3 hybridized electron pairs two of which are associated with the hydrogens and the other two form the lone

pair. However, this is not a very accurate description as, in a perfectly tetrahedral arrangement of the orbitals HOH angle should be 109.47° and such an arrangement is not found in liquid water. Also, molecular models that depicted a negative charge at the location of lone pairs are not accurate in description of the structure of bulk water [4].

The isolated water molecule in gas phase has an O-H length of 0.9584A and H-O-H angle of 104.45°. The charge distribution is determined by the method of calculation and the geometry but an approximate description would be a charge of –0.7e on the oxygen and charges og +0.35e on each of the hydrogens. The values of the OH bond length and the HOH angle are not maintained in bulk water and drift to about 0.97A and 106° according to neutron diffraction studies. Changes in the bond length and bond angles are also brought about by the cluster that a particular water molecule is associated and by interaction with solute ions. In general, molecular models of water use a bond length between 0.957A to 1A and angles of 104.52° to 109.5° [4].

An electron density map of the water molecule would show a minima in the electrostatic potential at the approximate location of the lone pairs and the water molecule has been reported to have an average Van der Waals of 2.8Å. The molecule is not spherical and has a variation of ±5% in the Van der Waals diameter[4].

As regards dimers, the most energetically favourable one is where one of the oxygen atoms is hydrogen bonded to a hydrogen atom of the other as shown in fig 1.1 :

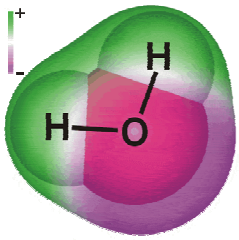

(a)

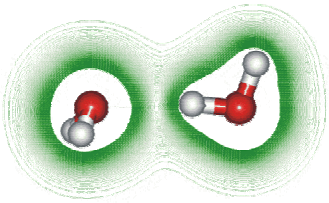

(b)

Fig 1.1a and b : A schematic representation of water molecule and the water dimmer-from[4]. The colors in (a) represent the charge with red being negative charge and green being positive charge.

1.1.2 Experimental methods for determining Structure of Bulk water.

The distinctive microscopic structure of amorphous materials can be determined reliably by a variety of experimental methods of which x-ray or neutron scattering studies are the popular methods used for studying. Scattering experiments involve probing the differential cross section ($d\sigma/d\Omega$) which is the ratio of the scattering cross section to the solid angle about the scattering angle [5]. This ratio is analyzed using the Born approximation to give the structure.

$$I(Q) = \frac{d\sigma}{d\Omega} = \left\langle \sum_{i,j=1}^{N} b_i b_j \exp(i\mathbf{Q}.\mathbf{r_{ij}}) \right\rangle \qquad 1.1$$

where the sums are over the nuclei or electrons , the b's are the scattering length for particle scattering of a given element or a form factor for phonon scattering; rij are the positions of the nuclei in particle scattering or the position of electrons in photon scattering and $Q=4\pi\sin(\theta/2)/\lambda$ is the momentum transfer for the elastic scattering process λ being the wavelength. In actual data analysis, one also has to account for other effects like incoherent scattering, beam polarization, multiple scattering, inelastic effects, container absorption of radiation etc.

In the x-ray scattering method the electronic density distribution around a nucleus scatters the incident radiation and the scattering cross section depends on the square of the number of electrons involved. In water, this essentially means that the x-rays "see" the electron distribution around the oxygen and data analysis thus leads to the molecular

structure of the water atoms. However, the presence of the positive neutrons of hydrogens changes the spherical symmetry of the electron distribution around oxygen as seen in the previous section. Hence, besides this minimal effect, the x-rays do not “see” the hydrogen. Hence, accurate structure is determined by doing appropriate modifications during data analysis to account for the redistribution of electrons due to a) the presence of hydrogen and b) due the water being in liquid state [6].

Neutron scattering differs from the above method in that the incident radiation of neutrons interact with all the nuclei and thus the hydrogens can be spotted more accurately. In case of water, there has been some success and general preference with neutron scattering experiments using heavy water where the coherent scattering length of the deuterium is 6.67fm as compared to -3.74fm with hydrogen and this results in better scattering by the hydrogen atoms. From diffraction measurements for heavy water, light water and mixtures of the two, one can extract the pair correlation functions of all the species. However, use of heavy water has in inherent disadvantage in that the structure of heavy water itself is more ordered than that of regular water [5].

The x-rays have wavelengths of about 0.5 – 2A and are generated inhouse by bombardment of high energy electrons on a target metal. A synchrotron source, can also be used to give a high intensity radiation and this is an advantage while collimating the beam to a small diameter and also requires lower exposure times. The Q ranges are typically around 0.3A-1 to 15 A-1.

Diffractometers used in neutron scattering also rely on the synchrotron or on spallation sources for neutrons. The spallation sources have higher intensity and neutrons of a greater span in wavelength.

The scattered signal is captured by detectors of a given area (dA) positioned at a given distance ,L and measures the flux of radiation scattered into the solid angle element $d\Omega = dA/L^2$.

For data analysis, the scattered intensity in x-rays is now split into two components, one corresponding to self scattering by individual molecules, also known as the molecular form factor $\langle F(Q)^2 \rangle$ and a second arising from intra molecular scattering, S(Q). With the approximation that the scattering is done by spherical electron clouds, the experimental intensity is now defined as [5]:

$$I(Q) = \sum_{ij} x_i x_j f_i(Q) f_j(Q) \frac{\sin Q r_{ij}}{Q r_{ij}} + \sum_{i \le j} x_i x_j f_i(Q) f_j(Q) S_{ij}(Q) \qquad 1.2$$

where x_i is the atomic fraction of species *i*, $f_i(Q)$ is the *Q* dependent atomic scattering factor for atom i and r_{ij} is the intramolecular distance between the centers of the electron clouds. The intermolecular correlation function then follows from the Fourier transform relation given by [5]:

$$S_{ij}(Q) = 1 + 4\pi\rho \int_0^\infty r^2 dr [g_{ij}(r) - 1] \frac{\sin Qr}{Qr} \qquad 1.3$$

Thus, we get g(r) which is a direct relation to the structure of bulk water. However, the above underlines only the basic equations for determining the structure. In actual analysis, there are several correction factors (to account for unwanted radiation from sample containers, absorption of some intensity by the sample, geometry of the sample, polarization of the source, multiple scattering, incoherent scattering or Compton effect, non-spherical geometry of the scattering electron cloud and deviations due to chemical bonding) that have to be applied to the raw data.

In neutron scattering, we split the differential cross section into self and distinct components as [5] :

$$\frac{\mathrm{d}\sigma}{\mathrm{d}\Omega}=\left(\frac{\mathrm{d}\sigma}{\mathrm{d}\Omega}\right)^{\text{self}}+\left(\frac{\mathrm{d}\sigma}{\mathrm{d}\Omega}\right)^{\text{distinct}} \qquad 1.4$$

The unwanted effect of incoherent scattering is isolated in the self scattering term and the liquid structure factor is then given by

$$S(Q)=\frac{\left[\left(\frac{\mathrm{d}\sigma}{\mathrm{d}\Omega}\right)^{\text{distinct}}+(b_O^2+2b_H^2)\right]}{(b_O^2+2b_H^2)^2} \qquad 1.5$$

This can be rewritten in terms of molecular form factor <F(Q)2> and a scattering function DM(Q) containing all the intermolecular correlations as

$$S(Q)=D_M(Q)+\left\langle F(Q)^2\right\rangle \qquad 1.6$$

The pair correlation function g(r) can be determined by Fourier transform of DM(Q)

$$4\pi r\rho_M(g_L(r)-1)=\frac{2}{\pi}\int_0^{\infty} QD_M(Q)\sin(Qr)\mathrm{d}Q \qquad 1.7$$

Use of isotopic substitution with heavy water allows for obtaining all the three pair distribution functions. Again there are corrections that need to be applied to the above equations to account for inelastic scattering.

Another important factor to be accounted for in structure determination by above methods is the experimental truncation of S(Q) in Q space.

1.1.3 Water structure at ambient conditions [5]

The radial distribution function(RDF's) and partial distribution functions(PDF's) are the commonly used data for gathering structure information about any amorphous

material. Experimental methods are used to determine the structure factor and Fourier transformation is used to obtain the RDF's and PDF's. The details of the pair distribution function will be listed out in a later chapter.

A good indication of the molecular structure of water is the nature of the O-O PDF. It is only recently that water structures calculated by x-ray and neutron scattering methods have started agreeing with each other. A key factor in determining the exact height of and shape of the first peak in O-O PDF is the scattering of wave vectors above $7A^{-1}$.

Nevertheless, one of distinct features revealed by both the methods is the tendency of water molecules to form a tetrahedral structure of four water molecules surrounding a central molecule. The nearest neighbour O-O distance is around 2.75A and this distance is maintained even in ice.(ref3) This is evident from the coordination of oxygen ontained by integration of PDF till the first minima.

Figure 1.2 shows a comparison of experimentally obtained PDF's of O-O pair based on neutron data and x-ray data. The given data shows excellent agreement between both the methods, primarily because the data by Soper (indicated by Soper 2000 in the O-O pdf) is based on new potential based reverse Monte Carlo analysis of previously obtained neutron results. Earlier data of neutron analysis used to give the first peak location at around 2.75 and a height of 2.2. The OH and HH PDF can be obtained only by neutron diffraction technique using heavy water substitution.

It is also customary to use the total pair correlation function for water or D2O as given in equation (8) to compare the experimental structure of water with simulation results.

$$G(r)=0.498g_{DD}(r)+0.421g_{OD}(r)+0.089g_{OO}(r) \quad 1.8$$

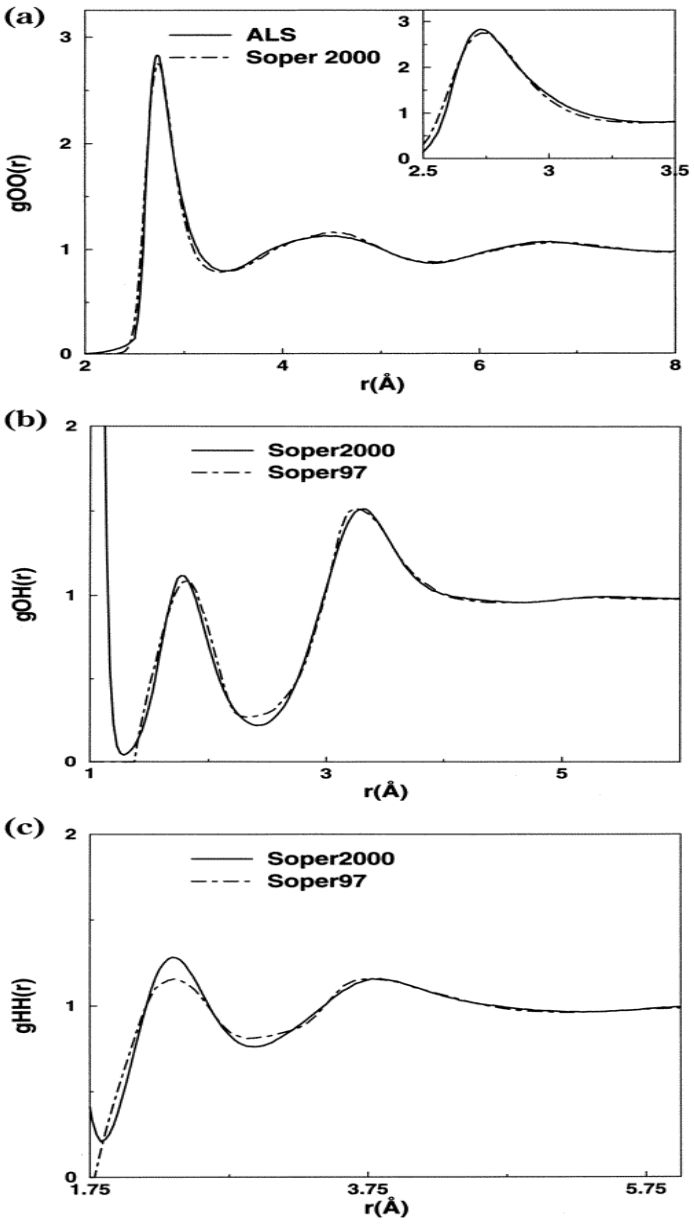

Fig 2.2 : (a) Comparison of O-O PDF obtained by neutron diffraction (Soper 2000) and x-ray diffraction (ALS). (b) and (c) are comparison of Soper's original data (Soper97 and newly analyzed data (Soper2000). Figures from [5]

Besides the above mentioned short range structures, it is also thought that combinations of these smaller clusters can result in the formation of larger clusters in a collapsed high density state or an open low density state [4]. The larger clusters could be close to the ordered structures found in crystalline ice or sometimes dodecahedral or icosahedral clusters. There are a variety of propositions as to the exact nature of these large clusters - however, all of them are based on an extensive network of hydrogen bonds which are preserved upto 85% even at temperatures of around 100 C. The presence of icosahedral has been reported in [4] based on x-ray diffraction of water nanodrops. A dynamic equilibrium that also shifts between open and closed structures based on ambient conditions serves as a possible explanation of the anomalous properties of water like temperature of maximum density and pressure viscosity behaviour.

1.1.4 Thermodynamic and transport properties of water.

The equilibrium properties like volume, entropy enthalpy and internal energy can be obtained from the Gibbs energy (or Helmholtz energy) based on standard thermodynamic relations. Other important properties like specific heat capacities, compressibility can also be derived from the equilibrium properties. Experimentally however, it is the equilibrium properties that are determined and the calculated Gibb's energy is used for designing the phase diagram. There are a number of standard experimental techniques for the evaluation of the properties and a discussion of all of them is beyond the scope of this work [4].

The International Association for the Properties of Water and Steam (IAPWS) sets and maintains the thermodynamic data of water. The latest standard , Industrial Formulation 1997 (IF97) replaced the earlier one IFC67 [7]. Among the various

properties that are standardized as an equation by IAPWS are the density, specific internal energy, specific enthalpy, specific entropy, specific isobaric heat capacity, specific iscochoric heat capacity, the dynamic viscosity and thermal conductivity all as a function of temperature and pressure and the values at saturation state, the boiling point as a function of pressure and the vapor pressure as a function of temperature. This data is made available in several steam table books.

The phase diagram of water, which is another important tool for the study of behavior of water, over a wide range of temperature and pressure is as shown in figure 1.3 [4]. One of the anomalous behaviors of water is evident from negative slope of the like separating the liquid and solid which implies that the melting point decreases with increasing pressures.

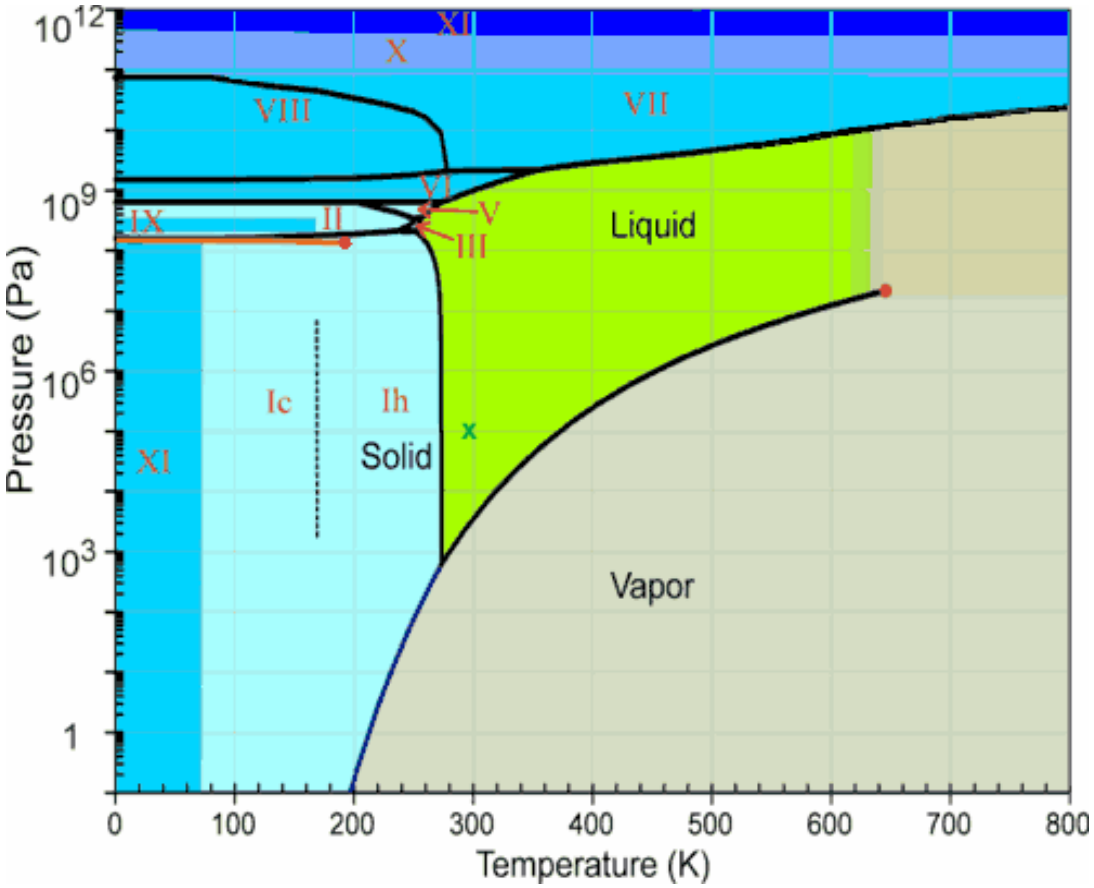

Fig 2.3 Phase diagram of water over a wide range of conditions. (from [4])

A discussion about the properties of water is not complete without a mention about the anomalous properties of water. Some of the unique properties of liquid water are its unusually high phase transition temperatures and physical properties and the negative coefficient of thermal expansion at low temperatures in liquid , the negative volume change on melting and the existence of a density maximum. Though it is conceivable that many of the anomalous properties (available literature can concieve as many as 40 [4]) can all be explained based on a few aspects of the electronic and structural behavior of clusters, the fact that these properties are not what is expected of a typical liquid is what makes water a unique liquid. Indeed, the presence of these unique properties is what results in the life sustaining capabilities of the earth.

Properties of the liquid at ambient conditions, defined as a temperature of 298K and 1 bar pressure, is one of the primary criterion to be reproduced by any simulation of water.

Classified under transport properties are the shear viscosity, which gives a measure of the transport of momentum, the thermal conductivity and the diffusivity. Calculation of the transport properties involves not only evaluation of these based on behavior during molecular collisions but also behavior during collision due to intermolecular forces and ultimately leads to the understanding of the intermolecular forces themselves.

The self diffusion coefficient is the one of the transport properties of water that has been paid attention by molecular models of water as it is an indicator of the influence of hydrogen bonds in the translational motions [4] and viscosity [8]. A common method

employed for determining the self diffusion coefficient is the spin-echo technique of nuclear magnetic resonance, in which the decay of the spin echo has an exponential relation with the self diffusion coefficient [8].

The thermodynamic properties of water at far from ambient conditions are also well investigated in literature and can be summed up by the Pressure-Volume-Temperature (PVT) data and the equation of state. Experimental methods for determination of far from ambient conditions can be either static mentods for low and moderate pressure regimes and dynamic for high pressure regimes. In the dynamic method a shock wave, generated by an explosion, is propagated at a supersonic velocity into the sample and the properties are determined on either side of the shock front [8].

Reliable experimental techniques for evaluation of viscosity and thermal conductivity do exist though the evaluation of self diffusion coefficient is more of a challenge.

Table 1 gives some of properties of liquid around the ambient conditions that are relevant to this work.

Property	Value and reference
Density at 298K	0.997 g/cc [7]
Temperature of maximum density	277.1 K [7]
OH distance	0.957Å in gas [4]
HOH angle	104.5 in gas [4]
Characteristic lines in frequency spectra	3657cm^{-1}, 1594cm^{-1} and 3758cm^{-1} for the molecule, and 3277cm^{-1}, 1645cm^{-1} and

	3490cm^{-1} in bulk water for the primary modes. [4]
Cohesive energy	10.40Kcal/mol [9]
Self diffusion coefficient	2.27cm^2/s [4]
Dipole moment	1.854D in gas and 2.95D in liquid at 300K [4]

Table 1.1 : some of the relevant properties of liquid water.

1.2 A brief on silica.

Vitreous silica (v-SiO_2) has been a subject of extensive study because of its technological significance and because it provides a reasonable insight into the glassy state. Significant progress has been made in the understanding of glass formation and the structure of v-SiO_2 by experimental techniques and more recently by the use of molecular dynamics especially in the detailed analysis of the atomistic motions and complex microstructures.

1.2.1 Glass formation.

In lieu of a proper definition, some of the common features that are accepted as being present in all glasses are the lack of a long range order, the lack of sharply defined melting point in solid state and the inability to cleave in specific directions. Thus, there are a wide variety of organic and inorganic compounds that can form glasses [10].

Two approaches can be adopted to explain glass formation. The atomic approach, based on correlating the nature of chemical bonds and the geometric shape of the groups involved to glass formation, was first put forward by Goldschmidt [11] .Accordingly the criterion for glass formation in oxide systems was based on the ratio of metal-oxide ionic

radii lying between 0.2-0.4 which would lead to tetrahedral packing. This theory served as a groundwork for later studies and Zachariasen [12] extended this to formulate what was later known as the continuous random network theory. The essential outline of this theory describes four rules for formation of oxide glasses – 1) the oxygens may not be linked to more than 2 atoms of the metal 2) the metal ion must be surrounded by only a small number (3 or 4) oxygens 3) the oxygen polyhedra thus formed share corners with each other to fill three dimensional space and 4) at least 3 corners of a polyhedron has to be shared. Two other important theories based on atomic approach were Smekal's [13] [10]mixed bonding hypothesis where the nature of bonds in a glass are a mixture of ionic and covalent bonds, and Sun's [14] [10]bond-strength criterion whereby a correlation was drawn to show that oxides of stronger bonds were capable of forming glasses more easily because they were incapable of breaking and reforming bonds that is required for crystallization.

A more recent approach has been based on the rate of crystal nucleation and growth in melts. According to this approach, liquids form glasses on quenching if the rate of cooling is high enough to suppress nucleation and growth of crystals. Thus, the glass forming capabilities of a materials can be determined based on the time temperature transformation (TTT) diagrams and by manipulating the cooling rate many more materials including metals are being quenched into a glassy state [10].

1.2.2 Structural properties

As noted before, a commonly used benchmark for MD simulations is the compliance of the simulation results to experimental properties. The molecular structure of vitreous silica is easily evaluated by x-ray and neutron scattering studies. Information

on local bonding in silica have been made available through EXAFS, NMR and ESR techniques. The vibrational spectra of silica can be Infrared, neutron and Raman scattering studies. In recent times molecular dynamics and reverse Monte Carlo simulation techniques have served to refine the results obtained by traditional experimental techniques and thus measure the bond lengths and bond angle distributions to a high level of accuracy [15].

Crystalline silica undergoes phase transitions from α-quartz to β-quartz at 574.3°C, then to hexagonal packed tridymite at 867°C and then to β-cristobalite at 1470°C before finally melting at 1727°C. The common feature between all these structures is the three dimensional framework of SiO_4 tetrahedra which is found in glass also. Silica glass is similar to β-cristobalite and H.P.tridymite w.r.t bonding, density, position of the first diffraction peak leading and vibrational spectrum and this leads to the belief that they have a close structural relationship in the short length scales. These similarities lead to the view of glass as being formed by rotational distortions and displacements of un-deformed SiO_4 tetrahedra of the abovementioned phases [15]. Some of the Key structural features of vitreous silica are given in table 2.

Density	2.2-2.4 g/cc [16]
Bond lengths[17]	
Si-O	1.62
Si-Si	3.10
O-O	2.64
Bond angles[17]	
O-Si-O	109.6

Si-O-Si	142.0

Table 1.2 : Structural properties of Vitreous silica.

1.2.3 Vibrational spectrum of silica

The vibrational spectra of simulated silica serves to validate the dynamic properties and the effectiveness of the potentials used. Indeed, a static structural model is a prerequisite for effectively evaluating the vibrational density of states. A central force model [18] or a simple random network cluster of Bell and Dean [19]serves well to explain the fundamental vibrational modes of amorphous silica. There are three main modes that are observed in the vibrational spectrum of silica and the peaks around 400 cm^{-1}, 800 cm^{-1} and 1150 cm^{-1} correspond to the rocking, bending and stretching modes of vibration of the bridging oxygen in Si-O-Si. Additional peaks at around 150-200 cm-1 are also seen and these are attributed to the correlated motions in bulk silica. The partial frequency spectrum of silicon and oxygen, when considered separately, show that the oxygen atoms dominate contributions in the high frequency lines at ~1150 cm^{-1} and at low frequency bands and significant contribution of silicon arises only around the 800-900cm^{-1} range.

A point of much interest with regards to the vibrational spectrum is the presence of D1 and D2 peaks at ~500 cm-1 and 600 cm-1. The origins of these peaks are not very well understood and have been attributed to inherent defects (hence the assignment D1 and D2) and the presence of surfaces as their intensity is increased for porous glasses and undensified silica gels [20] [21].

1.3 Water in confined spaces

The interaction of water with solid surfaces and the changes in properties when restrained by the presence of interfaces has attracted a lot of attention of theoretical and experimental studies in recent times. This is conceivable because in many common natural situations water is found attached to a substrate or contained in small voids of porous materials - typical examples being water constrained in clays, zeolite cages, rocks and sandstone, water interacting with the surface of biological macromolecules, proteins and membranes. Many technological applications also involve water in constrained geometries like hydrophilic wafer bonding, interactions between drugs and bio-molecules, de-pollution, corrosion and catalysis studies.

Surface Force Balance (SFB) experiments can be used to study the properties of confined and layered water. In these experiments, optically smooth mica surfaces interact with each other through an interface of water between them. The motion of these mica surfaces can be recorded using white light interferometry and the normal and shear forces exerted between the two surfaces can be measured by sensitive springs attached to the surfaces. Thus the shear viscosity, which indicates the fluidity of the confined water is studied [22]. Such studies have indicated that confined water retains its fluidity even at confinement to sub nanometer levels.

In studying solutions of water, solvation dynamics refers to the rate at which solvent molecules (in this case –water) arrange themselves around a solute molecule. Water is considered a universal solvent because it of the range of solutes that it can accommodate and its fast solvation dynamics. This effect is attributed to the low frequency modes of vibration caused by the hydrogen bonded network. Confinement of water results in an additional slow component (nano second mode) in the solvation

dynamics of water besides the usual sub picosecond mode. This effect is important in biological systems where interaction of water molecules confined in proteins and in micelles [23] . In the above work, the solvation dynamics of water confined in reverse micelles was studied and the emergence of the slow component is attributed in part to the disruption of the hydrogen bonded network.

Neutron scattering studies and Nuclear Magnetic Resonance (NMR) can also be used to characterize nano-confined water. NMR studies are done on elements that have a net spin on the nucleus by applying an external magnetic field and recording the splitting of the spin energies of the nuclei in response to the external field. The extent of distribution of the nucleons in the split energy levels is a function of the structure of the nucleons and thus this method allows us to probe the static structure of materials.

The common NMR techniques used for characterization of water/ice systems in confined geometries are listed in [24] and include measurement of changes in frequency spectra, changes in spin-lattice or spin-spin relaxation times, measurement of the translational diffusion coefficient or direct measurement of the magnetization transfer as a function of time.

Though there are several experimental techniques available for studying water in confined spaces, difficulties in probing the nano-confined water-substrate interface by experimental methods necessitates the use of computational simulations to study the interactions.

1.3.1 Water and nanoporous glasses.

One of the main considerations in all the water-interface studies is the affinity of the substrate to water. Weakly attractive and non reactive surfaces are classified as

hydrophobic surfaces. A drying transition is expected to be formed at a hydrophobic interface and the phase transition behavior is modified to produce co-existence curves of lower liquid density [25]. Computational studies of hydrophobic hydrations shows that the dipole vector of most of the bulk water molecule lies parallel to the interface and the dipole vectors of the molecules at the interface are perpendicular to the interface[26]. Other experimental and theoretical studies have shown that the presence of an interface may induce earlier freezing [27]. The freezing or solidification behavior has been attributed to the loss of degrees of freedom Besides changes in the static structures, changes in vibrational density of states has also been observed in hydrophobic substrates.

The other type of substrate commonly encountered is the hydrophilic or reactive substrate. Silica forms a typical hydrophilic surface and the reacts with the water to form silanols. The reactivity of silica with water is well documented and finds applications in a variety of fields. Fourier Transformed Infrared Spectroscopy studies of properties of water in zeolite cages which is a has demonstrated the shift in frequency spectrum of water to lower frequencies in both coordinated motions of molecules and in the fundamental OH stretching modes [28].

Another interesting result that has been observed is the late onset of crystallization when water is confined in silica or clay membranes in lamellar confinement. This peculiarity can thus be used to super-cool water to much below its normal crystallization temperatures for studying the glass transition and fragility [28]. Fragility here is dependent on the viscosity and relaxation time following an Arrhenius behavior with change in temperature. This can thus be used to indicate the glass transition temperature. It is to be noted that the viscosity of water under such confinements is still below the

liquid viscosity and hence the film is to be classified as glassy water or supercooled liquid. The above mentioned investigation into the glass transition revealed that glass transition in super-cooled water is in the 160-180K range or 136K depending on interpretation of the results.

Studies with hydrated mesoporous silica structures of various pore size and geometries by Liu et al. [29] confirm the slowing of both translational and rotational dynamics of the confined water and this effect is enhanced by lowering the temperature. The change is not strongly influenced by the pore morphology.

Neutron diffraction studies by Bruni et al. [30] has shown the contrast between the structures of bulk water and interface water. The study also served to explain the effect of Vycor™-water correlation interfering with the neutron scattering data. Furthermore, proper interpretation of data of neutron scattering for Vycor™-water interactions should include, the excluded volume effects to account for regions in Vycor™ where water is not allowed [31].

By measuring the static permittivity of a system of water in Vycor™ glass at high temperatures, Heijima and Yao [32] experimentally determined that the boiling point of the confined water is increased to about 15K above its bulk boiling point. However, the enthalpy of vaporization is still close to that of bulk water. This large increase in boiling point is also attributed to the reactivity of water with silica. The same studies also noted the suppression of the critical temperature to ~623K.

A summary of results obtained by neutron scattering and NMR studies is listed by Webber and Dore [24] and include :

1) Depression in crystallization temperature depending on pore geometries. The crystallization is noted to appear in the bulk phase and not that the surface of the substrate.
2) Lowering of the frequency spectrum with respect to bulk water.
3) Enhanced hydrogen bonding with reduction in temperature.
4) Formation of defective forms of cubic ice in pores with diameters greater than 30nm.
5) Hysteresis in ice nucleation and melting.

The above work however, lists increased diffusion rates and increased mobility at the interface in pores compared to ice. In general, it is recognized that the diffusion coefficient is lower in the confined ambience as compared to the bulk. The above study was a review of water confined in mesoporous silica.

A review paper of confinement studies of many different materials by Christianson [33] also lists the formation of cubic ice in water confined to mesoporous glasses.

Aided by experimental methods and molecular dynamics simulations, studies by Gallo, Ricci et al. [34] [35]have shown the effectiveness of MD simulations in the study of water confined in Vycor™ glass. The study demonstrated the change in static structure in that the water layers closer to and in contact with the Vycor™ surface form lesser hydrogen bonds and are not tetrahedrally coordinated and this is offered as the explanation for the lowering of crystallization temperature as hydrogen bond formation is required for the structure of all crystalline forms of ice. A later study by the same group [35] with the aid of molecular dynamics simulations also demonstrated the formation of

high density layers of water close to the glass surface which have a structure different from the almost bulk-like water that is present farther away from the hydrophilic surface. The water away from the wall did, however differ from bulk water in that it resembled ambient water only when cooled to 270K thus demonstrating a 28K under cooling.

Computational studies of water interacting adjacent to hydrophobic and hydrophilic surfaces have been conducted earlier [36]. In these studies, the hydrophobic surfaces were modeled either by a flat surface or a corrugated surface that interacted with the molecular water model through a Lennard-Jones type interaction. The hydrophilic surface was chosen to be silica but there was no direct interaction between the silica and the water molecules. Instead, a hydrated silica surface was formed by attaching hydrogens to the non bonded surface oxygens of the silica and the interaction was studied. The results of these studies indicated the higher propensity of the water molecules near the surface to form hydrogen bonds with the surface silanols rather than with other bulk water molecules. This resulted in a change in orientation and hence the dipole of water molecules near the surface being different from the bulk.

Simulations of water-glass system with interaction levels resembling physisorption have been studied by Puibasset and Pellenq [37]. In this case, the glass substrate was assumed to be rigid and the water molecules were non dissociable, however, there has been a good agreement of the simulations with thermodynamic and structural results. This study was also able to imitate the intricate pore structures of Vycor™ glass.

An important aspect that needs to be considered in water-glass interaction is the dissociation of water to form silanols. The substrate also needs to be a reactive and

should resemble the real oxygen terminating surfaces of real glass. Computational studies of water interacting with silica surfaces with emphasis on silicon wafer bonding and formation of siloxanes and silanols in gels has been investigated earlier by this group [38-40]. These simulations used atomic water models where the water molecules were capable of dissociation and reaction with the silica surface based on a fixed charge Coulomb term and a short range interaction based on BMH potentials. Earlier results by this group have indicated the relaxation of the silica surfaces by the presence of water and the formation of siloxane bonds across a layer of water as would be the case in silicon wafer bonding. The reaction between a water monolayer and a silica surface has also been studied and this indicates the clustering of water molecules on the free surface. The explanation for this was that sites on the silica surface that already have an attached water molecule or a defect or a silanol are more reactive and at low concentration of water, there sites accumulate the water molecules. Also, the energy barrier for attachment of a water molecule to a defective oxygen in silica surface is much higher than the energy barrier for attachment of the water molecule to a hydroxyl group or an other water molecule.

From the literature survey, it was thus inferred that there is a vast scope for understanding of the interfacial phenomena with the use of computational studies with a dissociable potential for water and a uniform description of interactions across water and silica and a water potential that is capable of reacting with a non rigid substrate.

2. REVIEW OF COMPUTATIONAL METHODS

2.1 Varieties of techniques.

Computational techniques are very widely used in the study of material systems and are particularly useful in studying the molecular and atomic behavior of materials by classical treatment. There are a variety of techniques available, most of them assuming some form of additive, spherical interaction potential between the particles. The essential aim of any of these computer experiments is to obtain a set of equilibrium positions and velocities of a set of particles and determine the physical properties of the system based on these. The choice of the method depends on the properties and mechanisms that need to be studied and the limits of the compuer. In general, the techniques can be classified as static or dynamic. All of the methods are detailed in literature [41] [42] [43] [44] and here a brief overview of some of them is presented with more details on Molecular Dynamics techniques.

In static techniques, otherwise known as stochaistic techniques the equilibrium atomic configurations are calculated based on variational, lattice statistic or Monte Carlo methods [45] [42].

In the variational technique, particles are moved individually to a new location of zero force based on the constraints imposed the the potential equations. When done iteratively for all the particles, the net result gives the energetically most favorable configuration for the system.

Monte Carlo techniques are pseudo-dynamic in that a series of static atomic configurations are obtained and the calculated properties are obtained by averaging over these configurations. This is called the Ensemble average and is considered equivalent to

the time average of properties. However, these configurations are from random points in the phase space and are not related by time. A probability function based on the Boltzman factor of exp(-E/kT) is used as a weighing factor for calculating the ensemble average. Thus the average of any property can be summed as [42]:

$$\langle A \rangle = \int A(\mathbf{R}) W(\mathbf{R}) d\mathbf{R} \qquad 2.1$$

where

$$W(\mathbf{R}) = \frac{\exp(-U(\mathbf{R})/k_B T)}{\int \exp(-U(\mathbf{R}')/k_B T)} \qquad 2.2$$

The above is a very crude description of the rationale behind Monte Carlo simulations and direct application of the above method becomes impractical due to the computational load.

The Metropolis Algorithm is a very convenient Monte Carlo method for conducting molecular simulations. In this method, the probability of choosing a configuration is based on the probability of existence of the configuration and hence, the average does not need the weighing factor. Thus, a sequence of steps that can be used in the method would be to select an atom, move it from R_i to $R_i+\Delta R$ and calculate the change in potential energy as ΔU and accept the new move only if $\exp(-\Delta U/k_B T)$ is less than a system generated random number and if the new move is not acceptable then return the atom to its original position. Proceeding this way for all the atoms over several configurations, one arrives at a set of quasi-equilibrium configurations.

The other way of calculation of new positions is based on lattice statistics, where, where the new positions are calcaulated simultaneously or atoms after minimizing the energy of the system Accordingly, the atomic displacements of a single lattice are

converted into an infinite superlattice of non-interacting primary lattices. The phonon amplitudes of the initial primary lattice are used to calculate the realspace displacement and hence the energy of the atoms in the primary cell. This results in a set of equilibrium atomic configurations.

As can be easily inferred, since the ensembles calculated by the static methods are not related by time, special methods like kinetic Monte Carlo methods have to be devised to calculate the dynamic properties of the system.

2.2 Molecular dynamics.

The present work deals only with Molecular Dynamics simulations and hence a more detailed overview of the principles of molecular dynamics follows.

The essential idea behind Molecular Dynamics is to calculate a set of atom positions and velocities as it would move in a real system. The classical many body system can be described by the many body Hamiltonian and the dynamics of the system can be solved for using Newton's laws of motion. Thus, the Hamiltonian (total energy) of a system of N particles can be written as [42] [44]:

$$H = \sum_{i=1}^{N} \frac{p_i^2}{2m_i} + \sum_{i>j}^{N} U(r_{ij}) \qquad 2.3$$

where p_i and m_i are the momenta and mass of the i^{th} particle $V(r_{ij})$ is the interaction potential between particles i and j separated by a distance r. The forces acting on each particle at a time t are obtained from

$$F_i(r) = -\frac{\partial}{\partial r} U(r) \qquad 2.4$$

The temperature of the system at any time would be given by

$$T = \frac{1}{3Nk}\langle \sum_{i=1}^{N} m_i v_i^2 \rangle \qquad 2.4$$

Initially, a Gaussian distribution of velocities are assigned to a random ensemble of atoms based on the desired temperature.

Then the particles are moved from their initial positions based on their velocities as given below [45]:

$$X_i(t+\Delta t) = X_i(t) + \Delta t\, v_i \qquad 2.6$$

This results in a new set of position and velocity coordinates at a time $t+\Delta t$ and the velocities at the new position are given by:

$$v_i(t+\Delta t) = v_i(t) + \Delta t.F_i/m \qquad 2.7$$

and the procedure is repeated again by evaluating the forces at the new positions. The above mentioned scheme is a very simplistic view of the process and there are various algorithms for implementing the above procedure for a system with $N\sim10^3$-10^4. Thus, one ends up with a set of values for the positions and momenta of all the particles in the system at different times.

One of the issues of these simulations is finding similarities between a simulated system of N~1000 particles and a real system of $\sim10^{25}$ particles. In atomistic simulations this is overcome by performing simulations with periodic boundary conditions. This means that the simulation box containing the N particles is considered to be a repeating unit with the periodicity equal to the dimension of the box. Thus an atom in the primary box would feel the force from its neighbors in the adjacent box, but due to periodicity, there is no need to calculate explicitly the positions of the atoms in the non-primary

boxes. This results in the properties of the simulated ensemble resembling those of the bulk [44] [41].

2.3 Statistical treatment of the results of MD simulations :

Statistical thermodynamics allows us to evaluate some of the physical properties of an ensemble obeying Boltzmann statistics. The probability of finding the ensemble in a given energy state E is proportional to $\exp(-E_i/k_BT)$. The ensemble average of physical properties of a system as given in equation 3.1 and 3.2. In ergodic systems, the ensemble average of any property is equivalent to the time average as given by [42]:

$$\langle A \rangle = \lim_{t \to \infty} \frac{1}{t} \int_0^t A(t)dt \qquad 2.8$$

Based on the above premise, the following equations can be used to define the physical properties of interest.

Pressure is given as [44, 46] [47] [48]:

$$P = \rho k_B T + \frac{\rho}{3N} \sum_{i>j}^{N} \langle r_{ij} \cdot F_{ij} \rangle \qquad 2.9$$

where ρ is the number density.

One also defines a partial distribution function between two species of the system from [44] [42] :

$$g_{ab}(r) = \langle (d\overline{n_b}/dr) / (4\pi r^2 \rho_b) \rangle \qquad 2.10$$

where n_b is the number of particles of species b around a particle of a.

This can be thought of as the average non-normalized probability of encountering an atom of species b at a distance of r from an particle of species a. This can again be averaged over all the species to give a radial distribution function g(r) which is

proportional to the probability of encountering any particle in ensemble the at a radial distance of r from any other particle. The distribution functions are used to estimate the structure of the material being studied. Most experimental methods give only an indirect measurement of the structure through x-ray and neutron scattering by measurement of the structure factor which is a Fourier transform of the distribution functions.

The self diffusion coefficient of the atoms in the system is given by [44]:

$$D = \frac{1}{6\tau}\langle [r_i(t) - r_i(t+\tau)]^2 \rangle \qquad 2.11$$

where τ greater than relaxation time for the system to arrive at equilibrium. Equation 3.11 is based on the Einstein expression for transport coefficient.

The velocity autocorrelation is calculated using [49]:

$$\gamma(t) = \frac{\left\langle \sum_i v_i(t_0) \cdot v_i(t_0 + t) \right\rangle}{\left\langle \sum_i v_i(t_0) \cdot v_i(t_0) \right\rangle} \qquad 2.12$$

where t_o is an arbitrarily chosen starting time.

Fourier transform of the autocorrelation function is gives the frequency spectrum as [49]:

$$D(\omega) = \int_0^\infty \gamma(t) \exp(i\omega t) \mathrm{d}t \qquad 2.13$$

where D(ω) is the intensity of vibration at frequency ω.

The fluctuation of the potential energy can be used to estimate the heat capacity at constant volume by [43] [50]:

$$C_v = \frac{\langle \phi^2 \rangle - \langle \phi \rangle^2}{k_B T} + \frac{3Nk_B}{2} \qquad 2.14$$

The dipole moment is calculated based on the charge and position of the atoms as follows [43] [42]:

$$D = \frac{1}{N}\sum_{i=1}^{N}\sum_{\alpha=1}^{n} q_i^{\alpha} r_i^{\alpha} \qquad 2.15$$

The index α is over all the atoms in a particular molecule and the initial summation gives the dipole moment of a single molecule, and the index *i* is over all the molecules.

Thus, it can be seen that many properties of interest can be derived based on the simulation results. A note of caution about simulation results at this point – Even though simulations allow us to probe the experimentally inaccessible systems and conditions, the eventual aim of these simulations is to provide insight into the micro - mechanisms in the system being studied. Thus, even with significant agreement between simulation results and macroscopic properties, the molecular mechanisms could be vastly different in reality and the agreement is based on one of the many possible solutions.

A more detailed analysis of the programs and algorithms used for the simulations and analysis is given in the next section.

2.4 Experimental set up and details of programs.

In this section, some experimental details of the molecular dynamics procedure are elaborated. Some of the important aspects of the functioning of the code are detailed below.

2.4.1 Condition for energy conservation in MD simulations.

The total energy of the system in an MD simulation is given as the sum of its kinetic and potential energies. When there is no change to the system conditions like

pressure or temperature, real systems do not undergo change in their total energy. Imposing this condition on MD simulations we have :

$$H = K.E + P.E = \sum (\frac{p_i^{\ 2}}{2m_i} + U(r_i)) = \text{constant}$$

$$\Rightarrow \frac{\partial}{\partial t} H = 0 = \frac{\partial}{\partial t} \sum (\frac{p_i^{\ 2}}{2m_i} + U(r_i))$$

$$\Rightarrow \frac{2 p_i \dot{p}_i}{2m_i} + \frac{\partial U}{\partial r_i} \dot{r}_i = 0$$

$$\Rightarrow F_i \dot{r}_i + \frac{\partial U}{\partial r_i} \dot{r}_i = 0 \qquad 2.16$$

Thus, it is seen that the force being a derivative of the potential (as indicated in equation 2.4 and equation 2.16) is a sufficient condition for energy conservation. In the simulations, as will be apparent from future discussions, the force is not a smooth derivative of the potential. Also, the calculation of higher order derivatives of force and actual movement of atoms is not exact and due to numerical approximations, equation 3.4 is not held true. Hence, energy is not conserved in the current simulations and the criterion of energy conservation has not been a critical factor in determining the success of the simulations.

2.4.2 Algorithm for force calculations

In all the following simulations, the Nordseick - Gear fifth order predictor-corrector algorithm was used to determine the positions and velocities of the atoms. A tabular array of the forces and potentials are calculated and stored at the beginning of the program at the initialization step. Then the move subroutine moves the atoms by the Nordseick Gear Algorithm [42] [41]. This involves three steps –

(i) the predictor step involving prediction of the position and its derivatives upto the fifth order based on taylor expansion of $r_o(t)$. Thus,

$$r_m(t) = \frac{1}{m!}\frac{d^m r_0(t)}{dt^m}(\Delta t)^m \qquad 2.17$$

defines the m^{th} derivative of the position $r_o(t)$. By Taylor expansion of all the derivatives, we get :

$$r_o(t+\Delta t) = r_0(t) + r_1(t) + r_2(t) + r_3(t) + r_4(t) + r_5(t) \qquad 2.18$$

$$r_1(t+\Delta t) = r_1(t) + 2r_2(t) + 3r_3(t) + 4r_4(t) + 5r_5(t) \qquad 2.19$$

$$r_2(t+\Delta t) = r_2(t) + 3r_3(t) + 6r_4(t) + 10r_5(t) \qquad 2.20$$

$$r_3(t+\Delta t) = r_3(t) + 4r_4(t) + 10r_5(t) \qquad 2.21$$

$$r_4(t+\Delta t) = r_4(t) + 5r_5(t) \qquad 2.22$$

$$r_5(t+\Delta t) = r_5(t) \qquad 2.23$$

Thus, the general formula for $r_m(t+\Delta t)$ is given by :

$$r_m(t+\Delta t) = \sum_{n=0}^{5-m} \frac{(5-n)!}{m!(5-n-m)!}\frac{1}{n!}\frac{d^n r_o(t)}{dt^n}\Delta t^n \qquad 2.24$$

(ii) error evaluation based on difference between the predicted forces and actual forces at the new positions. Once the derivatives are predicted, the forces on the atoms at the new positions are read from the table created at the start of the program and the new accelerations are computed. The difference between the read acceleration and the accelerations predicted by equation 5.5 is called the error signal and is used to correct the positions and all its derivatives [45].

$$\varepsilon_{r2} = \frac{F}{2m}\Delta t^2 - r_2(t+\Delta t) \qquad 2.25$$

(iii) the corrector step where the corrections – the error signal multiplied by constants are added to the new position and derivatives resulting in

$$r_m^c(t+\Delta t) = r_m(t+\Delta t) + C_m \varepsilon_{r2} \qquad 2.26$$

The correction constants C_m are chosen so as to minimize the net error. The values used for the fifth order Nordseick Gear Algorithm are [45]C_0=3/20 ; C_1=251/360 ; C_2 =1 ; C_3= 11/18 ; C_4=1/6 and C_5=1/60.

2.4.2 System specifics.

In all the simulations for this work, a spherical cutoff was used with the cutoff radius of cutoff being 10A. Both, NVE (constant N, Volume and Energy) and NPT (Constant N, Pressure and Temperature) ensembles were used in the simulations depending on the quantities being measured. The type of ensemble used has also been mentioned in the sections discussing the results.

3.DEVELOPMENT OF POTENTIALS

Pairwise additive potential functions provide a very convenient method to describe inter-particular interactions in molecular dynamics simulations [44]. Though the actual interaction between two atoms is much more complicated, the use of an additive pair potential in conjunction with a three-body term is computationally convenient and sufficiently accurate. A good potential equation should be amenable to reproduction of different effects and at the same time have parameters simple enough to be easily determined.

3.1 Formula for potential and interpretation of the terms.

The potentials used in the current work consist of the electrostatic part and a short range nuclear part with a repulsive and dispersive term. This is based on a pair potential for rigit water developed by Guillot and Guissani [9]. The pair interaction between two atoms is written as :

$$U_{tot}(r_{ij}) = U_{electrostatic} + U_{repulsive} + U_{dispersive} \qquad 3.1$$

where

$$U_{electrostatic}(r_{ij}) = \frac{q_i q_j}{r} + \frac{q_i^d q_j}{r}\,\mathrm{erf}\left(\frac{r_{ij}}{\sqrt{2}\xi}\right) + \frac{q_i q_j^d}{r}\,\mathrm{erf}\left(\frac{r_{ij}}{\sqrt{2}\xi}\right) + \frac{q_i^d q_j^d}{r}\,\mathrm{erf}\left(\frac{r_{ij}}{2\xi}\right) \qquad 3.2$$

$$U_{rep}(r_{ij}) = A_{rep}\,\frac{\mathrm{erfc}\left(r_{ij}/2\xi_r\right)}{\left(r_{ij}/2\xi_r\right)} \qquad 3.3$$

$$U_{disp}(r_{ij}) = -C_6/r_{ij}^6 \qquad 3.4$$

Most of the parameters in the above equation can be easily determined based on ab-initio data or based on the structure of the molecule. The electrostatic part consists of

four terms which involve the direct point charges (q's) and diffuse charges (q^d's) in all the possible combination. The physical significance of having both q and q^d is to mimic the effect of charge variation as a function of intermolecular distance. Thus, an atom is modeled as having a fixed charge q which decays to a lower charge of $q-q^d$ based on the variation parameter ξ. Though, in the present work, a fixed value for ξ is used for all the systems, use of such a potential allows the convenience of being able to model like species over different phases and compounds. The details of the variation of the potential with change in parameters is given in a later section. The dispersion and repulsion terms are short ranged and reduce to insignificant values by about 4.5Å.

In contrast to the electrostatic terms with is present between all the interactions because of non-zero q's for all atoms , the repulsion and dispersion terms act only between specific species. While in some cases they are present to mimic quantum mechanical effects like the C_6 and A_{rep} in O-O interactions , in other cases they are introduced as a convenience to fix certain molecular parameters like the A_{rep} and ξ_r in O-H interactions used to fix the OH distance.

This feature has also been exploited to depict changes in molecular parameters with change in physical conditions. While the exact nature of the changes in parameters can be determined accurately only by quantum mechanical methods or ab-intio calculations, in the present work the changes have been based on reproducing the property at the changed conditions, while also having a sensible physical interpretation. Specifically, since the OH bond length is determined by the parameter repulsion term in OH interactions, the OH bond length was changed with changes the pressure and temperature of liquid water.

The determination of the parameters with change in temperature and pressure were done on a trial and error basis for obtaining the appropriate thermal expansion curve for water at 298K and the equation of state between 273K and 298K and 1 atm and 8000 atm pressure. The changes in ξ_r are specific only to water and not for silica. This is reasonable in fact because of the liquid phase in water is expected to undergo a larger transformation in its thermodynamic phase range mentioned as compared to silica which is expected to be solid in the entire range.

However, in the mixed systems of water and silica, maintaining charge neutrality dictates that the q's and q^d's are always at a constant ratio and hence, the charge terms and ξ in silica also remain fixed in the above temperature range. While silica could have been simulated with different values for q and q^d initially, the condition of charge neutrality dictates that a constant ξ should be used for silica simulations at least in the case of silica-water systems. Thus, in the current simulations, an oxygen from silica is indistinguishable in terms of parameters from an oxygen in water.

Thus, as an example in a system of water and silica, ξ can be kept at a constant value for the quenching steps of silica and at a different constant value while interacting with water. This allows for having different effective charges for a particular species (which in the above case is oxygen) over different phases. In the inhomogenous systems, a simple method for evaluating the effective charges based on an ambience dependant ξ can be devised. Hence, in the above example, while oxygen atoms deeply embedded in the silica would have the initial constant value of ξ, an oxygen atom closer to the water/silica interface would have a different value based on its neighbors. Although this method is not as simple as the one used in the present work, it gives a greater accuracy by

taking into account ambience effects while not involving extra calculations for charge changes that usually result in a compromise in the computational time that is generally found in other electronegativity equalization methods [51] [52].

Table 3.1 gives the values of the parameters used for the different interactions at 298K. As discussed before, the value of ξ for the OH interaction is dependant on the temperature and pressure and the equation determining this dependency is given below table 3.1.

	ξ_r in Å	A_{rep} in J	C_6 in J/m^6
OH	0.2001	2.283×10^{-16}	-
OO	0.6100	4.25×10^{-17}	4.226×10^{-18}
HH	-	-	-
SiO	0.3730	2.67×10^{-16}	7.00×10^{-18}
SiSi	0.640	7.00×10^{-17}	-
SiH	0.350	5.00×10^{-16}	3.80×10^{-18}

Table 3.1 : Values of parameters used at 298K and 1atm pressure.

To calculate the parameter $\xi_{r\text{-}OH}$ the method adopted was as follows:

I) Perform NPT simulations of water at a given temperature and 1 atm pressure with different values of $\xi_{r\text{-}OH}$ and select the $\xi_{r\text{-}OH}$ that gives the right value for density (a difference of a maximum of 0.2% from the experimental value) as appropriate for that temperature.

II) Obtain $\xi_{r\text{-}OH}$ vs P plots for different fixed temperatures and higher pressures thus obtaining a set of ξr-OH vs P equations as shown in fig 3.1.

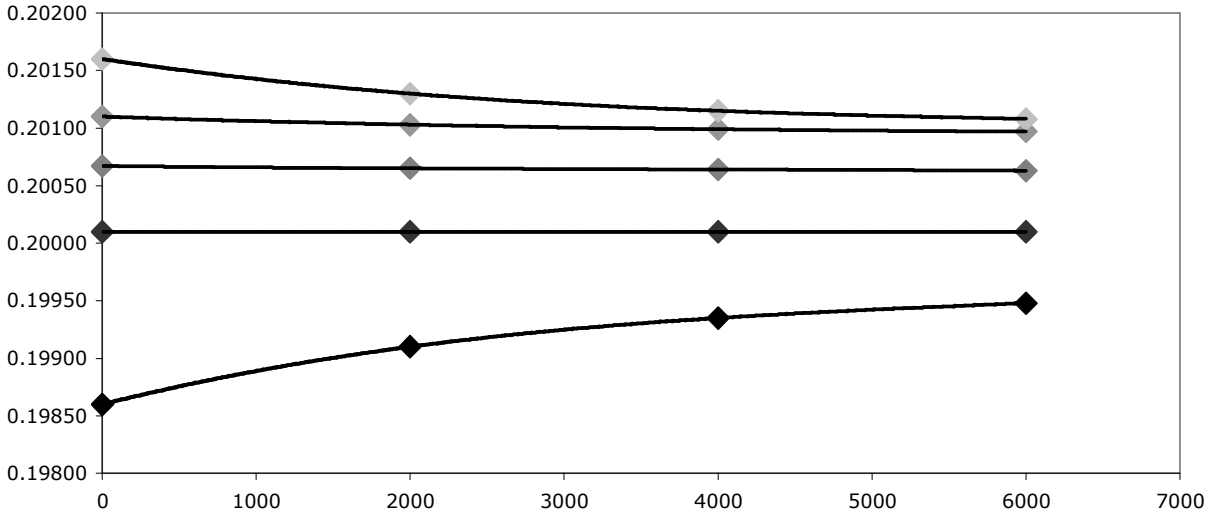

$xir(P,273) = 2.715301E\text{-}15P^3 - 4.758361E\text{-}11P^2 + 3.344732E\text{-}07P + 1.985997E\text{-}01$

$xir(P,298) = 2.001000E\text{-}01$

$xir(P,323) = -2.086287E\text{-}16P^3 + 2.503544E\text{-}12P^2 - 1.417966E\text{-}08P + 2.006700E\text{-}01$

$xir(P,348) = -2.092542E\text{-}16P^3 + 5.011051E\text{-}12P^2 - 4.420719E\text{-}08P + 2.011000E\text{-}01$

$xir(P,373) = -1.462486E\text{-}15P^3 + 2.754983E\text{-}11P^2 - 1.993494E\text{-}07P + 2.016002E\text{-}01$

Fig 3.1 – Plot of xr-OH vs P for 5 different temperatures showing the displayed equations. The lighter dots indicate higher temperature. Note that there is no variation in xr with P at a temperature of 298K and this is reflected in the equation also.

III) Plot the coefficients of xr-OH vs P as a function of temperature to obtain the final equation for $\xi_{r\text{-}OH}(T,P)$.

Thus, the variation of ξ_r with T and P for water is given by the following equation.

$$\xi_r^{OH}(T,P) = \sum_{m=0,n=0}^{m=5,n=3} A_{mn} \bullet T^m \bullet P^n \qquad 3.5$$

where the matrix A_{mn} has value as given table 3.2 :

Table 3.2a: The A-matrix of equation 12 columns A(:,0)-A(:,2)

0.655726502	-1.04442689×10^{-2}	8.31892416×10^{-5}
3.403472×10^{-4}	-3.986929×10^{-6}	1.742261×10^{-8}
-4.057853×10^{-8}	4.677537×10^{-10}	-2.007873×10^{-12}
1.657262×10^{-12}	-1.838785×10^{-14}	7.549619×10^{-17}

Table 3.2b: The A-matrix of equation 12 columns A(:,3)- A(:,6)

-3.07929142×10^{-7}	5.44770929×10^{-10}	$-3.73609493\times10^{-13}$
-3.364186×10^{-11}	2.419996×10^{-14}	0
3.800411×10^{-15}	-2.672717×10^{-18}	0
-1.355453×10^{-19}	8.939302×10^{-23}	0

The values obtained for q^d_H from the above equations were rounded off to the 5^{th} decimal place and the q's and q^d's for oxygen and silicon were calculated as multiples of q^d_H and are given in table 3.3. The fixed charge q for a species is exactly twice the negative of diffuse charge and the multiplying factor for different species is equal to the valence state of the species. The constant ratio was maintained so as to preserve the charge neutrality of the system. The dependance of q on temperature was chosen such that the charge decrease by less than 2% over the range of temperature where water is in liquid state at 1 atm pressure.

The value of ξ was fixed at 24A for all the pairs. As will be shown in section 3.4, this was partially based on the fact that the potential equations changed asymptotically with increasing ξ and beyond ξ=12Å the change in the potential and force curves and the properties of the system was negligible in the sphere of influence of radius 10Å.

Table 3.3 : Charges on different species at 298K. e is the electronic charge and is equal to 1.6×10^{-19} C.

	$q/e(=-2xq^d/e)$	q^d/e
H(v=1)	0.452	-0.113
O(v=-2)	-0.904	0.226
Si(v=4)	1.808	-0.452

The potentials and forces for the interacting species are plotted in figure 3.1(a) and (b). As can be seen, the presence of the dispersive C_6 term in O-O interactions results in a sharp fall in the O-O potential and force at low separation distances, but the barrier of the Oxygens to get so close as to become attractive is more than 20 times the equilibrium energy and it is unlikely that the oxygens will become repulsive at short distances.

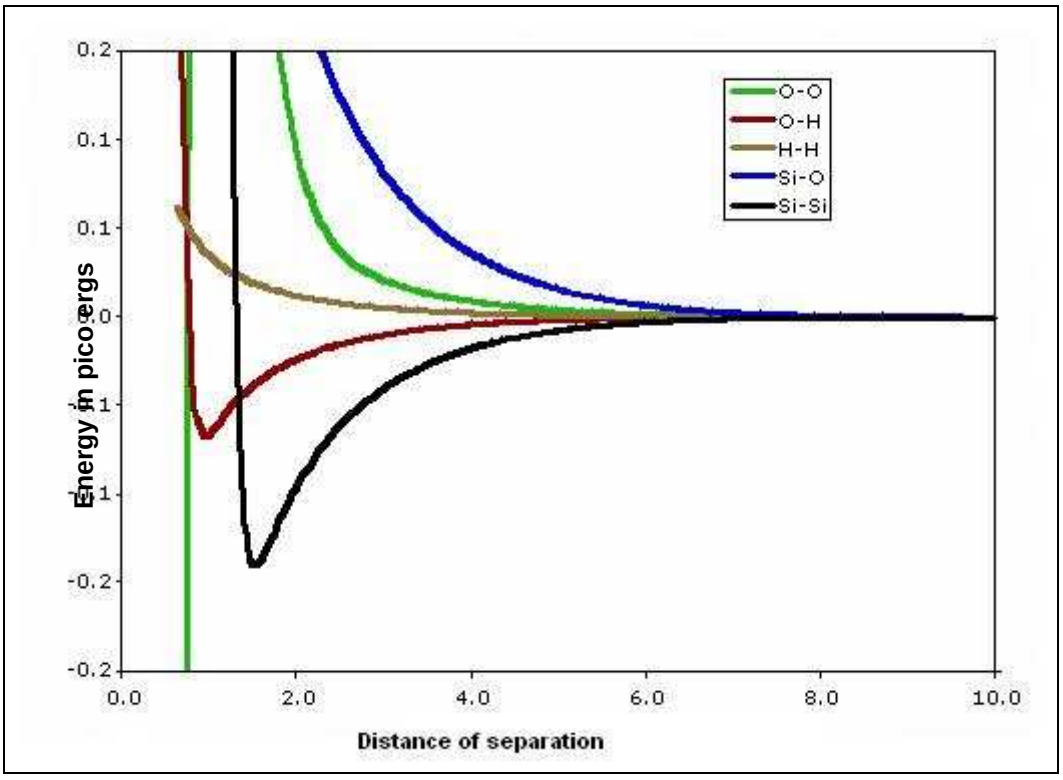

(a)

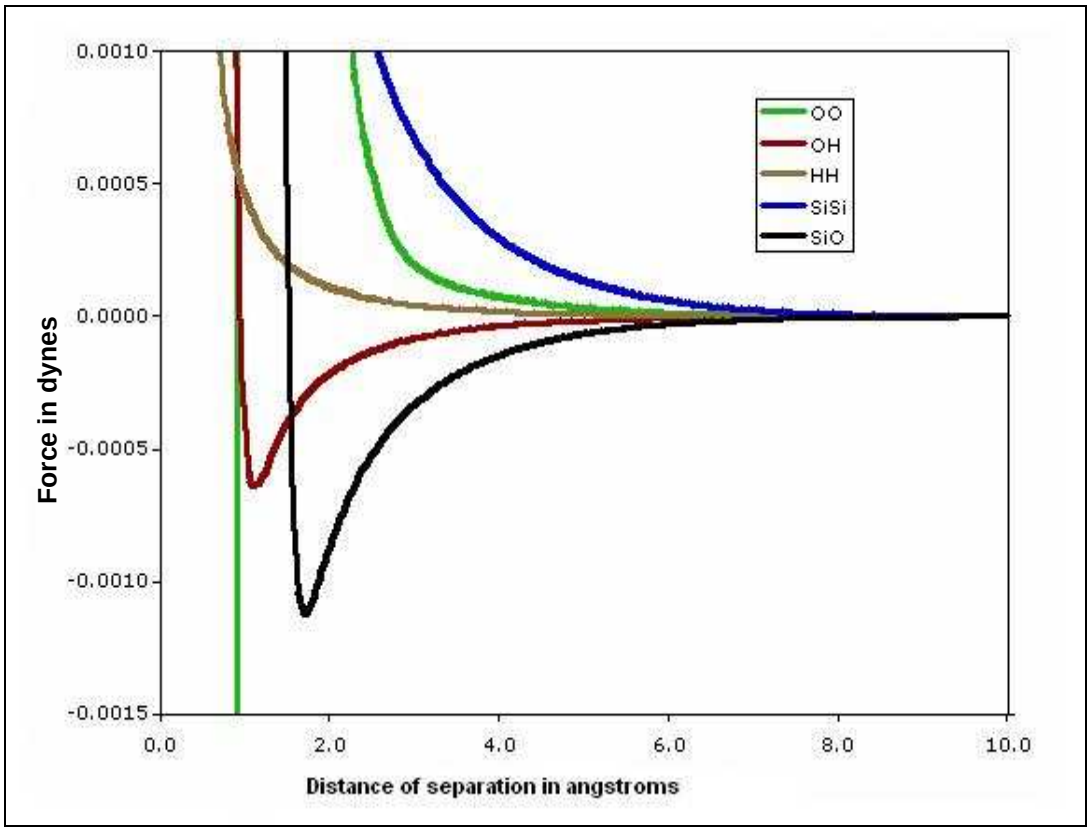

(b)

Fig 3.2 (a) and (b) showing the variation of interatomic potential and forces as a function of the distance of separation.

Note that all the potentials and forces approach zero at r->Rc (=10Å). This is because of the Wolf summation and the erfc term. This will be discussed in section 3.2.

Another feature that has been incorporated, but not used in the potential is the calculation of potential based on reduced radius at low separations. In this method, r is substituted by $(r^3+1/\gamma^3)^{(1/3)}$ thereby allowing the potential to taper off at short separations while remaining unaffected at higher distances. This is generally used in like species interactions and allows the species to get closer without increasing the pressure.

3.2 Long range electrostatic terms.

The electrostatic terms in the potential function are long range interactions and have non-zero values even at R_c. However, it will be computationally expensive and impractical to evaluate the electrostatic energy and forces by summing interactions over all the atoms. Hence, spherical truncation of the electrostatic terms after careful manipulation is required for evaluation of these forces and potentials.

3.2.1 Wolf summations

Thus, to evaluate the potential energy and calculate the forces, the method formulated by Wolf [53] was used which was a modification to the Ewald method of accounting for long range summations.

In the case of a simple fixed charge system, over each point charge, a Gaussian charge distribution with a half width of β , whose total charge density is equal to the point charge but of opposite sign of the point charge is superimposed. Another set of Gaussian charges with charges of opposite sign to the previously superimposed distributions is introduced for neutralizing the first component. Thus the total potential is split into two components as given by

$$U^1(r) = \sum_{i<j} \frac{q_i q_j}{r} - \frac{q_i q_j}{r}\operatorname{erf}(\frac{r}{\beta})$$
$$\Rightarrow U^1(r) = \sum_{i<j} \frac{q_i q_j}{r}\operatorname{erfc}(\frac{r}{\beta}) \qquad 3.6$$

and

$$U^2(r) = \sum \frac{q_i q_j}{r}\operatorname{erf}(\frac{r}{\beta}) \qquad 3.7$$

The total energy ($U^1(r) + U^2(r)$) is thus subdivided and the value of β is chosen such that there is a rapid convergence of $U^1(r)$ with increasing r. In Ewald summations, $U^2(r)$ is Fourier transformed and is evaluated as a reciprocal space component of the total energy. However, with a judicious choice of β, $U^2(r)$ becomes a small correction to U^1 and is equivalent to the self term given by :

$$U^{self} = \left(\frac{\mathrm{erfc}(R_c / \beta)}{2R_c} + \frac{1}{\beta\sqrt{\pi}} \right) \sum_{i=1}^{N} q_i^2 \qquad 3.8$$

where R_c is the radius of truncation.

Evidently, the self term is independent of the distance of separation and being a constant does not appear in the force equations.

In disordered systems, one also has to include the expression for charge neutralization (U^{neut}) which is the limit of 3.10 at r approaches R_c [53].

A similar analogy can be made for all the electrostatic terms in the potential equation described in eq. 3.2. Thus the final equation for the electrostatic terms to be used in the simulations is given by :

$$U^{net}(r_{ij}) = U^{tot}(r_{ij}) - U^{Neut} - U^{Self}, \qquad 3.9$$

where

$$U^{tot}(r_{ij}) = \left[\begin{array}{l} \frac{q_i q_j}{r} + \frac{q_i^d q_j}{r} \mathrm{erf}(\frac{r_{ij}}{\sqrt{2}\xi}) + \frac{q_i q_j^d}{r} \mathrm{erf}(\frac{r_{ij}}{\sqrt{2}\xi}) \\ + \frac{q_i^d q_j^d}{r} \mathrm{erf}(\frac{r_{ij}}{2\xi}) \end{array} \right] \times \mathrm{erfc}(\frac{r_{ij}}{\beta}) \qquad 3.10$$

and

$$U^{Neut} = \lim_{r_{ij} \to R_c} \left(U^{tot}(r_{ij}) \right) \qquad 3.11$$

The above equations, thus explain the handling of long range electrostatic interactions. It is to be noted that while the equations for force which are obtained by differentiating the above equations with respect to r_{ij} do not contain U^{self} , the neutralization term does appear to allow the forces to be zero at $r=R_c$.

The applicability of the above equations was validated Ma and Garofalini [54], and also by studying the stability induced by the above equations in water. The following plots of the average potential energy of a system of 648 stabilized water molecules indicate the stability of the potentials with equation 3.14. The stability of the potential energy when the Wolf correction is applied and the lack of stability when using equation 3.2 without long range electrostatic corrections is shown in figures 3.3. These energies were caculated for a system of 50Åx50Åx50Å of silica glass run for 50fs (50 MD moves).

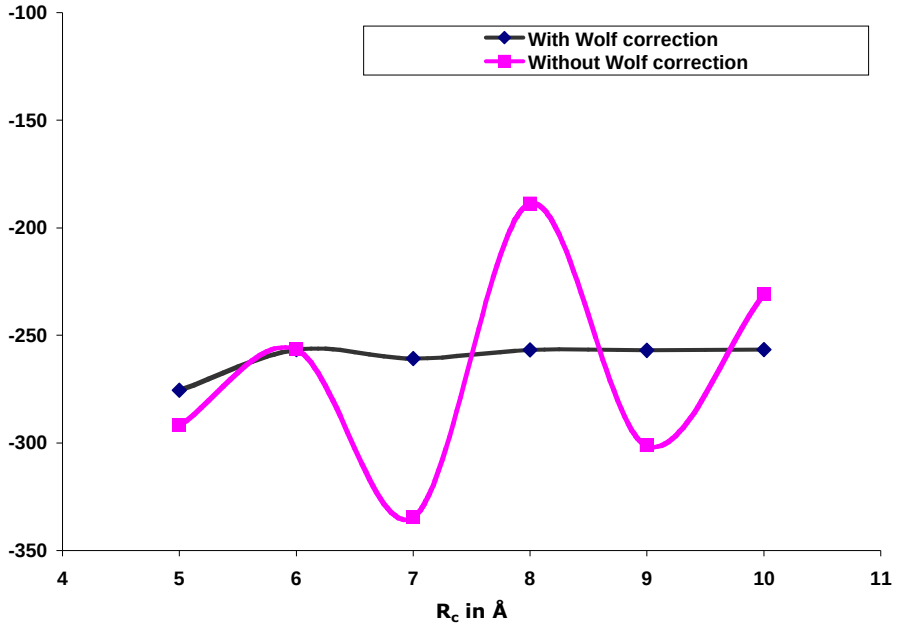

Fig 3.3 Show the change in potential energy of the system with time with different R_c's.

3.3 Charge calculation.

In general, charges on atoms are calculated based on the derivatives of the potential around the atoms, *i.e*., by considering the potential of an electron or other unit charges around a given atom. However, in the present work, the potentials are themselves based on the charges on the atoms and have not been defined for the case of a single electron. Hence, in the present case, the charges are determined according to the reaction between atoms of like species. Thus, consideration of Maxwell's equation on the integration of flux over an enclosed volume is used to define charges. Accordingly, to evaluate the charges on hydrogen, we take the instance of a central hydrogen atom and evaluate the charge due to the presence of another hydrogen at a distance r.

$$\oint \vec{\mathrm{E}} \cdot d\vec{\mathrm{A}} = \frac{q}{\varepsilon_0} \qquad 3.12$$

Where **E** is the electric field intensity through the area element *d***A** of a spherical enclosure (at a distance r from the charge being considered), ε_0 is the permittivity constant and q is the charge on either of the hydrogens. The electric field intensity itself is defined as the force per unit charge felt by the second hydrogen because of the central hydrogen and can be written as F/q. Thus,

$$\frac{1}{q}\oint \vec{\mathrm{F}} \cdot d\vec{\mathrm{A}} = \frac{q}{\varepsilon_0}. \qquad 3.13$$

The forces are in the radial direction and integration over the spherical volume gives us the the coulomb law expression:

$$\begin{aligned} \left|\vec{\mathrm{F}}\right| &= \frac{1}{4\pi\varepsilon_0}\frac{q^2}{r^2} \\ \Rightarrow q &= \sqrt{4\pi\varepsilon_0 r^2 \left|\vec{\mathrm{F}}\right|} \end{aligned} \qquad 3.14$$

The charges between two hydrogens evaluated by Eq.3.18 is plotted as a function of the separation in Fig 3.4. Charges can also be evaluated based on the potential energy as a function of distance and it would be equivalent to Eq. 3.14 only in the particular case where |F| = |U|/r. As can be seen from Eq.3.10, in the present case, the forces cannot be obtained from the potential by the above method and hence the charges calculated based on potentials and forces would be different from each other. In the present work, charges calculated based on the force equation is considered more authentic because, the atom positions and dynamics are determined by the forces and do not depend directly on the potential energies.

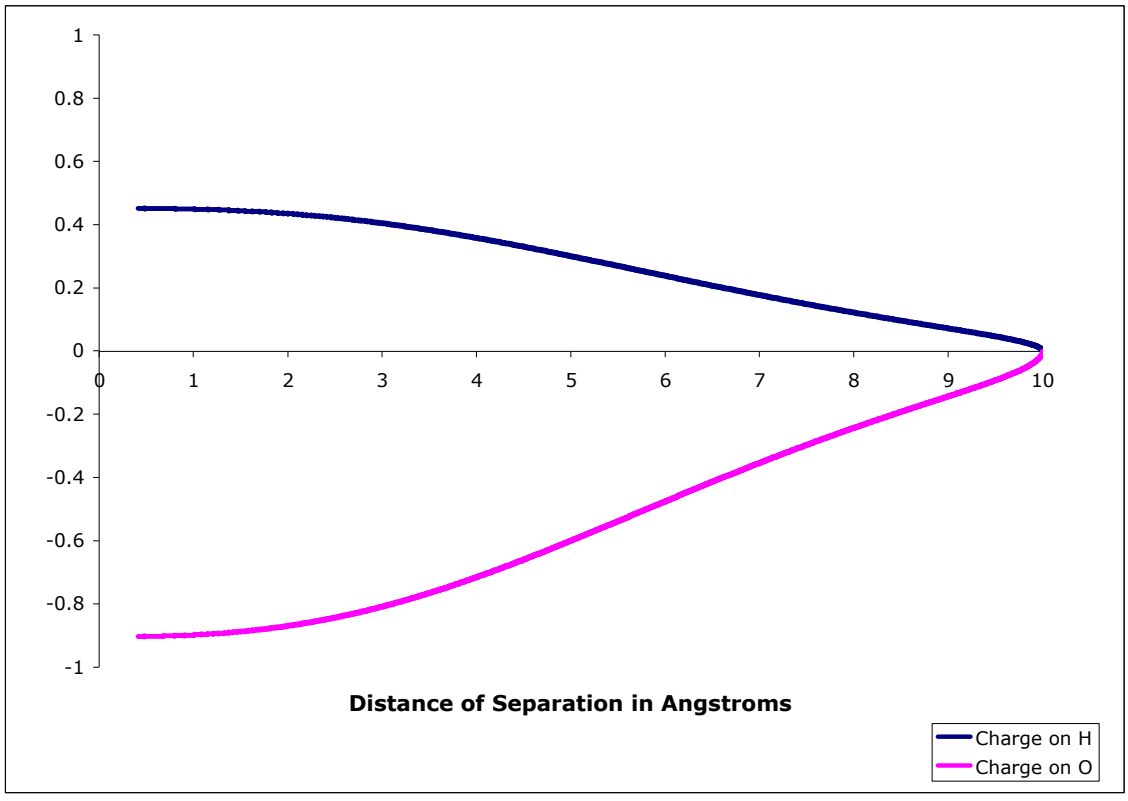

Fig 3.4 Charges as a function of distance of separation calculated according to equation 3.14. The oxygen charges are exact double and negative of the hydrogen charge and

charges on any other species are obtained based on valency of the species. As a further example charge on Si with a valency of +4 is 4 times the charge on Hydrogen.

The presence of a charge profile instead of a fixed point charge, is one of the important benefits of using the diffuse charge terms in conjunction with the Wolf term. Modeling of charge variation and charge transfer in molecular dynamics is usually done by setting up a separate set of equations not unlike the regular equations used for solving position and velocities but involving charges and fictitious charge masses. [51-53]. While these methods are effective in reproducing structure and properties , the extra set of equations for charge transfer calculations consume considerable computational time. This is even more so because in certain simulations involving charge transfer, the charge transfer equations are solved many more times for every step of positional equations to attain reasonable results[55]. Having charge profile with an effective pair potential results in the convenience of presenting charge transfers without consuming computational time because in such a situation case the charge transfer equations are coupled to the position/velocity equations and changes in intermolecular distances can be viewed as being caused by the change in charges.

The charges as seen in Fig. 3.4 are exactly zero at $r=R_c$. This is because of the use of the Wolf sum for long range electrostatic forces. As mentioned in section 3.2, Ewald summation technique is the other method of accounting for long range interactions. If the Ewald method is used, the reciprocal space term of the total potential energy is also summed up explicitly in calculation of the forces – i.e equation 3.7 is Fourier transformed to evaluate $U^2(k)$. The implication of using the Ewald sum in the charges is that the net charges do not go to zero and instead, they stabilize at a value of $q+q^d$. The curvature and

the start of descent of the charges from q is dependent on ξ in both Ewald summations and Wolf summations. However, in case of Wolf summation, the charge profile approaches the above figure asymptotically with increasing ξ and the above profile is closest to a value of ξ ~ 2.15 A when used with the Ewald sum. (Fig 3.4).

In using the Wolf summations, the effect of charge transfers have also to be viewed from the perspective that these equations imply a steady decrease in the effective charges with increasing intermolecular distance as explained above. This is however not a major concern in modeling of small molecules like water because a majority of the charge transfer occurs usually between first neighbors and within the molecule and the agreement between the Ewald and Wolf charge profiles is reasonable till the first intermolecular distance of 2.8A. (Fig 3.4)

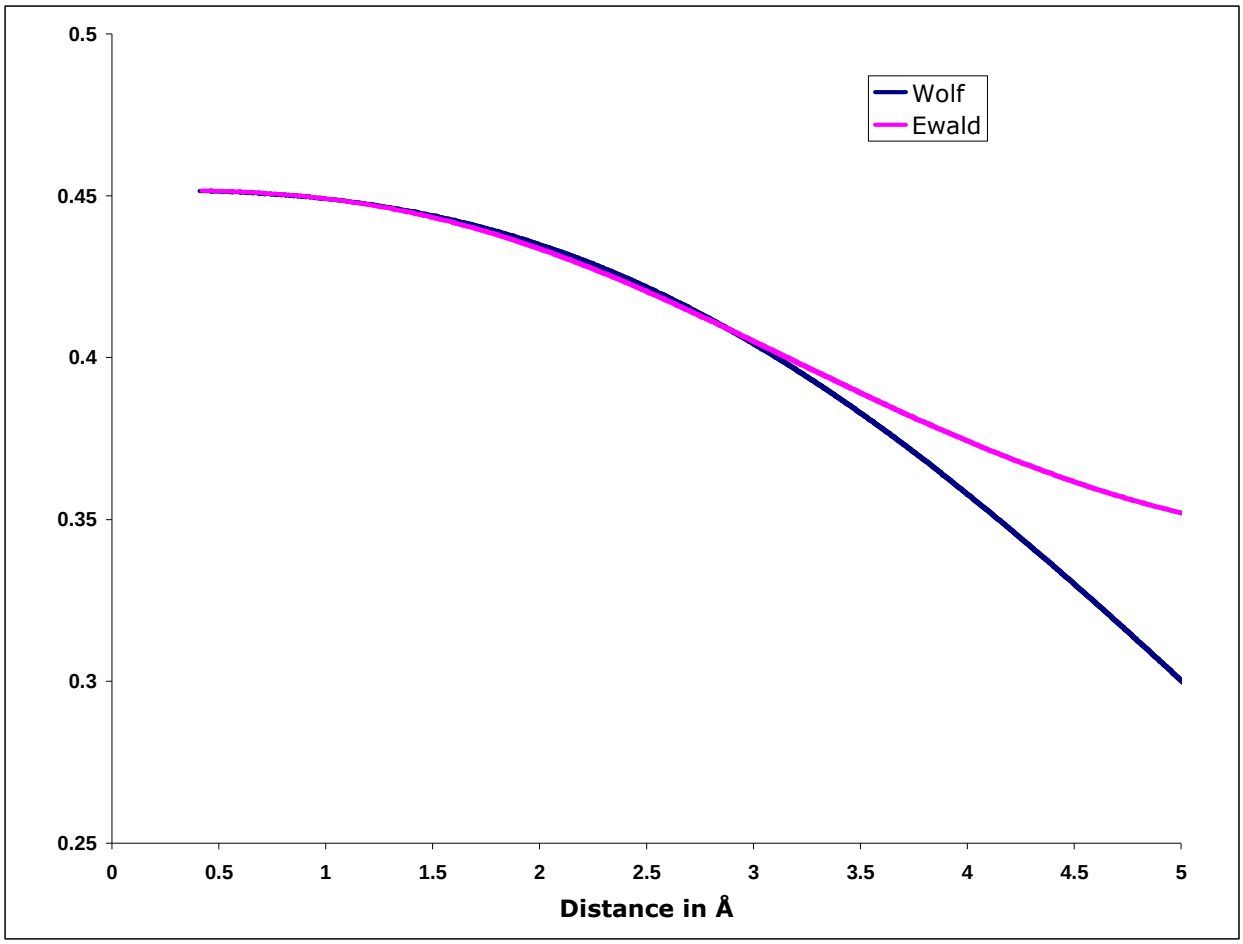

Fig 3.5 The charge as a function of separation distance – Comparision using Wolf sum and Ewald sum shows that the charges are close to each other till 3Å.

3.4 Three body potentials.

3.4.1 Need for three body terms

From the expression for the pair potential it is apparent that the force between two hydrogen atoms is always repulsive. While this may be acceptable in molecular structures with high level of tetrahedral symmetry like methane or silica, in case of water molecule it would result in the HOH angle settling close to 180^{o}. To prevent this, we introduce a three body potential.

The threebody potential used in the present is defined by [56]:

$$U_3(r_1,r_2,\theta)=\begin{cases}\lambda\exp\left\{\dfrac{\gamma}{r_1-r_c}+\dfrac{\gamma}{r_2-r_c}\right\}\times(\cos\theta-\cos\theta_c)^2 & \text{for } r_1,r_2 < r_c \\ 0 & \text{for } r_1,r_2 \geq r_c\end{cases}$$

3.19

where, r_1 and r_2 are the distance between the oxygen and the hydrogens 1 and 2 and θ is the HOH angle (Fig 3.6), θ_c is fixed angle parameter of "target angle" , rc is the range over which the three body forces act and λ and γ are parameters with units of energy and distance

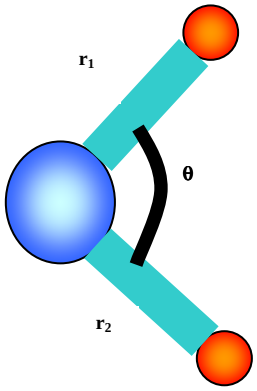

Fig 3.6 definitions of r_1,r_2 and θ.

This type of threebody forces have been successfully used to regulate angles in previous simulations of silica and other heterogenous systems by this group[38-40].

3.4.2 Action of three body forces.

The nature of the three-body potential is such that it increases the energy of the molecule with deviation of the subtended angle from the target value. The value of the energy parameter l is chosen to be such that the three body potential is a very small fraction of the total energy. The forces are calculated as a derivative of the above potential and are split into a radial component along the direction of r_1 and r_2 and a non

radial component that brings the 2 hydrogens closer. The change in the potential energy of the molecule as a function of the subtended angle is given in fig 3.7.

3.4.3 Modifications to the target angle.

The threebody forces act in addition to the already existing pair forces. The target angle defines the angle of minimum potential if only the threebody force were acting or if the pair potential was unchanging in the region of target angle. However, since the pair potential increases with the angle of minimum potential occurs at a value higher than θ_c

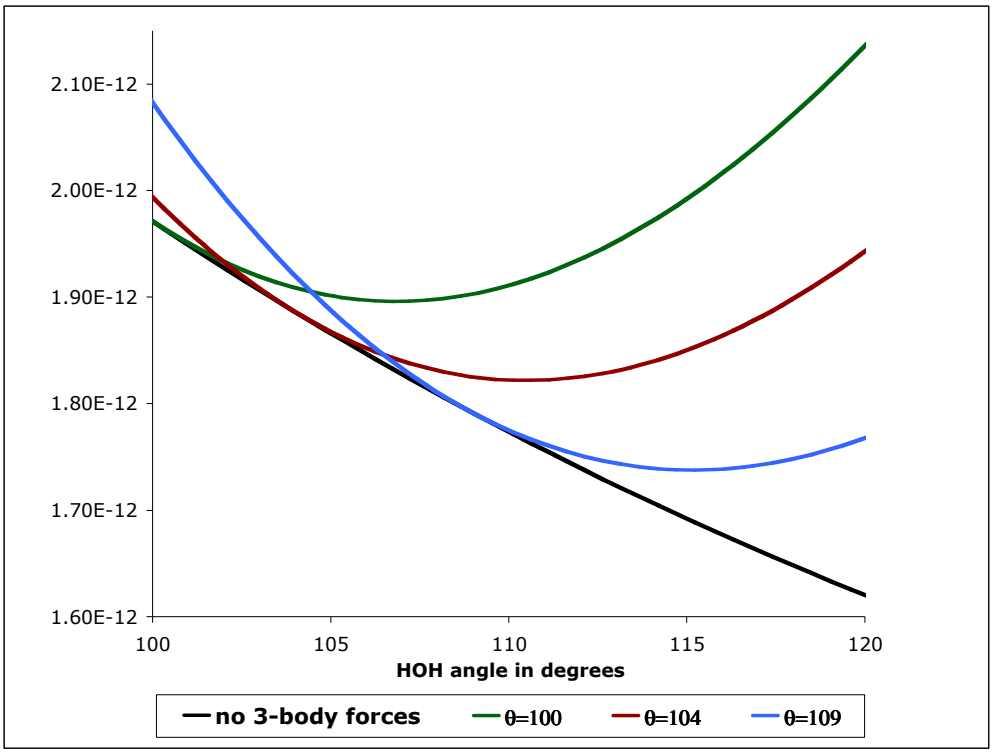

as can be seen in figure 3.7 Effect of changing target angle on the nature of the curves and the rationale behind

introducing different values for the target angle.

Thus, if the target angle is maintained at 104, which is the experimental value observed in water, the minimum of the net potential occurs at around 112^o. This effect

was pronounced in the case of single molecule where the HOH angle settled at 112^o with a target angle of 104^o. In the case of bulk water, ambient forces resulted in a lowering of the angle to 109^o with the same target. While most of the simulations use an angle of 109^o and while angle values of 104^o-109^o are acceptable for simulation results, 112^o was deemed unfit to be used for the molecule. Thus, a target angle of 100^o was chosen as the input parameter which allows the angle of minimum potential to be at 109^o and results in bulk water having an average angle of 104^o.

Fig 3.8 shows the effect of varying γ, and r_c on the H-H potential. Though decreasing γ or increasing r_c produces the effect of making the angle of minimum potential to be closer to the target value, using these parameters to produce the abovementioned effect results in the potential well being sharper which results in greater change in forces with slight change in H-H distances. This is an undesirable effect in that it heats the system and also results in greater deviation in the energy of the system after equilibriation.

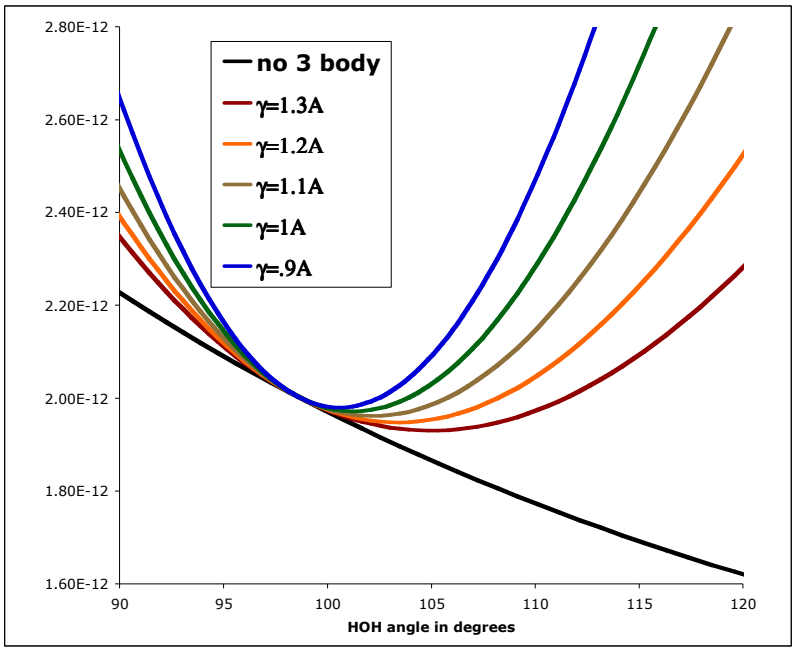

Fig 3.8 (a) (in previous page)

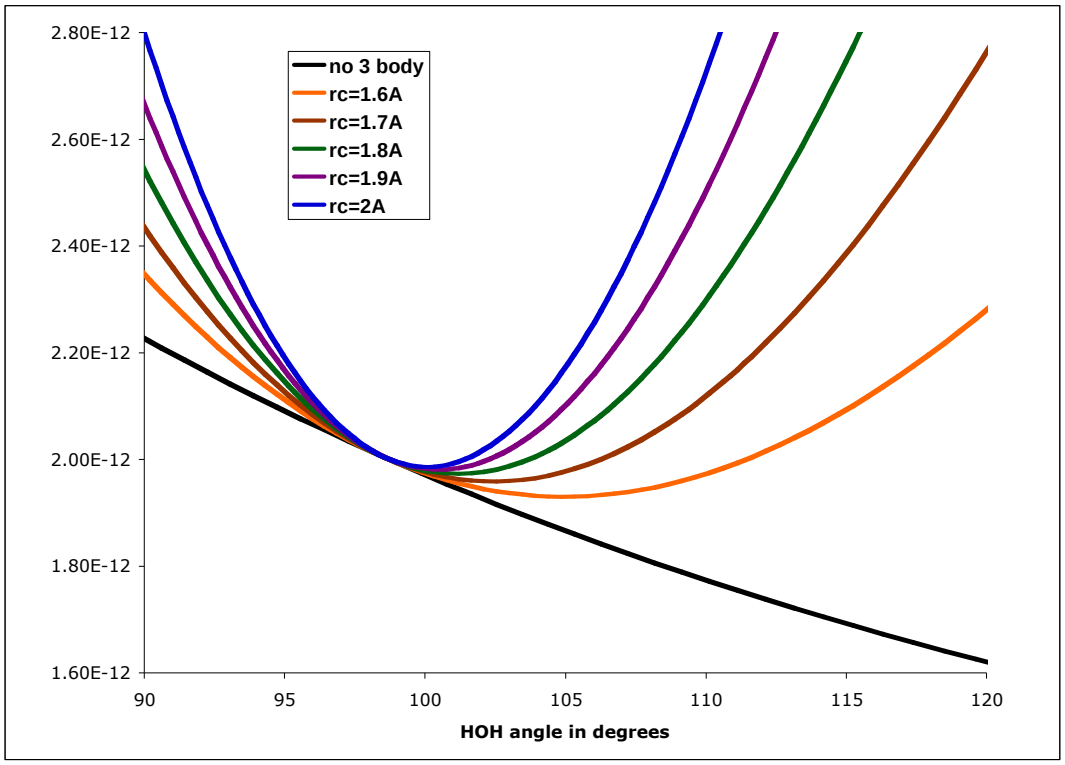

Fig 3.8(b)

Fig 3.8 a and b - Effect of γ and r_c on the HH potentials. The energies in figures 3.7 and 3.8 are compared relative to the HH pair potential without the 3body forces. The brown curve in fig 3.8(a) and orange curve in 3.8 (b) are the curves used in the simulation and the rest of the curves are for demonstrating the effect of varying the 3 body parameters. Similar plot can also be made for energy variation as a function of H-H distance however, plotting the threebody potential as a function of the angle gives a better perspective. The OH distances were kept at a constant value of 0.97A for all cases.

3.5 Change in molecular structure with modification of parameters .

In the present work, as detailed above, the $\xi_{r\text{-}OH}$some parameter of the water potential was modified and made to vary depending on ambient conditions. These

modifications lead to changes in the structure of the water molecule. A correlation between the changes in the molecule and the parameters needs to understood before the effect can be utilized to get appropriate properties for bulk water. The most important parameter change that was affected was changing the value of $\xi_{r\text{-}OH}$ in water with temperature and pressure as given in equations 3.5 to 3.8. The change in the structure of water molecule due to this parameter change can be understood based on fig.3.8 where the pair equilibrium OH distance, which is the distance at which the pair forces between oxygen and hydrogen equals zero, has been plotted as a function of $\xi_{r\text{-}OH}$. The actual OH distance depends not only on this theoretical value but also on the three body forces and the HH repulsions.

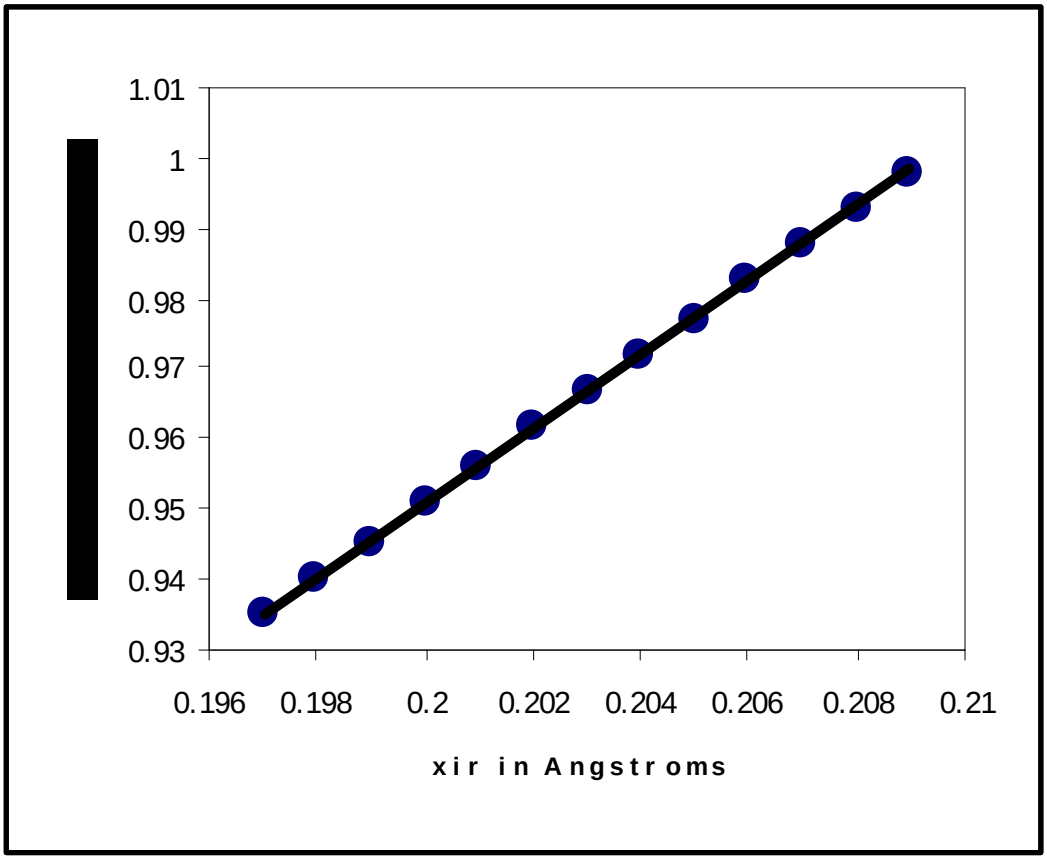

Fig 3.9 : Plot of variation of theoretical OH distance based on pair forces with change in the potential parameter ξ_r. These distances were calculated by plotting out the OH forces for different values of parameters ξ_r and interpolating the forces to zero.

While experimental value for the OH distance in the single water molecule is around 0.948A and about 0.967A for bulk water, changing the value of ξr allows us to adjust this distance in the simulation from 0.94A to around 1A. The effect of changing the OH distance manifests as change in the local structure and since the density of bulk water is dependant on the local short range structure, a corresponding change in the bulk density of water is also expected.

More details about the correlation between the bulk density / structure and the ξr parameter will be demonstrated in a later chapter.

4. SUMMARY OF APPENDED MANUSCRIPTS

This chapter contains the summaries of the appended manuscripts. The first manuscript is already published in journal of physical chemistry and this contains all the results pertaining to using the potential for developing water. It also contains the results that we obtained in the simulations of water and some details of how the potential was trained to simulate the properties of water. The second paper contains results of how the water model was used to study the interaction between silica surface and water vapor. Some of the observed mechanisms are also presented as results in this paper. The third paper contains the results of structural and diffusional properties of water confined between two slabs of silica separated by ~3nm.

4.1 Manuscript I: "Dissociative Water Potential for Molecular Dynamics Simulations"

In this publication we discuss the development of the potential and its application in building the model of water. The results presented show the structure, vibrational spectrum, diffusion coefficients, coefficient of thermal expansion of the simulated water are very close to experimental results for water. An important reason for the coefficient of thermal expansion being accurate is that the parameter $\xi_{r\text{-}OH}$ is varied as a function of temperature and pressure. As is indicated in the paper, a strong correlation between $\xi_{r\text{-}OH}$ and the structure and OH distance is observed as indicated in fig 4.1(a) and (b). However, even though the OH distance is increases, the dimmer distance is observed to reduce as indicated in fig 4.2. Thus, although the $\xi_{r\text{-}OH}$ parameter decreases the density of the single molecule by making it larger, the overall effect is one of increasing the density of bulk water by bringing the water molecules closer. Accordingly, when the OH distance is

increased with temperature, the net effect is that the density of bulk water does not fall as rapidly as it would with a constant OH distance.

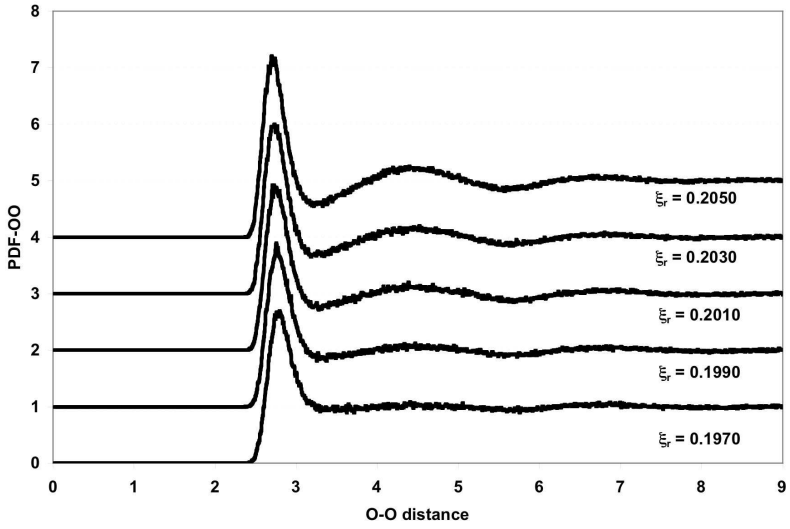

Fig 4.1(a) – Variation in the structure of water as a function of the $\xi_{r\text{-}OH}$ parameter as indicated by the O-O pair distribution function.

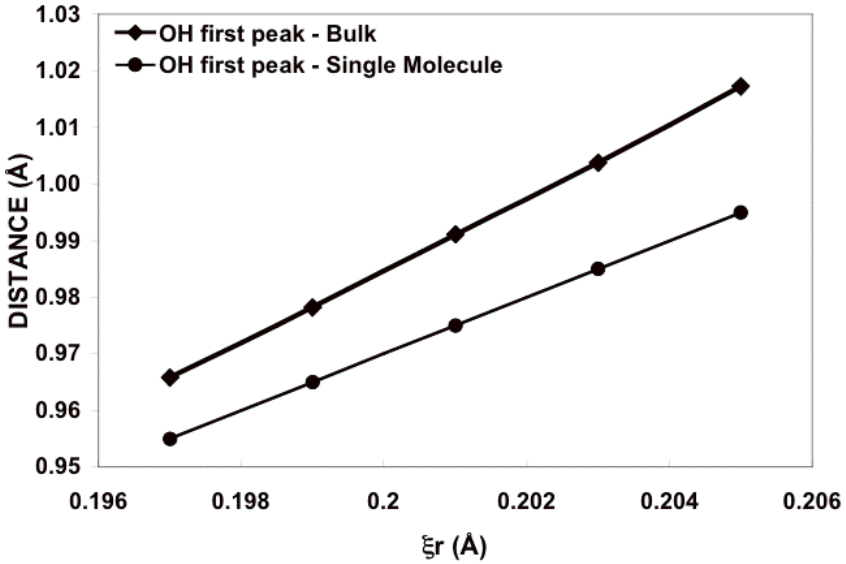

Fig 4.1(b) – Variation in the OH distance of the $\xi_{r\text{-}OH}$ parameter

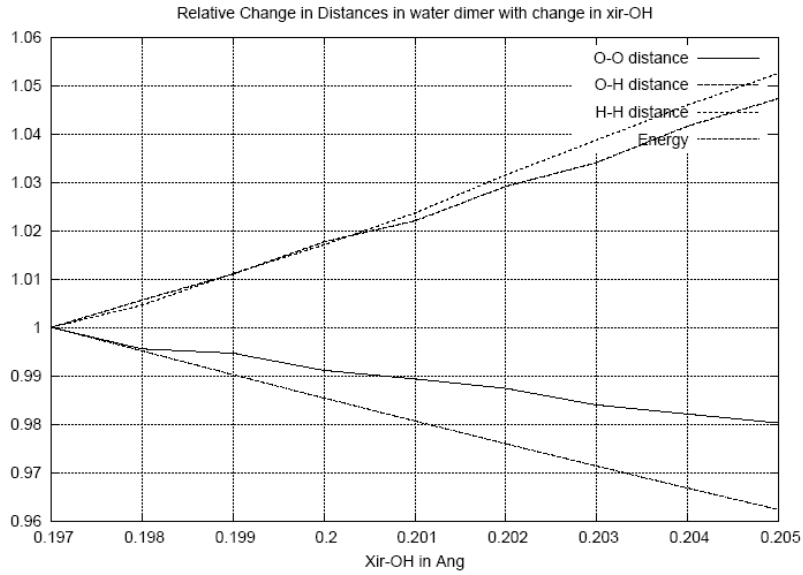

Fig 4.2 – Relative variation in distances between different species and the energy as a function of
the $\xi_{r\text{-}OH}$ parameter. All the distances and energies are normalized w.r.t to their values at ξ_{rOH}=0.1970Å.

The reproduction of the coefficient of thermal expansion is an important feature of this model as not many of the other models of water have reproduced the CTE to this level of accuracy. The variation of the density at the given temperature from experimental values is a maximum of 0.2% in the current model.

This paper also demonstrates the ability of this water to dissociate in the presence of a hydronium. Normal bulk water was not observed to dissociate and hence hydronium ion was introduced by placing an extra hydrogen atom close to a central water molecule in a cube. The complexes that were formed due to the presence of the hydronium was presented through snapshots of the graphics and the mechanisms of hydronium transfer were also investigated based on the distance between species during the transfer of the extra hydrogen.

4.2 Manuscript II: "Molecular Dynamics Simulation of Water Adsoprtion onto Silica Surfaces Using a Dissociative Water Potential"

This manuscript, gives the results of the study of interaction between water vapor and silica surface thus validating the use of the potential for studying silica-water interaction. Some of the observed mechanisms of silanol formation have been reported in this manuscript and density profiles as a function of distance perpendicular to the surface indicate penetration of molecular water upto 8Å below the surface besides the formation of sub-surface silanols.

Formation of hydronium was also observed at the surface of the glass and some of the mechanisms of the role played by the hydroniums in the formation of silanols and in the transport of protons at the surface is also shown graphically in this manuscript. The onset of diffusion of water molecules into open channels in the glass surface was also seen and is shown as a series of snapshots.

It was also observed that the adsorption of water at the surface led to saturation of the dangling surface oxygens by formation of silanols and the saturation of under coordinated silicons at the surface again by the formation of silanols. Adsorbed water molecules were also observed at the surface but these were few in number as can be seen in the concentration profile of various species. A co-relation between the number of remaining water molecules and the number of silanols was observed and is shown graphically in the manuscript.

Many of these mechanisms of silanol formation in the presence of surface water has been observed through ab-initio studies and QM calculations and that a model based

on simple pair potentials can reproduce these mechanisms indicate the effectiveness of the model in studying these interactions.

4.3 Manuscript III: "Water confined in Silica Nano layers: A Molecular Dynamics Study"

This paper details the structural changes in confined water. The computational set up in this case was to insert a 6.4nm x 6.4nm x 3.2nm slab of water between two slabs of vitreous silica. This set up was simulated at seven different temperatures for about 10ps each. The density profiles of the water was observed to indicated penetration of water into the silica slabs upto about 1nm deep. The difference between the structure of water in the interior of the 3nm film and at the interface clearly indicates that the water at the interior is closer to bulk water and the interfacial and penetrated water have a structure that is closer to high pressure water in the first neighbor level and closer to high temperature water beyond 4.5Å which indicates the formation of high density clusters under confinement. The structural changes in confined water are consistent with experimentally observed shoulder formation in the O-O pair distribution function. The diffusion coefficient of the confined water is also orders of magnitude lower than that of bulk water, which has also been observed experimentally.

As a consequence of the changes in structure, we were also able to observe a higher expansion coefficient of the confined water as given in fig. 4.4. The volume changes of glass was much less as can be seen in the graph and thus bears no contribution to the higher expansion of water. This higher expansion behavior has also been observed in experiments of water in confined geometries. Thus, the current model for analysis has

consistently produced results comparable to experiment and has been used to explain the structure and phase behavior of confined water.

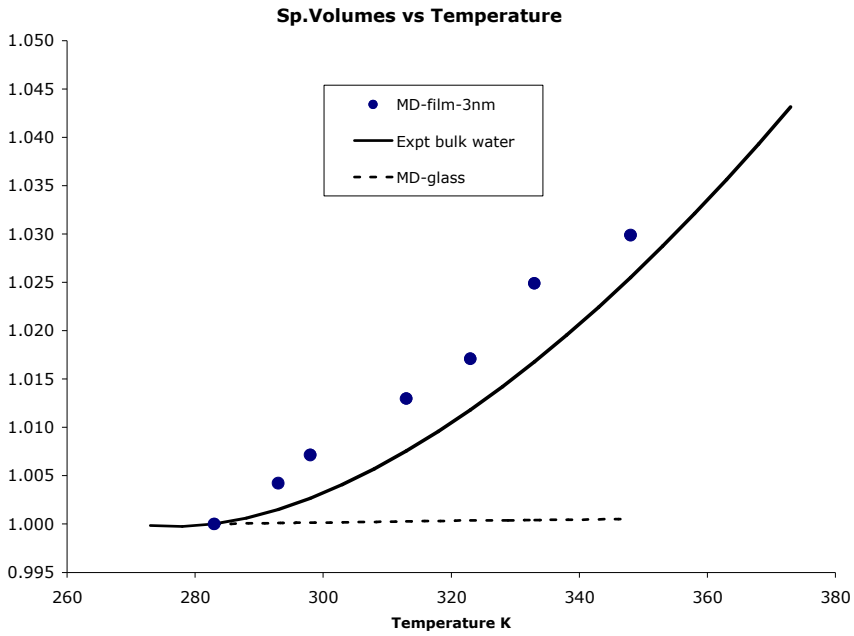

Figure 4.4 : Plot of the specific volume of confined water as a function of as compared to that of bulk water. The expansion of the confining glass is also indicated by the dotted line, showing that the volume expansion of glass is very low compared to that of water and it can thus have no contribution to the overall change in volume.

5. SUGGESTIONS FOR FUTURE RESEARCH

In this current thesis, molecular dynamic simulation methods were used to develop a model for dissociable water that could accurately reproduce the experimental physical quantities over a wide range of temperatures and pressures and this model was used to study the interaction between vitreous silica and water vapor and subsequently was also used to study the changes in structure of water when confined by nano slabs of vitreous silica. Based on the results there are two primary directions that future research can take.

The first would be to improve the potential function to include parameters for many other species like alkalis and alkaline earth materials. The modus operandi for obtaining parameters for other species would be try and replicate the structure and vibrational spectrum of the oxides of the species. As explained in the section on potential, the A_{rep} and ξ_r parameters can be used to fix the first neighbor distance and also the primary stretch mode (which is determined by the slope of F vs r Curve at the interaction distance. As an extension of the methods in developing parameters for different species, further refinement of the potential can be done by changing the ξ to simulate heterogenous structures with same materials. For example, in the current simulations, changing the the ξ value in silica would have produced different methods of interaction between water oxygen and silica oxygen. Such methods can be especially useful in simulating interaction between ionic and covalent materials where ξ can be varied as a function of the interacting neighbors. While using different ξ values would have resulted in many interesting interactions, it would also entail longer computational times because of the treatment of species of different ξ as a separate species. However, with the advent

of faster processors and computational times, these difficulties can be easily circumvented.

Another direction for future research would be to explore the effect of the geometry of the confining environment and on the structure and dynamics of water as well as studying the interaction. Studies in this direction do exist in literature, however none of these studies use a dissociable model for water and hence, using the above model would provide fruitful insights in understanding the behavior of water under confinement.

Needless to express, a combining both the above research prospects would also fetch interesting results and can find application in the fields of transport and diffusion behavior of ions in aqueous confined media and across media of different ionic nature, precipitation of minerals in biological media and simulation of metals and organic materials.

BIBLIOGRAPHY AND REFERENCES

1. Trickey, S.B., et al., *A perspective on multi-scale simulation: Toward understand water-silica.* J. Comp-Aided Mater. Design, 2006. **13**: p. 1-12.
2. Franks, F., *Introduction - Water, the unique chemical*, in *Water- A comprehensive treatise*, F. Franks, Editor. 1972, Plenum Press.
3. Guillot, B., *A reappraisal of what we have learnt during three decades of computer simulations on water*. Journal of Molecular Liquids, 2002. **101**: p. 219-260.
4. Chaplin, M. *Water Structure and Science*. 2007 [cited; Available from: http://www/lsbu.ac.uk/water.
5. Head-Gordon, T. and G. Hura, *Water Structure from scattering experiments and simulation.* Chemical Review, 2002. **102**: p. 2651-2670.
6. Narten, A.H. and H.A. Levy, *Liquid water: Scattering of x-rays*, in *Water: A comprehensive treatise Volume I*, F. Franks, Editor. 1972, Plenum press. p. 311-331.
7. *International Association for the properties of water and steam (IAPWS).* 2007 [cited; Available from: http://www/iapws.org.
8. Kell, G.S., *Thermodynamic and Transport Properties of Fluid Water*, in *Water-A comprehensive treatise*, F. Franks, Editor. 1972, Plenum press: New York.
9. Guillot, B. and Y. Guissani, *How to build a better pair potential for water*. J. Chem. Phys., 2001. **114**: p. 6720-6733.
10. Paul, A., *Chemistry of glasses*. 1982: Chapman and Hall.
11. Goldschmidt, V.M., *Skrifter Norske Videnskaps Akad.* I.Math-Naturwiss.K1 8: p. 7.
12. Zacharaisen, W.H., *The atomic arrangement in glass.* J. Am. Chem. Soc., 1932. **54**: p. 3841-3851.
13. Smekal, A., J. Soc. Glass. Tech, 1951. **35**.
14. Sun, K.H., *Fundamental Condition of Glass Formation.* J. Amer. Ceram. Soc., 1947. **30**(9): p. 277-281.
15. Keen, D.A. and M.T. Dove, *Local structures of amorphous and crystalline phases of silica SiO_2, by neutron total scattering.* Journal of Physics: Condensed Matter, 1999. **11**: p. 9263-9273.
16. Holloway, D.G., *The physical properties of glass*. 1973: Wykeham Publications.
17. Vashishta, P., et al., *Interaction potential for SiO2: A molecular-dynamics study of structural correlations.* Phys. Rev. B, 1990. **41**: p. 12197-12209.
18. Sen, P.N. and M.F. Thorpe, *Phonons in AX2 glasses: From molecular to band-like modes.* Phys. Rev. B, 1977. **15**: p. 4030-4038.
19. Bell, R.J. and P. Dean, *Properties of Vitreous Silica: Analysis of Random Network Models.* Nature, 1966. **212**: p. 1354-1356.
20. Garofalini, S.H., *Physical properties of silica*. 2002.
21. Geissberger, A.E. and F.L. Galeener, *Raman studies of vitreous SiO2 versus fictive temperature.* Phys. Rev. B, 1983. **28**(6): p. 3266-3271.
22. Klein, J., et al., *Fluidity of water and of hydrated ions confined between solid surfaces to molecularly thin films.* Journal of Physics: Condensed Matter, 2004. **16**: p. S5437-S5448.

23. Bhattacharya, K. and B. Bagchi, *Slow dynamics of constrained water in complex geometries.* Journal of Physical Chemistry A, 2000. **104**: p. 10603-10613.
24. Webber, B. and J. Dore, *Structural and dynamic studies of water in mesoporous silicas using neutron scattering and nuclear magnetic resonance.* Journal of Physics: Condensed Matter, 2004. **16**: p. S5449-S5470.
25. Brovchenko, I., A. Geiger, and A. Oleinikova, *Water in nanopores: II. The liquid-vapour phase transition near hydrophobic surfaces.* Journal of Physics: Condensed Matter, 2004. **16**: p. S5345-S5370.
26. Jedlovszky, P., *The hydrogen bonding structure of water in the vicinity of apolar interfaces: a computer simulation study.* Journal of Physics: Condensed Matter, 2004. **16**: p. S5389-S5402.
27. Zangi, R., *Water confined to a slab geometry: a review of recent computer simulation studies.* Journal of Physics: Condensed Matter, 2004. **16**: p. S5371-S5388.
28. Crupi, V., D. Majolino, and V. Venuti, *Diffusional and vibrational dynamics of water in NaA zeolites by neutron and Fourier transformed infrared spectroscopy.* Journal of Physics: Condensed Matter, 2004. **16**: p. S5316-S5297.
29. Liu, L., et al., *Slow dynamics of supercooled water confined in nanoporous silica materials.* Journal of Physics: Condensed Matter, 2004. **16**: p. S5403-S5436.
30. Bruni, F., M.A. Ricci, and A.K. Soper, *Water confined in Vycor™ glas. I A neutron diffraction study.* J. Chem. Phys., 1998. **109**(4): p. 1478-1485.
31. Soper, A.K., *Water condined in Vyor glass. II Excluded volume effects on the radial distribution functions.* J. Chem. Phys., 1998. **109**(4): p. 1486-1494.
32. Hiejima, Y. and M. Yao, *Phase behaviour of water confined in Vycor™ glass at high temperatures and pressures.* J. Phys.: Cond. mat., 2004. **16**: p. 7903-7908.
33. Christenson, H.K., *Confinement efects on freezing and melting.* J. Phys.: Cond. mat., 2001. **13**: p. R95-R133.
34. Gallo, P., M.A. Ricci, and M. Rovere, *Layer analysis of the structure of water confined in Vycor™ glass.* J. Chem. Phys., 2002. **116**(1): p. 342-346.
35. Ricci, M.A., et al., *Water in confined geometries: experiments and simulations.* J. Phys.: Cond. mat., 2000. **12**: p. A345-A350.
36. Lee, S.H. and P.J. Rossky, *A comparison of the structure and dynamics of liquid water at hydrophobic and hydrophilic surfaces - a molecular dynamics study.* J. Chem. Phys., 1994. **100**: p. 3334-3345.
37. Puibasset, J. and R.J.M. Pellenq, *A comparision of water adsorption on ordered and disordered silica substrates.* Phys. Chem. Chem. Phys., 2004. **6**: p. 1933-1937.
38. Litton, D.A. and S.H. Garofalini, *Modeling of hydrophilic wafer bonding by molecular dynamics simulations.* J. Appl. Phys., 2001. **89**: p. 6013-6023.
39. Feuston, B.F. and S.H. Garofalini, *Oligomerization in Silica Sols.* J. Phys. Chem., 1990. **94**(13): p. 5351-5356.
40. Martin, G. and S.H. Garofalini, *Sol-Gel Polymerization: Analysis of Molecular Mechanisms and the Effect of Hydrogen.* J. Non-Cryst. Sol., 1994. **171**: p. 68-79.
41. Allen, M.P. and D.J. Tildesley, *Computer Simulation of Liquids*. 1st Edition ed. 1987, New York: Oxford University Press. 384.

42. Pang, T., *An introduction to computational physics*. 1997: Cambridge university press.
43. Meyer, M. and V. Pontikis, *Computer simulation in materials science*. NATO ASI Series: E Applied Sciences. Vol. 205. 1991: Kluwer Academic publishers.
44. Woodcock, L.V., *Molecular dynamics calculations on molten ionic salts*, in *Advances in molten salt chemistry*. 1975, Plenum press.
45. Levine, S.M., *Silicate structure, relaxation and metal particle interactions using molecular dynamics computer simulations.*, in *Ceramics Science and Engineering*. 1990, Rutgers University: Piscataway. p. 190.
46. Tsai, D.H., *The virial theorem and stress calculation in molecular dynamics.* J. Chem. Phys., 1979. **70**(3): p. 1375-1382.
47. Anderson, H.C., *Molecular dynamics simulations at constant pressure and/or temperature.* J. Chem. Phys., 1980. **72**(4): p. 2384-2393.
48. Hunenberger, P.H., *Calculation of group based pressures in molecular simulations. !. A general formulation including Ewald and particle particle particle mesh electrostatics.* J. Chem. Phys., 2002. **116**(16): p. 6880-6897.
49. Garofalini, S.H., *Molecular dynamics simulation of the frequency spectrum of amouphous silica.* J. Chem. Phys., 1982. **76**(6): p. 3189-3192.
50. Lebowitz, J.L., *Modified virial theorem for total momentum fluctuations.* Phys. Rev., 1958. **109**(5): p. 1464-1465.
51. Rick, S.W., S.J. Stuart, and B.J. Berne, *Dynamical Fluctuating Charge Force Fields: Application to Liquid Water.* J. Chem. Phys., 1994. **101**: p. 6141-6156.
52. Mortier, W.J., S.K. Ghosh, and S. Shankar, *Electronegativity Equalization Method for the Calculation of Atomic Charges in Molecules.* J. Am. Chem. Soc., 1986. **108**: p. 4315-4320.
53. Wolf, D., et al., *Exact method for the simulation of coulombic systems by spherically truncated, pairwise r-1 summation.* J. Chem. Phys., 1999. **110**: p. 8254-8282.
54. Ma, Y. and S.H. Garofalini, *Modified Wolf Electrostatic Summation: Incorporating an Empirical Charge Overlap.* Molec. Sim., 2005. **31**: p. 739-748.
55. Ma, Y. and S.H. Garofalini, *Iterative fluctuation charge model: a new variable charge molecular dynamics method.* J. Chem. Phys., 2006. **124**: p. 234102-1-7.
56. Feuston, B.P. and S.H. Garofalini, *Empirical Three-Body Potential for Vitreous Silica.* J. Chem. Phys., 1988. **89**(9): p. 5818-5824.

MANUSCRIPT I : “Dissociative Water Potential for Molecular Dynamics Simulations”, T.S.Mahadevan and S.H.Garofalini, J.Phys. Chem. B **111**(30) 8919-8927 (2007).

Dissociative water potential for molecular dynamics simulations

T. S. Mahadevan and S. H. Garofalini

Interfacial Molecular Science Laboratory

Department of Materials Science and Engineering

Rutgers University

Piscataway, NJ, 08855

Abstract :

A new interatomic potential for dissociative water was developed for use in molecular dynamics simulations. The simulations use a multi-body potential, with both pair and three body terms, and the Wolf summation method for the long range Coulomb interactions. A major feature in the potential is the change in the short-range O-H repulsive interaction as a function of temperature and/or pressure in order to reproduce the density-temperature curve between 273K and 373K at 1 atm, as well as high pressure data at various temperatures. Using only the change in this one parameter, the simulations also reproduce room temperature properties of water, such as structure, cohesive energy, diffusion constant, and vibrational spectrum, as well as the liquid-vapor coexistence curve. Although the water molecules could dissociate, no dissociation is observed at room temperature. However, behavior of the hydronium ion was studied by introduction of an extra H^+ into a cluster of water molecules. Both Eigen and Zundel configurations, as well as more complex configurations, are observed in the migration of the hydronium.

Introduction :

Simulation and understanding of water has been an ongoing issue for over three decades and its importance cannot be overstated. While many water potentials exist[1-18], most are non-dissociating, being either rigid, or at most flexible. Because of the large number of papers regarding simulations of water, the reader is referred to a couple of excellent reviews currently available[19,20]. In general, the properties of water can be expressed fairly accurately over a narrow range of temperatures and pressures. One major problem has been the failure of these potentials to reproduce the density versus temperature curve over the liquid state range from 273K to 373K[13]. Even in cases where the temperature of maximum density is well reproduced, the potentials often fail at reproducing the rest of the density-temperature curve[18]. Since our major interest is in the behavior of water interacting with silica and silica pores and the atomistic evaluation of the anomalous expansion of confined water, the exact reproduction of the bulk liquid expansion becomes paramount. A new non-dissociative water potential recently developed reproduces the molecular state, liquid water, and the liquid-vapor co-existence curve extremely well[21]. However, we also want to include the dissociation of water onto the silica surface, similar to earlier simulations of water on silica[22], but with a more accurate water potential. Other dissociative water potentials exist, but are similarly not sufficiently accurate with respect to the liquid equation of state[10,23]. To obtain a more appropriate water potential, we modified the rigid water potential developed by Guillot and Guissani (GG) [15] so that it more accurately reproduced the features of bulk water, but also allowed for dissociation.

Dissociation also allows for the study of the hydronium ion, although the quantum nature of the proton makes a classical approach only approximate. The hydronium ion has been

previously modeled classically[24], with reasonable results. Two important structural models for the hydronium ion in water are the Zundel [25] complex, $H_5O_2^+$, with the H_3O^+ ion H-bonded to a normal H_2O molecule, and the Eigen [26] complex, $H_9O_4^+$, with the H_3O^+ ion H-bonded to 3 water molecules. Recent ab-initio path integral simulations showed that these two structure are limiting cases of more complex behavior[27].

We first describe the details of the potential function and modifications that were required, followed by the properties of the simulated water.

Computational Procedure:

The new dissociative water potential is a multibody potential with both two-body and three-body terms. The pair term is based on the rigid water potential developed earlier (GG) [15]. However, in our potential, intramolecular interactions are added. Also, because of the use of the Wolf summation to account for the long range nature of the Coulomb term, parameters in the original GG potential were modified. The potential is given as:

$$U_{2-body} = U_{qq} + U_{q^d q^d} + U_{qq^d} + U_{q^d q} + U_{rep} + U_{disp} \qquad (1)$$

where

$$U_{qq}(r_{ij}) = \frac{q_i q_j}{r_{ij}} erfc(\frac{r_{ij}}{\beta}) \qquad (2)$$

$$U_{q^d q^d}(r_{ij}) = \frac{q_i^d q_j^d}{r_{ij}} erf(\frac{r_{ij}}{2\xi_{ij}}) erfc(\frac{r_{ij}}{\beta}) \qquad (3)$$

$$U_{qq^d}(r_{ij}) = \frac{q_i q_j^d}{r_{ij}} erf(\frac{r_{ij}}{\sqrt{2}\xi_{ij}}) erfc(\frac{r_{ij}}{\beta}) \qquad (4)$$

$$U_{q^d q}(r_{ij}) = \frac{q_i^d q_j}{r_{ij}} erf\left(\frac{r_{ij}}{\sqrt{2}\xi_{ij}}\right) erfc\left(\frac{r_{ij}}{\beta}\right) \quad (5)$$

$$U_{rep}(r_{ij}) = A_{ij}^{rep} \frac{erfc(z_{ij})}{z_{ij}} \left(z = \frac{r_{ij}}{2\xi_r^{ij}} \right) \quad (6)$$

$$U_{disp}(r_{ij}) = \frac{-C_6^{ij}}{r_{ij}^6} \quad (7)$$

In the original GG potential, $q_i^d \sim -q_i/4$, so we made the constant relation $q_i=-4q_i^d$, using $q_H^d = -0.113$ and allowing O to be twice the -H values.

For the long range coulomb interactions, we use the Wolf summation[28] rather than the Ewald sum. The Wolf summation gives the coulomb energy contribution as:

$$E^{ele} = E_{(1)}^{ele} + E_{(2)}^{ele} = \frac{1}{2}\sum_{i=1}^{N}\sum_{j\neq i=1} \frac{q_i q_j erfc(r_{ij}/\beta)}{r_{ij}} + \frac{1}{2}\sum_{i=1}^{N}\sum_{j\neq i=1} \frac{q_i q_j erf(r_{ij}/\beta)}{r_{ij}} \quad (8)$$

The second term can be shown to be negligible with the appropriate choice of β and cut-off distance R_c, giving the energy as:

$$E_{(1)}^{ele} = \frac{1}{2}\sum_{i=1}^{N}\sum_{\substack{j\neq i \\ r_{ij}<R_c}} \left(\frac{q_i q_j erfc(r_{ij}/\beta)}{r_{ij}} - \lim_{r_{ij}\to R_c}\left\{ \frac{q_i q_j erfc(r_{ij}/\beta)}{r_{ij}} \right\} \right) - \left(\frac{erfc(R_c/\beta)}{2R_c} + \frac{1}{\beta\pi^{1/2}} \right) \sum_{i=1}^{N} q_i^2 \quad (9)$$

We have employed the Wolf summation in simulations of SiC[29] and variations of the Wolf summation have been applied to simulations of water[30].

In the original GG potential, the charge distribution on the each atom is modeled with a point charge on the atom plus a diffuse charge that reduces the net charge as a function of the distance from the atom based on the error function. The application of a diffuse charge distribution to a water potential has been previously discussed[31]. A modified version of their potential has been elegantly applied to water in a recent paper[21], in which they also discuss the benefits of a diffuse charge model on achieving both high density and low density behavior. In the GG potential, the diffuse charge contributions to the total charge of an ion i varies as a function of the distance based on the q^d_i term, which is opposite in sign to the q_i term, thus reducing the effective charge on ion i as a function of the distance between an ij pair and the value of ξ. In the present case, the coulomb potential is also reduced by the long range summation parameter β in the erfc term in equations 2-5. The smaller the value of ξ, the more rapidly the contribution of the diffuse charge on the total charge increases to its maximum. In our case, ξ is set large so that the diffuse charges contribute only slightly to the total charge. However, this is offset by the erfc term of the Wolf summation in equations 2-5. The pair potential acts between all pairs of atoms and does not distinguish between different molecules. This enables a uniform description for the interactions within and between molecules that depends only on the distance between the atoms. This results in a fully atomistic model of water that allows for dissociation. This also means that the dissociated species, $OH^{-\delta}$ and $H^{+\delta}$, retain their original charge contributions, q_i and q^d_i for each O and H ion.

Besides the above two body potential, a three body potential of the following functional form was also added to the overall interaction:

$$U_3(r_i, r_j, r_k) = \nu_3(r_{ij}, r_{ik}, \theta_{jik})$$

(10)

where

$$v_3(r_{ij}, r_{jk}, \theta_{jik}) = \lambda_{jik} \exp[\gamma_{ij}/(r_{ij} - r_{ij}^o) + \gamma_{ik}/(r_{ik} - r_{ik}^o)][\cos(\theta_{jik}) - \cos(\theta_{jik}^o)]^2 \quad (11)$$

for $r_{ij} < r_{ij}^0$ and $r_{ik} < r_{ik}^0$, and equals 0 otherwise. $r_{ij}^0 = r_{ik}^0 = r_{\alpha\beta}^0$ as given in Table 1c. The effect of this function is to modify the interaction between three atoms depending on their deviation from the ideal angle, $\cos(\theta^0_{jik})$. The use of such a function allows the water molecule to reach correct angles. The parameters used in the three body potential are such that only the H-O-H angles in water are regulated to 104.2˚ (ie λ exists only for jik = HOH and is identically zero for OOH or HHO or OHO). In order to achieve this angle, θ^0_{jik} was set to 100°, which in combination with the H-H repulsive interaction, created a minimum at 104°. The list of parameters finally selected are given in Table I(a-c).

The potentials were developed so that the simulated water matched the thermal expansion curve of water from 273K to 373K[32] (plus a data point at 263K[33]) and high pressure data at several temperatures. Additional simulations of bulk water using the resultant potentials were used to generate cohesive energy, structural data, vibrational spectra, liquid-vapor coexistence curve, and diffusion coefficients. In all of the simulations, the long range Coulomb interactions were handled by the Wolf summation[28], with a cut-off of 1nm. System sizes less than 1nm (individual molecule or small molecular clusters) were calculated using the full Coulomb interactions, without the Wolf

summation. The time step was 0.1fs in all simulations and the simulations used a fifth order Nordseick-Gear algorithm. NPT (constant number, pressure, temperature), NVT (constant number, volume, temperature) or NVE (constant number, volume, energy) ensembles were used.

Development of the potential:

In the current work, we modify the original GG potential[15] in order to create a dissociative water potential that very accurately reproduces the density-temperature relation of the liquid while maintaining good structure, cohesive energy, and diffusion coefficient. We do this by allowing the parameters to vary as a function of temperature and/or pressure. While many water models are able to accurately arrive at a reasonable structure and density near 298K, most falter at reproducing the thermal expansion curve. In general, the observed trend in simulations has been that the density of water has been found to decrease at a greater rate with increase in temperature than experimental data[18]. Previous studies have discussed the importance of the interactions at short distances on the accuracy of the interatomic potential[15,21]. An effective way of making our water model better represent real water was achieved by allowing a change in a parameter with environment. In the current work, we have chosen to vary the short range OH repulsive interaction via the ξ_r^{OH} parameter as a function of temperature and pressure.

The effect of this change in ξ_r^{OH} can be seen in properties of bulk water and the following three figures are a simple demonstration of this and are not meant to be definitive. The effect of the change in ξ_r^{OH} on the OH distance is shown in figure 1, and, as a consequence of the above change in OH distance, the energy of bulk water also changes,

as shown in figure 2. The simulations were of a system of 392 water molecules in a box of approximate dimensions 2.3nm x 2.3nm x 2.3nm. The NPT simulation was carried out at 1atm pressure and a constant temperature of 298K for 200,000 timesteps. Structural and diffusion data were gathered over the final 100,000 timesteps. While this is a very short run time, these simulations were only designed to show the relative effect of ξ_r^{OH} on properties. Figure 2 shows the cohesive energy of bulk water and was obtained by calculating the difference between the average energy of a water molecule in bulk water and the average energy of a single gas phase water molecule simulated with the same set of parameters. These energies may be different from those obtained in subsequent runs with final parameters and longer simulation times, but the trends are obvious. The effect of ξ_r^{OH} on the OO pair distribution function (PDF) is shown in figure 3. Small changes in ξ_r^{OH} cause changes in the OO PDF, especially the shape of the important second OO peak. Another consequence of changes in ξ_r^{OH} is the lowering in the self diffusion coefficient at 298K from 3.41×10^{-5} cm^2/sec to 1.08×10^{-5} cm^2/sec with increasing ξ_r^{OH}. Clearly, the short range repulsion term, moderated by the ξ_r^{OH} term, plays an important role in the simulated properties. This effect can be controlled with various methods, such as added polarization terms, variable charge terms, etc. As shown here and below, we see the direct effect of the short range term on properties.

In order to determine the correct values of ξ_r^{OH} that would enable the simulations to match experimental densities at various pressures (from 1atm to 6000 atm) and various temperatures (from 263K to 373K), a series of runs at each T and P were performed with various ξ_r^{OH} values, interpolating the value of ξ_r^{OH} to coincide with the experimental T and P. An initial molecular dynamics simulation of 392 water molecules in a periodic

cubic simulation box of starting dimensions 2.175nm x 2.175nm x 2.486nm was performed for $2.0x10^6$ steps at 298K in order to generate a starting water configuration for the subsequent runs to generate the final ξ_r^{OH} values. NVE conditions were used for the first 200,000 steps, with velocities scaled for the first 100,000 steps. The run was continued for another $1.8\ x10^6$ steps under NPT conditions at 1 atm. Nominal parameters of ξ_r^{OH} =0.1989 and q^d_H=-0.11299 were used for this initial run. The final configuration of this run was used as the starting configuration for the additional NPT and NVE runs to determine the correct ξ_r^{OH} parameters for a particular T and P.

Each simulation that was then used to determine the correct ξ_r^{OH} values at each T and P was run for $1x10^6$ steps. The densities averaged over every 2000 configurations were collected. The variation in densities over the entire run was around 2-3%, and the maximum variation was observed during the initial 15% of the moves. Thus for calculating the density of a particular simulation, the first 20% of the run was discarded and the average density for a particular temperature, pressure, and ξ_r^{OH} value was determined.

The ξ_r^{OH} values that resulted in densities from 263K to 373K at 1 atm pressure that were less than 0.2% from the experimental value[32] were selected as the appropriate value of ξ_r^{OH} at that temperature and pressure. The data point from 263K was taken from Hare[33]. Figure 4 shows the results of the simulations at 1 atm at temperatures between 263K and 373K, showing the excellent agreement with experiment. The final configurations from these runs were used as the starting configurations for all subsequent NPT, NVT, and NVE runs at the specific temperature.

The ξ_r^{OH} values obtained from comparison to the high pressure data from 2000atm to 6000atm[34] varied by less than 0.5%. Figure 5 shows the results of the simulations using the final ξ_r^{OH} values at five temperatures and several pressures each.

The ξ_r^{OH} values thus calculated from the data generating figures 4 and 5 were plotted as a function of pressure and temperature and polynomial equations were fitted to the above data. The resultant polynomials could be used to determine the appropriate value of ξ_r^{OH} for any temperature or pressure within the fitted range. The resultant equation in a simplified form is :

$$\xi_r^{OH}(T,P) = \sum_{m=0,n=0}^{m=3,n=5} A_{mn} \bullet P^m \bullet T^n \qquad (12)$$

where the constant matrix A(4,6) is given in Table I(d,e).

Other parameters are shown in Table I. The basis for the calibration in the present case has been adherence to the liquid EOS shown in figure 4 and the equation of state curves in figure 5.

Results:

Molecular Clusters:

Water clusters containing from 2 to 9 molecules were simulated for 500,000 timesteps at 50K using the final parameters shown in Table 1a-e and the ξ_r^{OH} value obtained at 263K, followed by a 20,000 move continuation run at 1K with the same parameters. The 50K run allowed for sufficient rearrangement of the molecules to sample low energy states, with the 1K run acting as an energy minimizer. The energies shown in figure 6 for the clusters are given as the average cohesive energy per molecule. Also shown are data

taken from reference 14, involving data from minimizations using 5 other water potentials (POL5/TZ, POL5/QZ, TIP4P/FQ, TIP5P, and MCDHO), plus data from ab-initio calculations. The high and low MD results in the figure are taken from the highest and lowest values from any of the classical potentials and are used to show the spread in data with different interatomic potentials. The trends are similar, with our simulations showing stronger cohesive energies (which would be consistent with the considerations presented by Guillot and Guissani[15] and our dissociative water potential, as discussed below.)

Bulk Water:

For data analysis, bulk water simulations with the correct ξ_r^{OH} values were continued from the standard starting configuration for $1x10^6$ steps under NPT conditions at 1 atm and 5 different temperatures. The positions and velocities were saved every 2000th step for subsequent data analysis. The averages for the structure and angles were taken from the final 50% of the runs. Further NPT calculations at 1atm were also used in the calculations of the liquid-vapor coexistence curve. An NVE ensemble continued from the standard starting configuration for up to $3x10^6$ steps was used for calculation of diffusion coefficients at several temperatures using the correct ξ_r^{OH} values. The vibrational spectrum of water was calculated from the Fourier transform of the velocity auto-correlation function. For evaluating the spectrum, the simulations were continued from the standard starting configuration of bulk water simulation for an NVE run of 100,000 timesteps with the correct parameters and densities, followed by a 20,000 step run for analysis of the spectrum. Temperature equilibration was carried out for the initial 10,000

steps of the 20,000 move run and these initial moves were discarded while calculating the velocity autocorrelation function from the final 10,000 saved configurations.

Figure 7 shows the results of the structure of water through the OO, OH, HH pair distribution functions (PDFs) at five different temperatures (7a-c) as well as a direct comparison to Soper's most recent experimental data[35] (7d). As can be seen, the PDFs show variations over the five temperatures. The variations are similar to results that were obtained previously [15]. The results of the PDFs at 298K are compared to experiment[35] in figure 7d and are similar to the comparison of several other simulations of water to experiment[18], although most other simulations do not have the nearest neighbor OH and HH peaks. Clearly, the OH and HH intermolecular pair distributions are precisely equivalent to the experimental data (2^{nd} and higher peaks). Only the first peaks are too sharp for OH and HH in comparison to experiment, although the locations are accurate. The inset shows an expansion of the OO PDF, with only a slight variance in the depth of the first minimum and maximum in the second peak, although locations are accurate.

Figure 8 shows a comparison between the OO PDF at 298K and 373K. The main differences are the lowering of the first peak maximum and an increase in the first minimum and slight increase in the location of the second maximum. These results are consistent with previous simulations[15,21] and experiments[35] showing similar shifts in the OO PDF with temperature.

The vibrational spectrum of the simulated bulk water is plotted as a function of temperature in figure 9. The primary modes of vibration in water at 298K have been experimentally determined to occur around 400-600 cm^{-1}, 1600 cm^{-1}, and 3600-3700cm^{-1}. The peak near 500 cm^{-1} shifts to lower frequency with increasing temperature, similar to

previous work[15]. The most significant effect of changing the temperature is the lowering of the frequencies of the *v2* mode and a slightly lesser decrease in the stretching mode as well as a broadening of the frequency spectrum in the *v1* and *v3* modes. The spectrum at 298K is similar to the experimental data, except the 1600 peak has shifted upwards, probably because of the combined HH repulsion and the HOH 3-body term in the potential function, as also evidenced by the narrow first peaks in the HH and OH PDFs. Nonetheless, the general form is very good in comparison to experiment.

Diffusion coefficients were calculated from the mean square displacement (MSD) of the water molecules in bulk water as a function of temperature. At each temperature, the simulations started from standard starting configuration and were run for $3x10^6$ steps (300ps) under NVT conditions (the correct volume for each T was applied for the NVT continuations). The MSD was averaged over the final $1.8x10^6$ steps. The diffusion coefficients were taken from the average of the slopes of multiple segments of the MSD curve.

Figure 10 shows the resulting values of D for several temperatures compared to experimental data[36]. The value at 298K was $2.45x10^{-5}$ cm^2/s, which is close to the experimental value of $2.3x10^{-5}$ cm^2/s.

The average dipole moment at 298K was determined to be 2.6D, consistent with the experimental values that range from 2.3D to 3.2D.

The cohesive energy of the simulated bulk water at 298K was calculated as the energy difference between the $1x10^6$ steps NPT run of 392 water molecules at 298K and an NVE run of 500,000 timesteps of 1 isolated molecule of water (the latter without the Wolf sum method). The value obtained was -11.18 kcal/mol, which is the value expected

for a simulation with a dissociative water potential. Guillot and Guissani[15] discuss the effect of intramolecular interactions and quantum effects in the intermolecular interactions in the liquid that are not present in rigid water potentials. With an experimental ΔH_{vap}^{exp} of 10.52 kcal/mol[15,20], the cohesive energy using the rigid water potential should be –10.4 kcal/mol. However, in our case, changes in the intramolecular interactions between the isolated molecule in the vapor and that in the liquid are taken into account. It is only the intermolecular quantum effects in the liquid that are not included in our simulations. Addition of the intermolecular quantum effects discussed by Guillot and Guissani[15] and the RT term would result in a cohesive energy of -11.23 kcal/mol, indicating that our simulation result of –11.18 kcal/mol is very close to the correct value.

In order to test the validity of the potential for reproducing the high pressure-high temperature data, an NPT simulation of bulk water at 5000 atm and 3000 atm were performed at five different temperatures. As anticipated, the variable potential reproduces the experimental density as a function of pressure fairly well, as shown in figure 11.

The liquid-vapor coexistence curve, shown in figure 12, was calculated from additional simulations at five higher temperatures, 398K, 448K, 498K, 548K and 598K starting from the same initial configuration, which had a density of 0.9919e23 atoms/cm^3. Runs of 4.0x10^6 moves were made for all the temperatures starting from a 2.2nm x 2.2nm x 5.0nm (xyz) box of water with 392 water molecules. The simulations included the liquid in contact with a vacuum on either side in the z dimension into which the liquid could evaporate. Densities were averaged over 5000 move increments over the last 1.0x10^6 moves and plotted as a function of z, from which the density of the liquid was

obtained from the hyperbolic tangent function. Results for the liquid at 548K and 598K showed less than a 4% deviation from the experimental data. Water molecules evaporate into the excess volume at the higher temperatures, although the curve fitting is less accurate for these data because only a few molecules evaporate below 498K and the excess volume may be a little too low at 598K, where the vapor is at 0.134g/cc.

Hydronium Ion Behavior:

A cluster of 64 water molecules with one H^+ ion added was used to evaluate hydronium behavior with this classical potential. The cubic simulation box size was 4.0nm per side. Two conditions were studied: one where the extra H^+ ion was placed near an O in a water molecule near the edge of the cluster and a second case where the extra H^+ ion was placed near an O in a water molecule near the center of the cluster. The former was an NVE run of $1x10^6$ steps at 298K with the full coulomb summation, with temperature equilibration for the first 100,000 steps. Within the one million steps, H^+ ion exchange occurs 6 times. This implies an average lifetime of ~17ps for the H_3O^+ ion. Periodic boundary conditions were not used and all the molecules remained together without the cluster disintegrating. Interestingly, the hydronium ion stays near the periphery of the cluster. In the second case, the NVE run was 500,000 steps. Three exchanges occurred in this timeframe, giving the same lifetime as the previous run. Also within this timeframe in the second run, the hydronium ion migrated (via these exchanges and motion) from the cluster center to the edge of the cluster. Previous studies have similarly seen hydronium migration to the surface [24,37]. Figure 13 shows the interaction distances between the exchanging H^+ ion and its two closest O ions (labeled O1 and O2) during a portion of the simulation during which a proton exchange occurred. The 0.0ps

on the timescale is an arbitrating starting point. Also shown is the O1-O2 distance between the two oxygen ions in the interacting hydronium-water pair, in which O1 is the oxygen in the hydronium ion at the start. The H-O2 distance oscillates as the O2 in the second water molecule approaches the exchanging H^+ ion. Near 0.5ps, the exchange occurs rapidly. A different exchange process involving different molecules is observed in figure 14. In this case, the H^+ ion is located equidistant between both the O1-O2 oxygen for nearly 0.3ps. In this particular example, the H^+ ion returns to its original oxygen, but within ~0.7ps later in this run does exchange to this same O2. This process of having the H^+ ion located equidistant between the two interacting O is consistent with CPMD studies of the hydronium exchange process[27].

Figure 15 shows four snapshots of hydronium exchanges observed during a portion of the simulations. Only ions near the hydronium are shown, with some ions looking undercoordinated because their attached neighbors are not within the frame of the image. While the H_3O^+ ion itself may diffuse, additional migration of a H_3O^+ complex occurs via proton exchanges between a H_3O^+ ion and neighboring water molecules, as shown in the figure (and previously discussed [27]). The figure shows the initial H_3O^+ ion, the O of which is labeled as 1 in (a), is in an Eigen complex, $H_9O_4^+$, changing to more complex structures during proton exchange. Zundel ($H_5O_2^+$) and Eigen configurations are observed in the figure and are only two of the multiple configurations occurring in the exchanges.

Conclusions :

Molecular dynamics simulations of water were performed using a multibody potential that allows for dissociation of water and varies with environmental conditions.

The major variable that changed with the environment was the short distance OH repulsive term. With small changes in that term alone, the thermal expansion of water at atmospheric pressure and the equation of state at high temperatures and pressures were reproduced. The resultant interatomic multibody potential was then used to simulate other properties. The room temperature properties of water that were accurately reproduced include the structure, the cohesive energy, the average dipole moment of the liquid, the diffusion constant, the vibrational frequency spectrum, and the transient Eigen and Zundel complexes of the H_3O^+ ion. In addition, the liquid-vapor coexistence curve was well reproduced.

Acknowledgements:

The authors wish to acknowledge funding from the DOE Office of Science, Division of Chemical Sciences, Geosciences, and Biosciences, grant number DE-FG02-93ER14385, and from the Division of Material Sciences, grant number, DE-FG02-97ER45642.

Table Ia: parameters of the two body potential.

Species	A_r (J)	ξ (Å)	ξ_r (Å)	C_6 (J-Å^6)
O-H	2.283×10^{-16}	24	f(T, P)	-
O-O	4.250×10^{-17}	24	0.610	4.226×10^{-18}
H-H	-	24	-	-

Table Ib: Charges on species

Species/multiple	q/e	q^d/e
O	-.904	+.226
H	+.452	-.113

Table Ic: Three body parameters :

Species	λ (ergs)	$r^0_{\alpha\beta}$ (Å)	γ (Å)	θ°_{HOH}
H-O-H	30×10^{-11}	1.6	1.3	100

Table Id: The A-matrix of equation 12 columns A(:0)-A(:,2)

0.655726502	$-1.04442689 \times 10^{-2}$	$8.31892416 \times 10^{-5}$
3.403472×10^{-4}	-3.986929×10^{-6}	1.742261×10^{-8}
-4.057853×10^{-8}	4.677537×10^{-10}	$-2.007873 \times 10^{-12}$
1.657262×10^{-12}	$-1.838785 \times 10^{-14}$	7.549619×10^{-17}

Table Ie: The A-matrix of equation 12 columns A(:,3)- A(:,5)

$-3.07929142 \times 10^{-7}$	$5.44770929 \times 10^{-10}$	$-3.73609493 \times 10^{-13}$
$-3.364186 \times 10^{-11}$	2.419996×10^{-14}	0
3.800411×10^{-15}	$-2.672717 \times 10^{-18}$	0
$-1.355453 \times 10^{-19}$	8.939302×10^{-23}	0

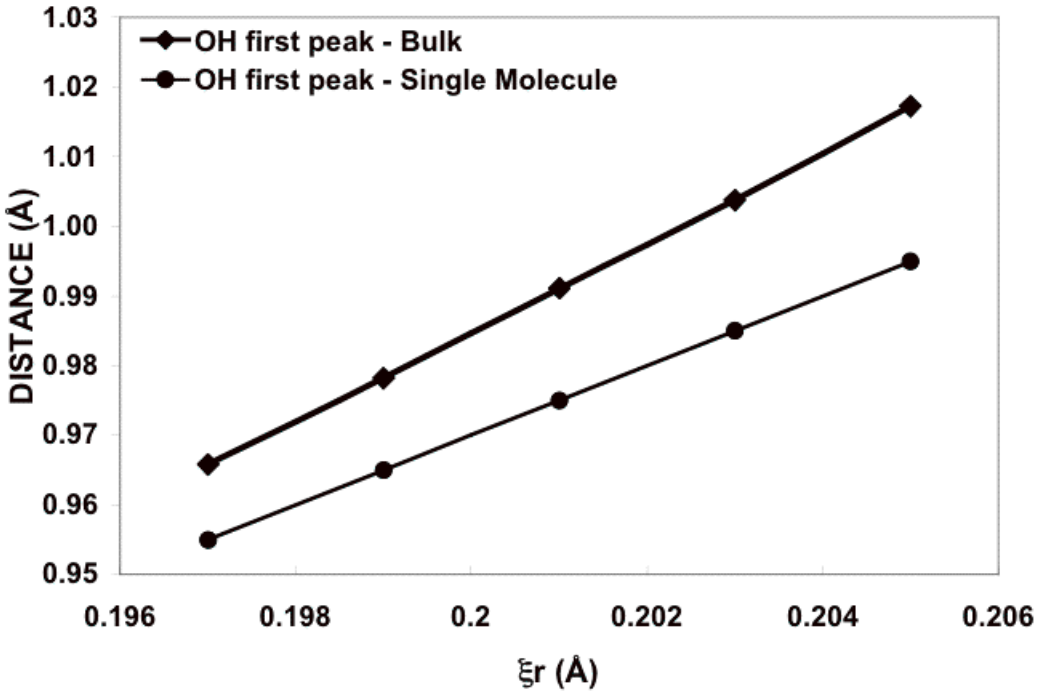

FIG 1.Variation in the OH distance in a single water molecule and within bulk water as a function of a term in the OH short-range repulsion, ξ_r.

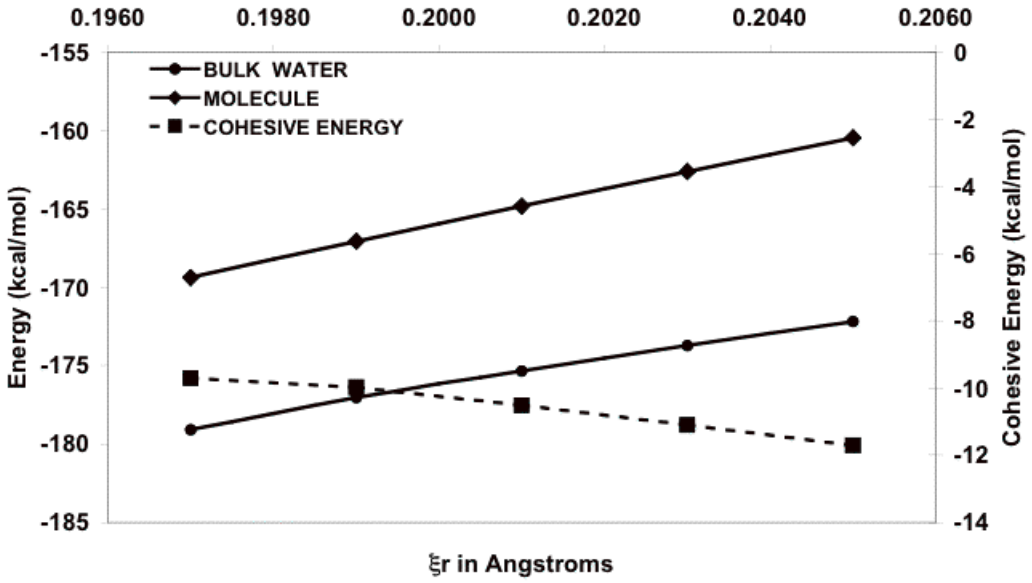

FIG 2. Variation in the energy in a single water molecule and bulk water as a function of the ξ_r term in the OH short-range repulsion (left axis) and the cohesive energy (right axis).

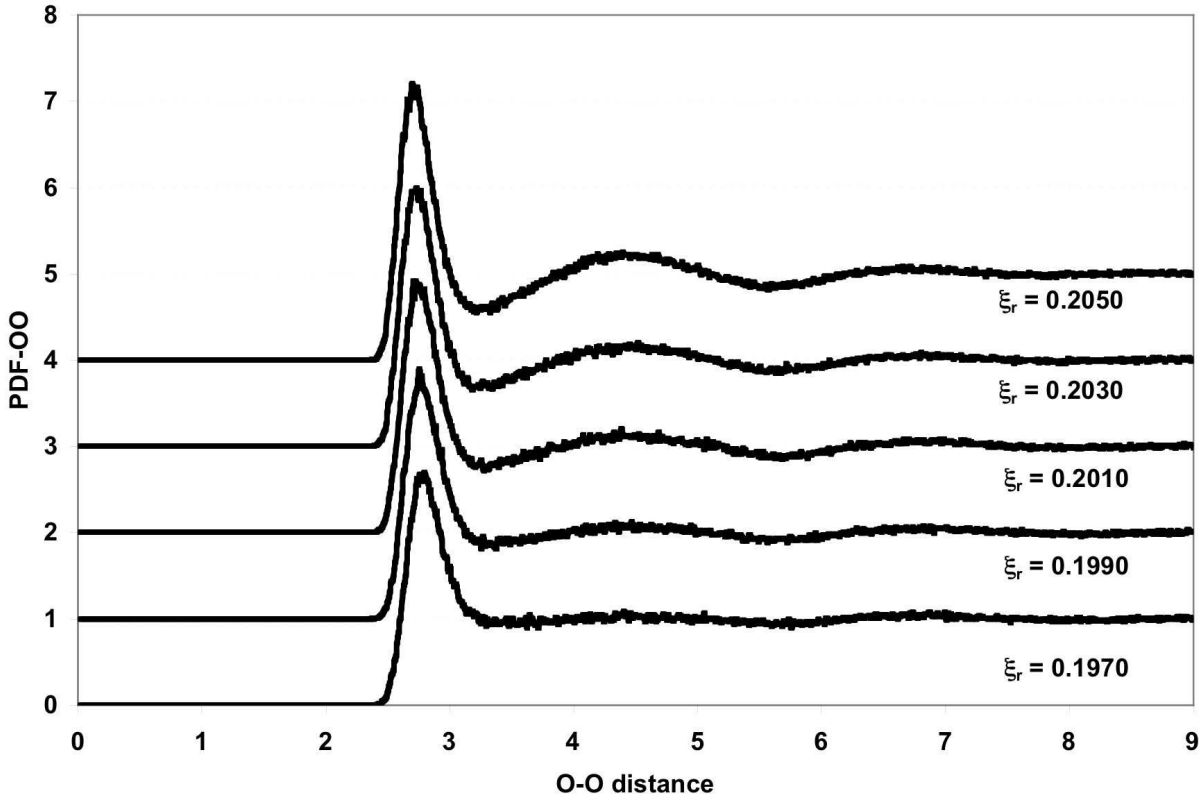

FIG 3. Variation in the OO pair distribution function (PDF) for bulk water as a function of the ξ_r term in the OH short-range repulsion.

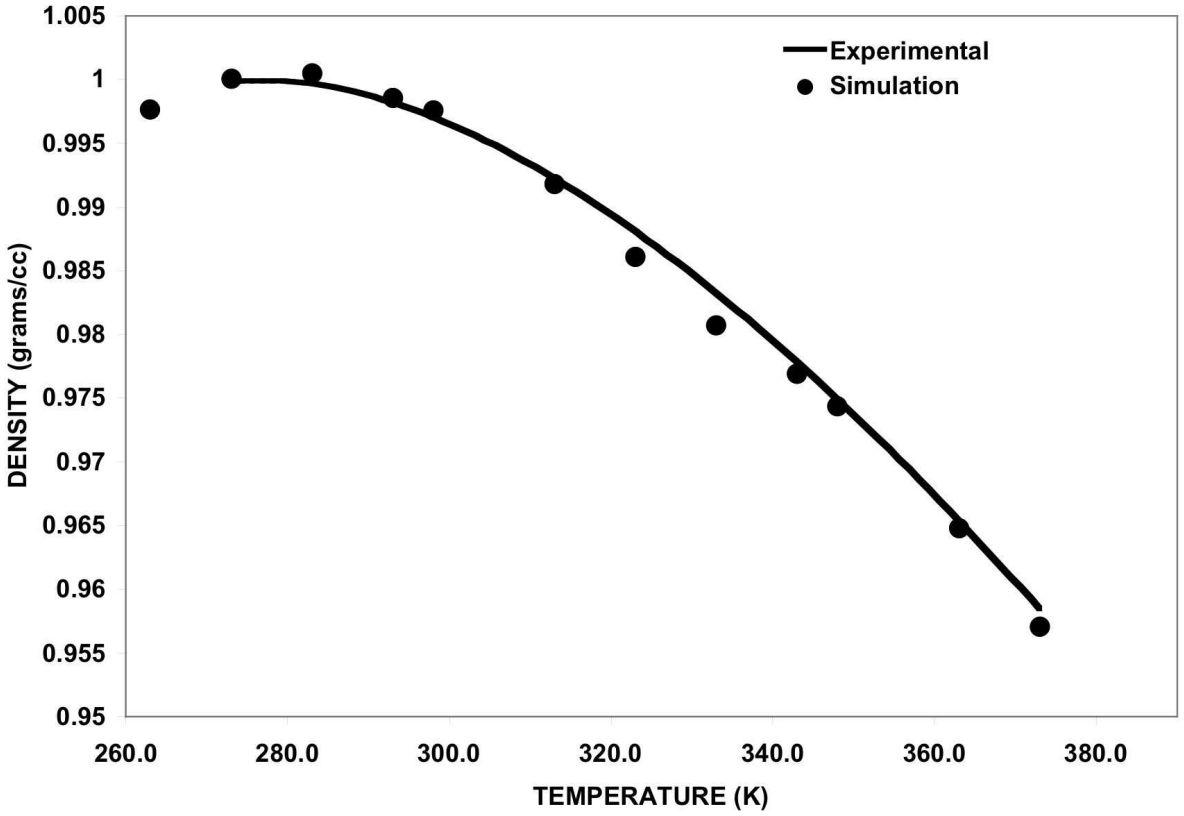

FIG 4. Result of optimizing the ξ_r term in the OH short-range repulsion on reproducing the density-temperature curve.

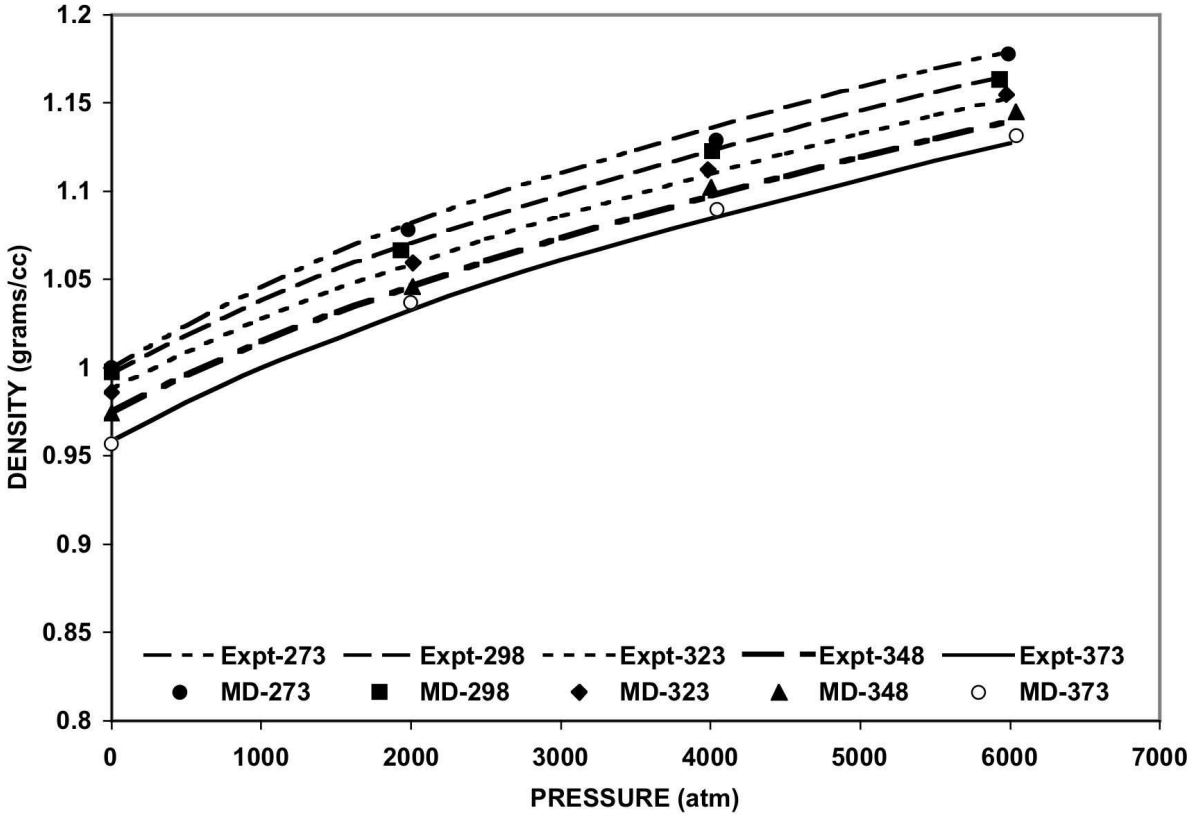

FIG 5. Result of optimizing the ξ_r term in the OH short-range repulsion on reproducing the density-pressure curve at four different temperatures.

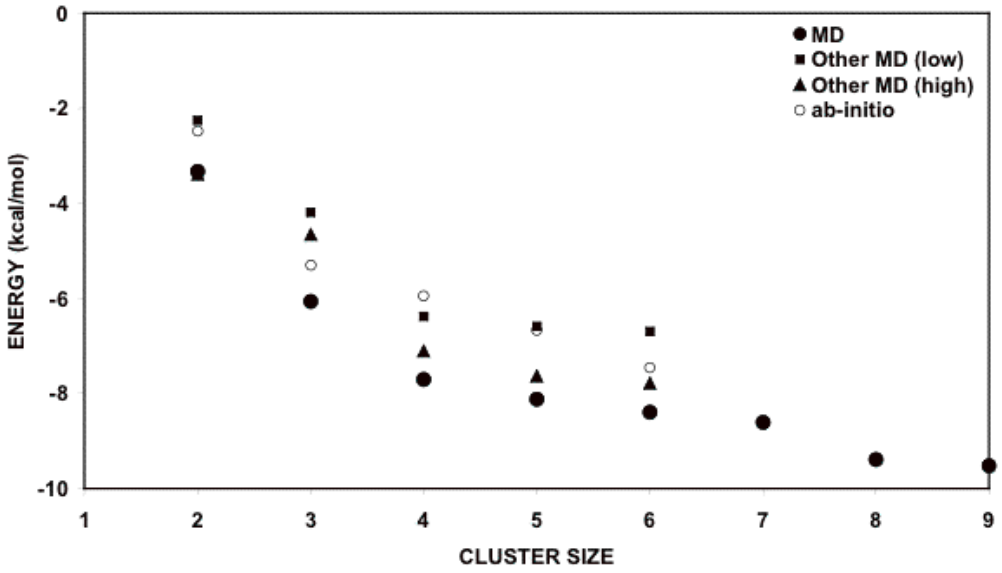

FIG 6. Cohesive energy per molecule of small water clusters at 1K using finalized parameters given in Table 1 and the ξ_r term in the OH short-range repulsion obtained at 263K. “MD” is the current data. Other data points come from reference 14, which contains data from other classical water potentials used in MD simulations (“other MD”) and ab-initio calculations, with the lowest (low) and highest (high) cohesive energy per molecule from the other potentials (see text).

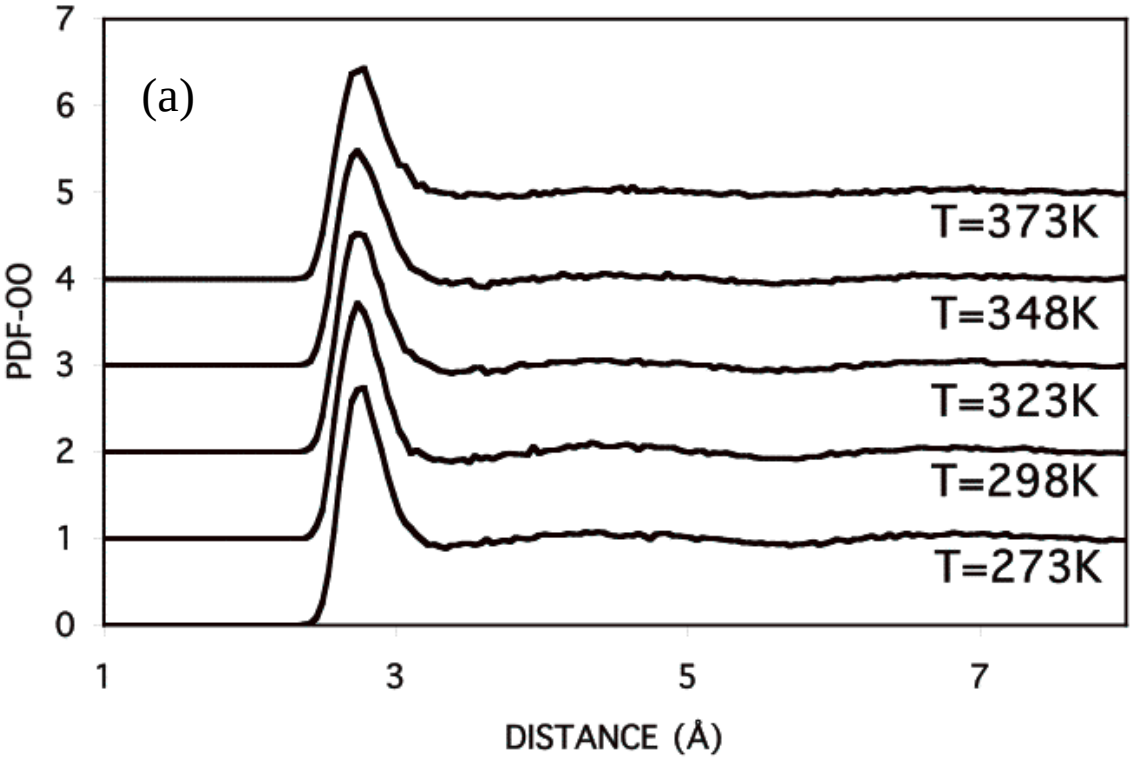

FIG 7. Pair distribution functions at different temperature for (a) O-O, (b) H-H, and (c) O-H pairs. (d) shows comparison between the MD simulations at 298K and experimental data[35] for all 3 pairs, as well as a larger scale comparison of the OO pdf in the insert.

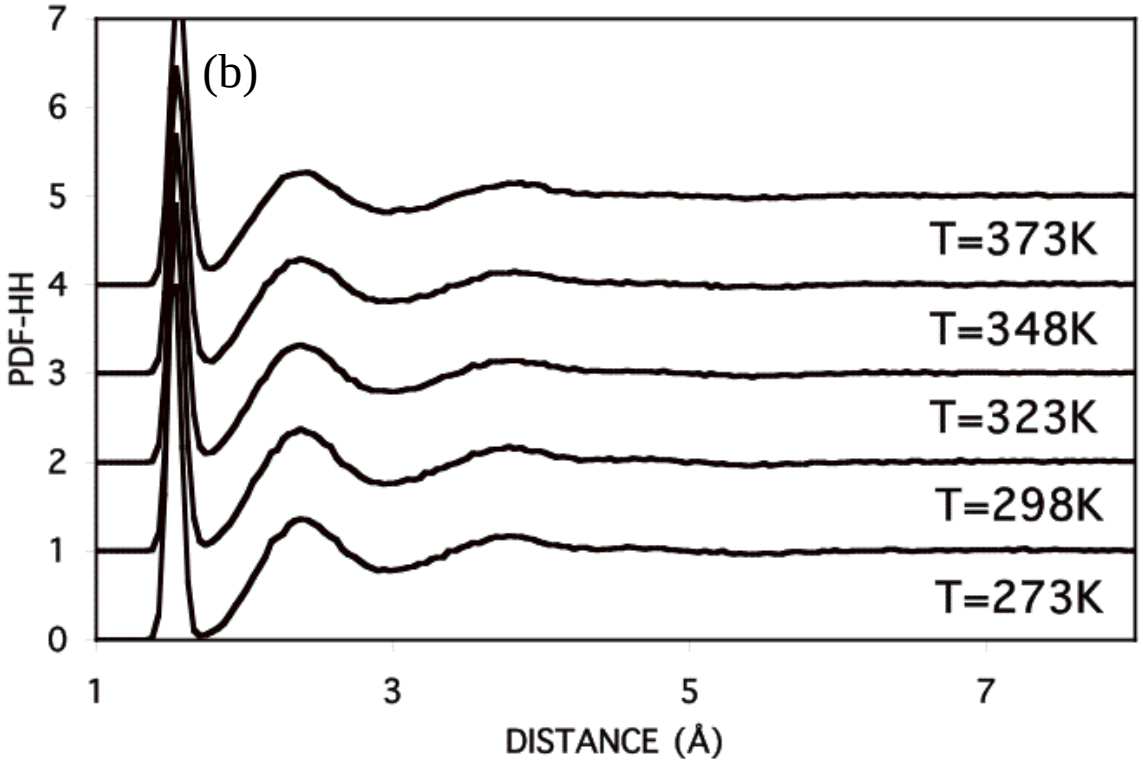
(b)
T=373K
T=348K
T=323K
T=298K
T=273K
PDF-HH
DISTANCE (Å)
0
1
2
3
4
5
6
7
1
3
5
7

Fig 7b

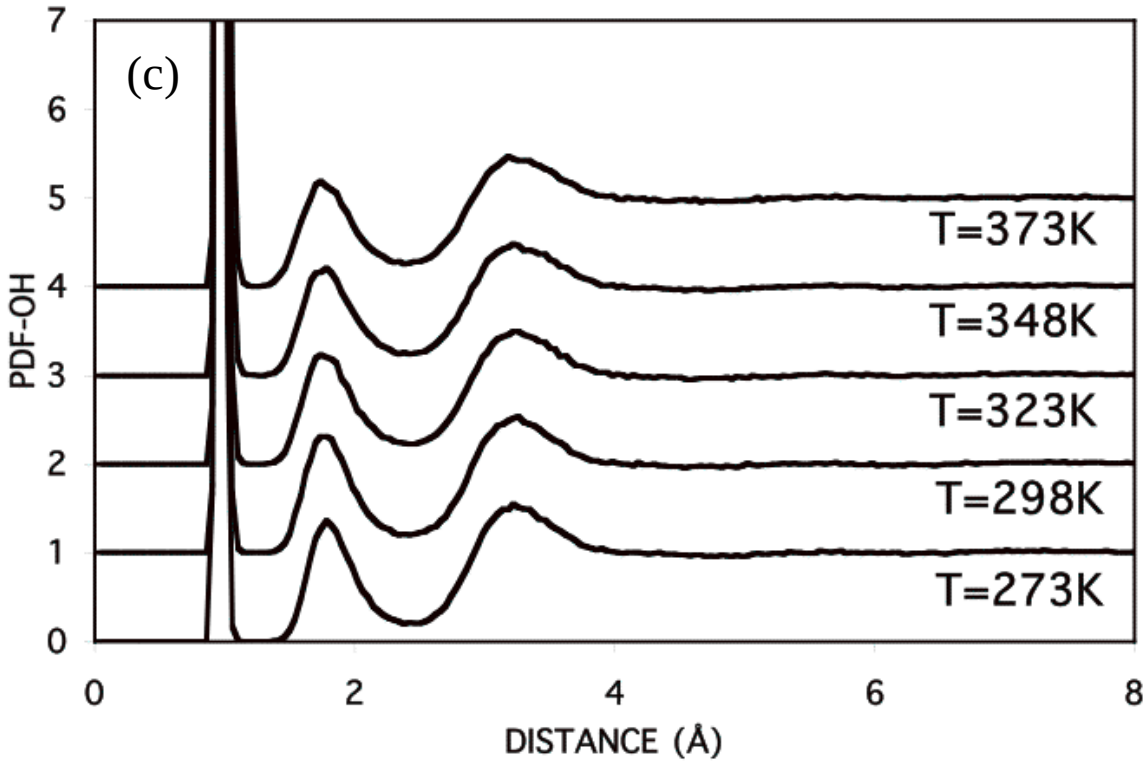
(c)
PDF-OH
DISTANCE (Å)
T=373K
T=348K
T=323K
T=298K
T=273K
0
1
2
3
4
5
6
7
0
2
4
6
8

FIG 7c

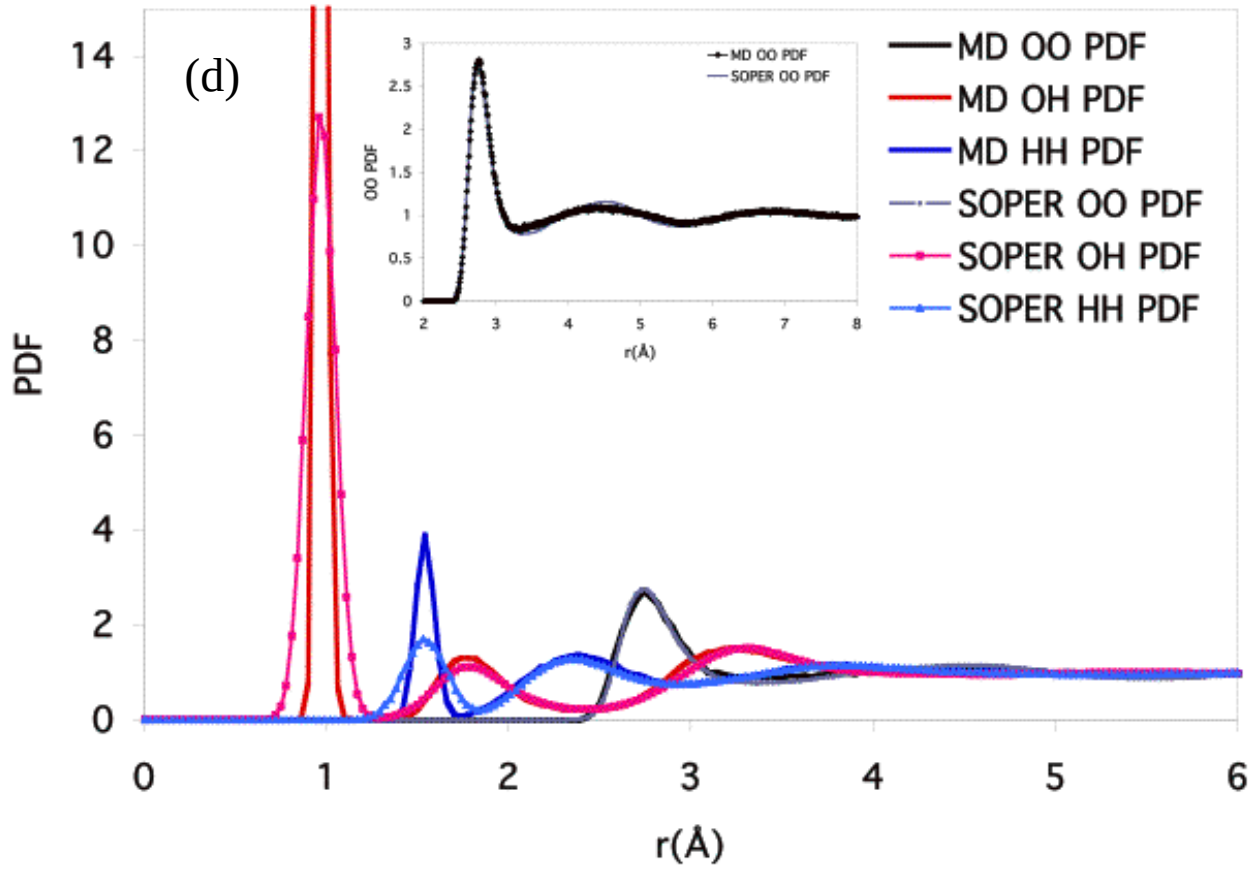
(d)
PDF
r(Å)
MD OO PDF
MD OH PDF
MD HH PDF
SOPER OO PDF
SOPER OH PDF
SOPER HH PDF
OO PDF
r(Å)
MD OO PDF
SOPER OO PDF

7d

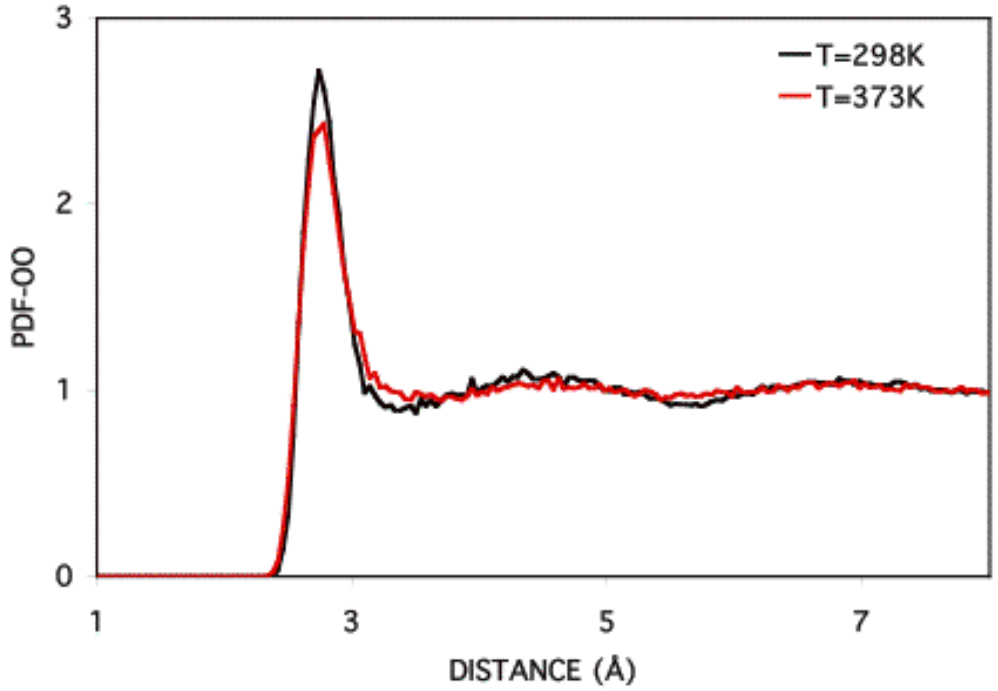

FIG 8. Comparison between the OO PDF at 298K and 373K, showing the loss of structure at the elevated temperature in the decrease in the first peak maximum and an increase in the first minimum.

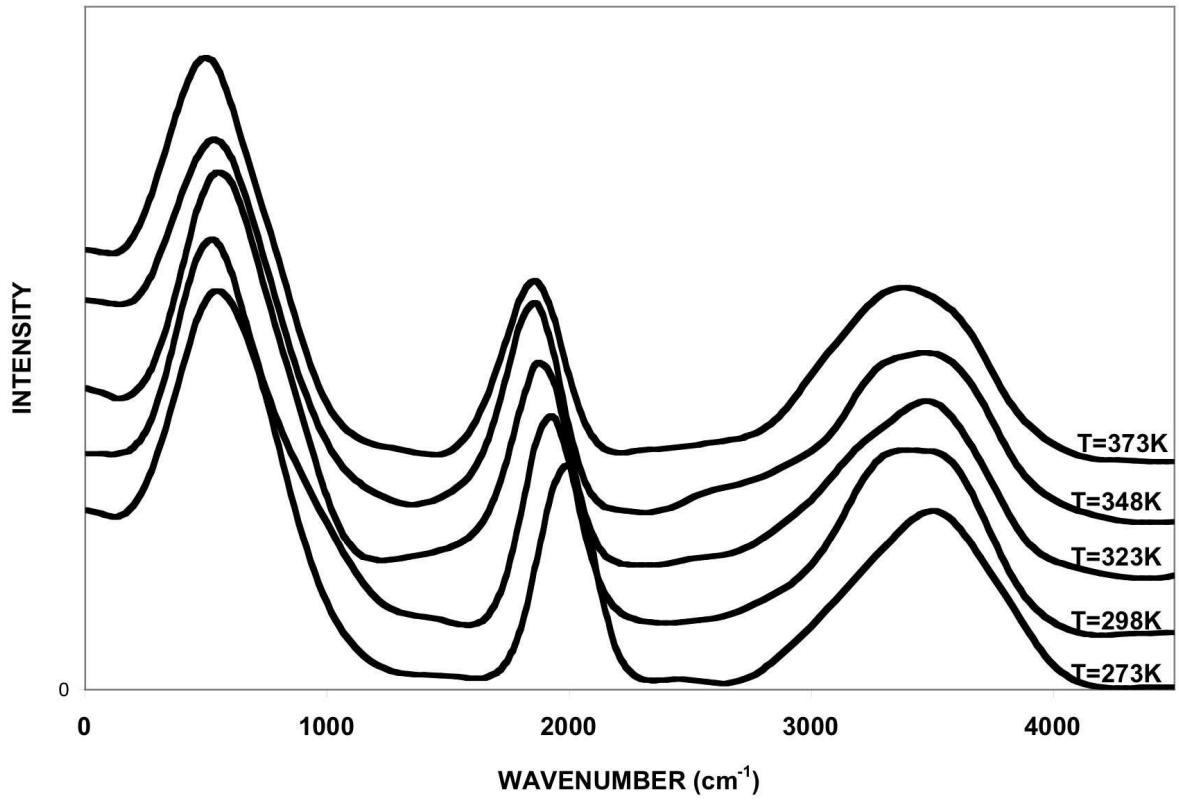

Fig 9. Vibrational frequency spectrum of simulated bulk water as a function of temperature.

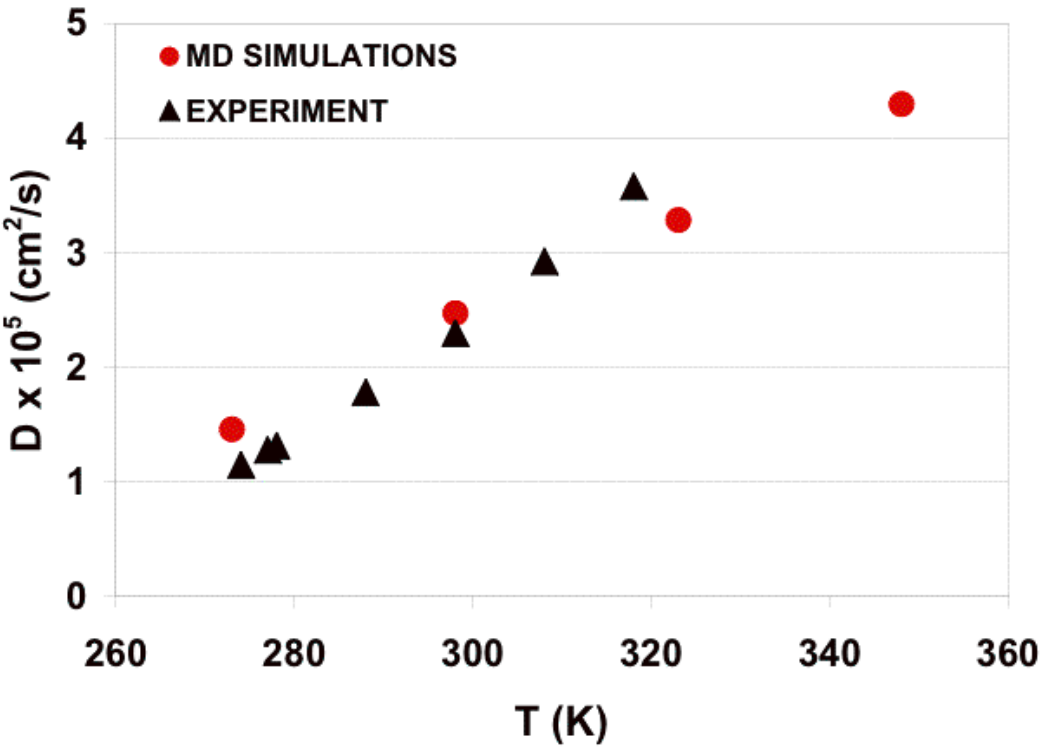

FIG 10. Diffusion coefficient, D (cm^2/s), as a function of temperature from the MD simulations versus experimental data (ref. 36).

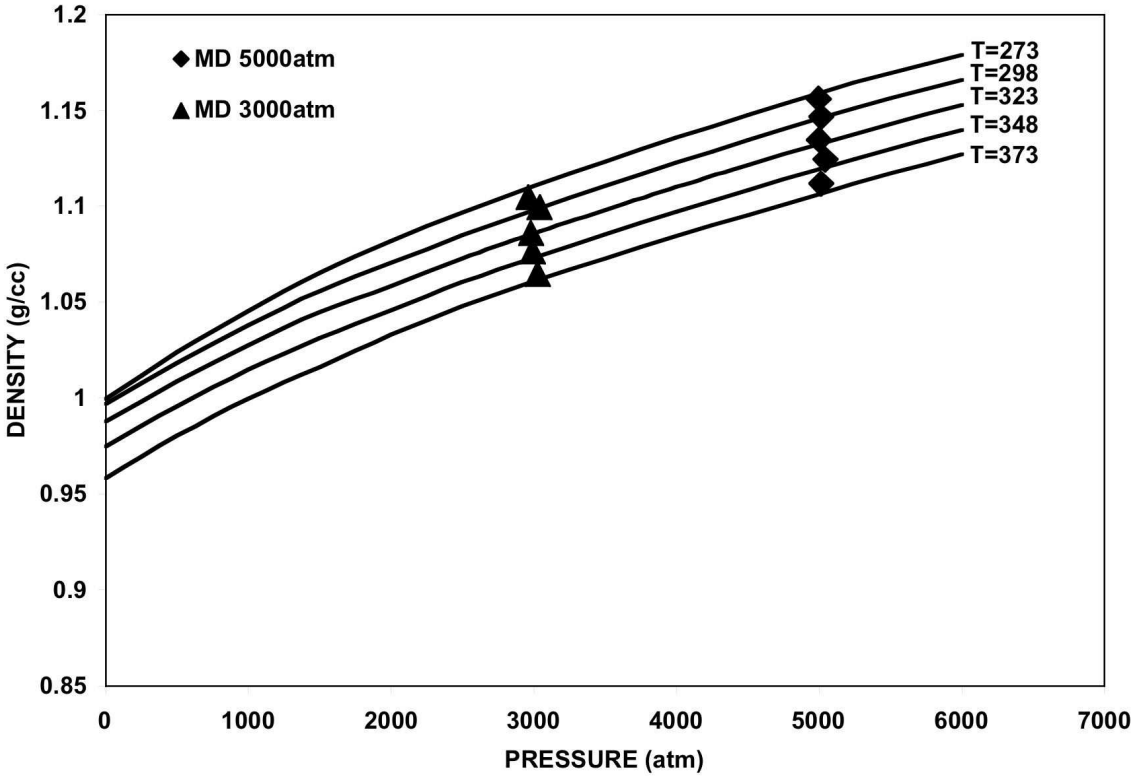

Fig 11. The density-pressure relation at 5000 and 3000 atm predicted from the simulations in comparison to the experimental data.

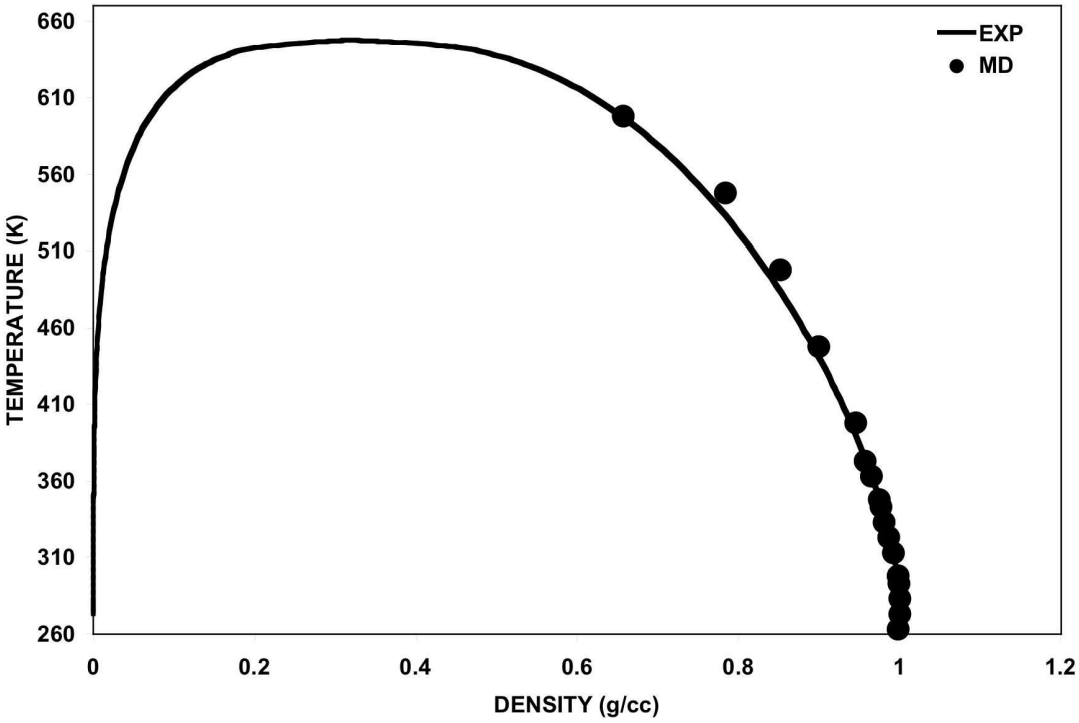

FIG 12. The liquid-vapor coexistence curve obtained from the simulations in comparison to experiment. The data at the four highest temperatures are predicted from the potential and functional form of ξ_r of OH obtained at the lower temperatures.

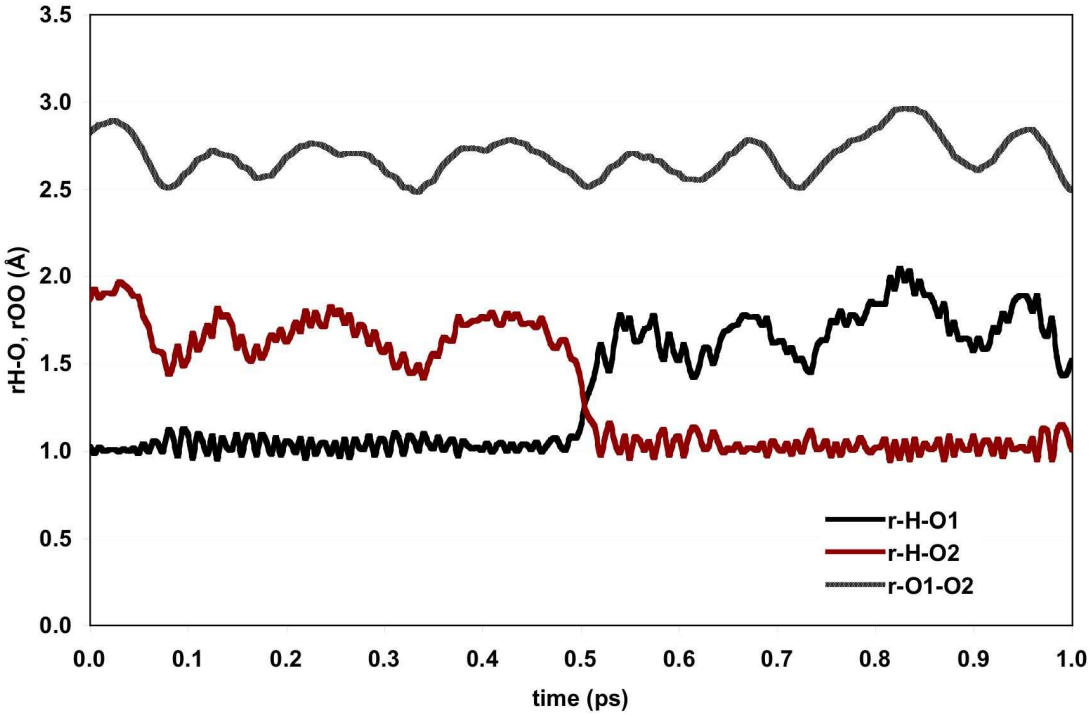

Fig 13. Variation in the HO distances for the reacting H of a hydronium ion during the H exchange with an adjacent water molecule. O1 is the oxygen in the starting H_3O^+ ion and O2 is the oxygen in the interacting H_2O. At ~0.5ps, the H_3O^+ ion is centered on the O2 oxygen. The O1-O2 separation distance during the reaction is also given, with large oscillations between 2.5Å and 3.0Å.

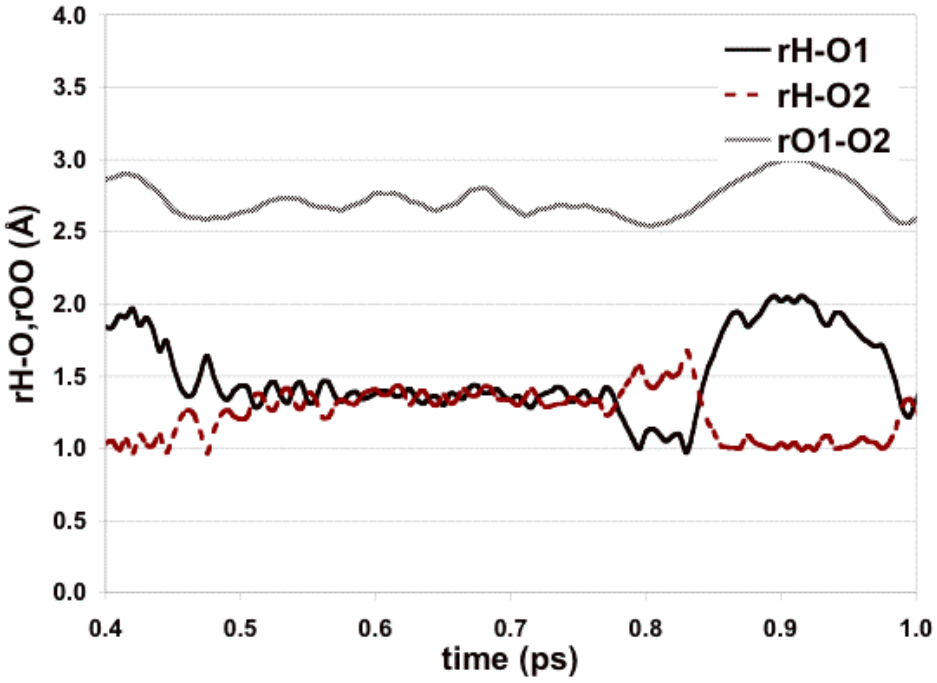

FIG 14. Additional example of hydronium exchange mechanism, where the exchanging H ion sits between both O, equidistant from each, from ~0.5ps to ~0.75ps, in this case returning to the original configuration. This pair continues to interact and does show a stable exchange of the proton at 1.7ps on this time scale (not shown here).

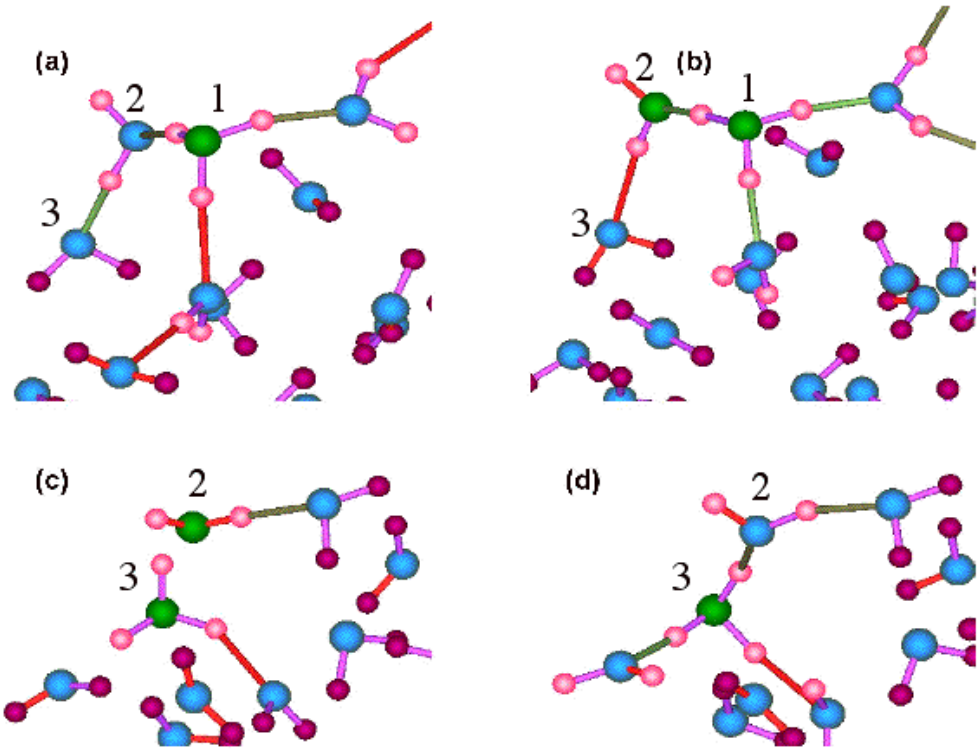

FIG 15. Snapshots of the reaction(s) of the H_3O^+ ion(s) with neighboring water molecules. Color scheme: green=O in H_3O^+ ion; pink=H attached to O within H_3O^+ ion or in H_2O molecules H-bonded to the H_3O^+ ion; blue=O, small red = H in other waters. Long 'bonds' drawn between O-H within 2.0Å showing covalent and H-bonded molecules. Three relevant O labeled by numbers 1, 2, 3. (a), Eigen-type complex with H_3O^+ ion (O1) H-bonded to 3 neighbors; (b) reacting H ion split between two O, O1 and O2, with O2 now also marked green; (c) between frames b and c, a second transfer of a proton occurs to the third water molecule (O3) which forms a Zundel complex. O1 has migrated out of the frame; (d) the O3 H_3O^+ is now in another Eigen complex.

References:

(1) Rahman, A.; Stillinger, F. H. *J. Chem. Phys.* **1971**, *55*, 3336.
(2) Rahman, A.; Stillinger, F.; Lemberg, H. *J. Chem. Phys.* **1975**, *63*, 5223.
(3) Stillinger, F.; Rahman, A. *J. Chem. Phys.* **1978**, *68*, 666.
(4) Jorgensen, W. L. *J. Am. Chem. Soc.* **1981**, *103*, 335.
(5) Jorgensen, W. L.; Chandrasekhar, J.; Madura, J. D.; Impey, R. W.; Klein, M. L. *J. Chem. Phys.* **1983**, *83*, 926.
(6) Weber, T.; Stillinger, F. *J. Phys. Chem.* **1982**, *86*, 1314.
(7) Jorgensen, W. *J. Chem. Phys.* **1982**, *77*, 4156.
(8) Zhu, S.-B.; Singh, S.; Robinson, G. W. *J. Chem. Phys.* **1991**, *95*, 2791.
(9) Sprik, M. *J. Chem. Phys.* **1991**, *95*, 6762.
(10) Halley, J. W.; Rustad, J. R.; Rahman, A. *J. Chem. Phys.* **1993**, *98*, 4110.
(11) Rick, S. W.; Stuart, S. J.; Berne, B. J. *J. Chem. Phys.* **1994**, *101*, 6141.
(12) Dang, L.; Chang, T.-M. *J. Chem. Phys.* **1997**, *106*, 8149.
(13) Mahoney, M. W.; Jorgensen, W. L. *J. Chem. Phys.* **2000**, *112*, 8910.
(14) Stern, H. A.; Rittner, F.; Berne, B. J.; Friesner, R. A. *J. Chem . Phys.* **2001**, *115*, 2237.
(15) Guillot, B.; Guissani, Y. *J. Chem. Phys.* **2001**, *114*, 6720.
(16) Izvekov, S.; Parrinello, M.; Burnham, C. J.; Voth, G. A. *J. Chem. Phys.* **2004**, *120*, 10896.
(17) Ren, P.; Ponder, J. W. *J. Phys. Chem. B* **2003**, *107*, 5933.
(18) Ren, P.; Ponder, J. W. *J. Phys. Chem. B* **2004**, *108*, 13427.
(19) Robinson, G. W.; Zhu, S.-B.; Singh, S.; Evans, M. W. *Water in Biology, Chemistry, and Physics*; World Scientific: Singapore, 1996.
(20) Guillot, B. *Journal of Molecular Liquids* **2002**, *101*, 219.
(21) Paricaud, P.; Predota, M.; Chialvo, A. A.; Cummings, P. T. *J. Chem. Phys.* **2005**, *122*, 244511.
(22) Feuston, B. P.; Garofalini, S. H. *J. Appl. Phys.* **1990**, *68*, 4830.
(23) Lussetti, E.; Pastore, G.; Smargiassi, E. *Chem. Phys. Lett.* **2003**, *381*, 287.
(24) Dang, L. *J. Chem. Phys.* **2003**, *119*, 6351.
(25) Zundel, G.; Metzger, H. *Z. Phusik. Chem.* **1968**, *58*, 225.
(26) Eigen, M. *Angew. Chem. Int. Edn. Engl.* **1964**, *3*, 1.
(27) Marx, D.; Tuckerman, M. E.; Hutter, J.; Parrinello, M. *Nature* **1999**, *397*, 601.
(28) Wolf, D.; Keblinski, P.; Phillpot, S. R.; Eggebrecht, J. *J. Chem. Phys.* **1999**, *110*, 8254.
(29) Ma, Y.; Garofalini, S. H. *J. Chem. Phys.* **2005**, *122*, 094508.
(30) Fennell, C. J.; Gezelter, J. D. *J. Chem. Phys.* **2006**, *124*, 234104.
(31) Chialvo, A. A.; Cummings, P. T. *Fluid Phase Equilibr.* **1998**, *150-151*, 73.
(32) Wagner, W.; Cooper, J. R.; Dittmann, A.; Kijima, J.; Kretzchmar, H.-J.; Kruse, A.; Mares, R.; Oguchi, K.; Sato, H.; Stocker, I.; Sifner, O.; Takaishi, Y.; Tanishita, I.; Trubenbach, J.; Willkommen, T. *ASME J. Eng. Gas Turbines and Power* **2000**, *122*, 150.
(33) Hare, D. E.; Sorensen, C. M. *J. Chem. Phys.* **1986**, *84*, 5085.
(34) Kell, G. S. Thermodynamic and Transport Properties of Fluid Water. In *Water-A comprehensive treatise*; Franks, F., Ed.; Plenum press: New York, 1972; Vol. 1.
(35) Soper, A. K. *Chem. Phys.* **2000**, *258*, 121.

(36) Mills, R. *J. Phys. Chem.* **1973**, *77*, 685.
(37) Kusaka, I.; Oxtoby, D. W. *J. Chem. Phys.* **2000**, *113*, 10100.

MANUSCRIPT II: “Water induced relaxation of silica surfaces with a long range dissociative water potential”.

T.S.Mahadevan and S.H.Garofalini

Water induced relaxation of silica surfaces with a long range dissociative water potential.

T.S.Mahadevan and S.H.Garofalini

Abstract:

Molecular dynamics simulations were performed to study the interaction between a film of water vapor and vitreous silica surface. The water was modeled by dissociative atomistic model and the potential used allowed for interactions between water and silica to form silanol bonds. The potential parameters were refined by studying the energetics of interaction between silicic acid and water molecule. We observe the mechanisms and rate of formation of silanols and note that the concentration of the silanols is consistent with experimentally observed results. The mechanism of hydronium ion formation and its role in the formation of silanols and proton transfer was also studied. The modification of the surface structure of the glass was analyzed quantitatively and the graphics depicting the formation silianols from breaking of surface siloxanes is also presented this study.

I) Introduction:

Silica and water are two of the most abundant materials found in nature and this abundance has lead to their use in many technological applications. [1] [2] [3] The study of interactions between water and silica provides important insights for many technological processes like wafer bonding in MEMS devices, mechanical strength and failure behavior of optical fibers, catalysis, expansion of water in geological systems and scaling of structural ceramic materials.[4] [5] [6, 7]Presence of water in vitreous silica has a profound influence in many of its thermal, mechanical and optical properties and

experimental techniques for studying these changes can easily provide information into the macroscopic aspects of the interactions. [8] However, the molecular interactions are trickier to be studied with experimental techniques and computational methods have become a useful tool to study the nano scale interactions in these material systems. Ab-initio and quantum chemical methods of computational studies have been applied to simulate molecular interaction between silicic acid and water. [9] [10-12] The results of these studies can be used to understand the interactions between glass surfaces or zeolites and water[13]. Ab-initio methods and quantum mechanical calculations are computationally exhaustive methods which, even in combination with classical MD methods can be used for studying only small local regions involving 100's of molecules at the most [14] [15]. Classical MD simulations have been used to study structural and energy changes in SiO_2-H_2O interactions using non dissociative water potentials or artificially inducing silanol formation[16] [17] [18].

This group has previously used molecular dynamics simulation techniques to simulate and study the properties of vitreous and crystalline silica with and water – silica interactions using BMH interactions and a three body interaction [6, 19]. These potentials have successfully simulated the structure and dynamics of bulk glasses and glass surfaces[20] and has been used to explain mechanisms of oligomerization in silica sols[21], and reactions in silicic acid molecular clusters[22] [23]. The low energy structures and energies of the H2O – $Si(OH)_4$ clusters were found to be comparable to ab-initio calculated energies. The normal reaction mechanism for the breaking of siloxanes and formation of silanols has been computationally verified to be as depicted schematically as shown in fig 1. For clarity, the bonds from the bridging oxygens

attached to the silicon are not shown. The five coordinated silicon that shows a stretched bond is a reaction intermediate. This reaction has been experimentally inferred [24] [25] [26] [27] and predicted through ab-initio[28] [29] and classical MD studies to occur preferentially at the sites that have most strained siloxane bonds.

While several potentials for prediction of water structure and properties exist [30], most of them are based on rigid molecules or at the most flexible but non dissociative models. Previous studies by this group was based on a BMH potential for water with certain RSL modifications for the water molecules. While that model was reliable for a short range structure of water, it did not reproduce the correct water structure of water more than first neighbor distances. Considering that the potential acts over only 5.5Å and that significant structural information of water exists till the third peak of the O-O pair distribution function at around 7Å, this BMH –type potential would be insufficient to study the effect of large sections of silica on water dissociation and clustering.

The authors have also used a diffuse charge based – dissociative potential to describe the structure of water over a large range of temperatures [31]. This dissociative water operates with a larger cut-off (10Å) for interactions and thus can be considered more appropriate for studying glass-water interactions. This potential was developed for using the dissociative water to study the anomalous expansion of water in nano-sized pores and gives results that have a close match to experimental structure and dynamic properties of water. In the current work, the relaxation of a silica surface in the presence of water is investigated using molecular dynamics with the new potential. The results of this study will eventually determine the suitability of this new potential to study atomistic

mechanisms of water-silica interactions while using simple, and relatively computationally inexpensive classical MD techniques that can work for large systems.

Following this introduction, section II provides a brief overview of the potential function followed by a description of the computational techniques in section III. Section IV describes the results of the acid- water molecular interactions and this is followed by results of vapor interacting with the silica surface in section V. Section VI shows the graphics of vapor –surface interactions and this is followed by conclusions in section VII.

II) Description of potential:

The dissociative water potential is based on the rigid water potential developed by Guillot and Guissani. In our potential, intra molecular interactions are added so as to include flexibility in the atomic simulations and polarizability. The two body potential is given by:

$$U_{2-body} = U_{qq} + U_{qdqd} + U_{qqd} + U_{qdq} + U_{rep} + U_{disp} \quad (1)$$

where

$$U_{qq}(r_{ij}) = \frac{q_i q_j}{r_{ij}} \times erfc(\frac{r_{ij}}{\beta}) \quad (2)$$

$$U_{qdqd}(r_{ij}) = \frac{q_i^d q_j^d}{r_{ij}} erf(\frac{r_{ij}}{2\xi^{ij}}) \times erfc(\frac{r_{ij}}{\beta}) \quad (3)$$

$$U_{qqd}(r_{ij}) = \frac{q_i q_j^d}{r_{ij}} erf(\frac{r_{ij}}{\sqrt{2}\xi^{ij}}) \times erfc(\frac{r_{ij}}{\beta}) \quad (4)$$

$$U_{qdq}(r_{ij}) = \frac{q_i^d q_j}{r_{ij}} erf(\frac{r_{ij}}{\sqrt{2}\xi^{ij}}) \times erfc(\frac{r_{ij}}{\beta})$$

(5)

$$U_{qdq}(r_{ij}) = \frac{q_i^d q_j}{r_{ij}} erf\left(\frac{r_{ij}}{\sqrt{2}\xi^{ij}}\right) \times erfc\left(\frac{r_{ij}}{\beta}\right) \quad (6)$$

$$U_{rep}(r_{ij}) = A_{rep}^{ij} \frac{erfc(z^{ij})}{z^{ij}} \left(z = \frac{r_{ij}}{2\xi_r^{ij}} \right) \quad (7)$$

$$U_{disp}(r_{ij}) = \frac{-C_6^{ij}}{r_{ij}^6} \quad (8)$$

The values of the parameters used for the different atom species are given in table I. in general $q_i = -4q_i^d$ and the charge on silica is 4 times the charge on hydrogen and oxygen has twice the charge on hydrogen. The wolf sum is used to handle the inclusion of the long range terms in the Madelung potential. The details of the calculation of Wolf sum is given in an earlier paper by the authors. One of the effects of using the wolf summation is the presence of the complementary error function term in the charge based parts of the potential function. This does not appear in the repulsion and dispersion terms as they are short range. In summary, the final effect of using the Wolf summation is to induce a correction term for all the charge based terms of the potential giving the final equation as:

$$E_{(1)}^{ele} = \frac{1}{2} \sum_{i=1}^{N} \sum_{\substack{j \neq i \\ r_{ij} < R_c}} \left(\frac{q_i q_j erfc(r_{ij}/\beta)}{r_{ij}} - \lim_{r_{ij} \to R_c} \left\{ \frac{q_i q_j erfc(r_{ij}/\beta)}{r_{ij}} \right\} \right) - \left(\frac{erfc(R_c/\beta)}{2R_c} + \frac{1}{\beta \pi^{1/2}} \right) \sum_{i=1}^{N} q_i^2 \quad (9)$$

The above pair potential does not distinguish between molecules and acts between all the atom pairs. Wolf summations with the above modification has been successfully employed by this group in Simulations of SiC and water.

Besides the two body potential as described above, a three body potential of the following form was also added to the equation.

$$v_3(r_{ij}, r_{jk}, \theta_{jik}) = \lambda_{jik} \exp[\gamma_{ij}/(r_{ij} - r_{ij}^o) + \gamma_{ik}/(r_{ik} - r_{ik}^o)] \times [\cos(\theta_{jik}) - \cos(\theta_{jik}^o)]^2 \quad (10)$$

The main purpose of having a three body potential is to fix the angles in the water molecule at 104° and SiO2 tetrahedral angle at 109°, and it acts only for $r_{ij} < r_{ij}^0$ and $r_{ik} < r_{ik}^0$. λ exists only for HOH, SiOSi and OSiO triplets and is identically zero for all other triplets. The effect of the three-body equation on a j-i-k triplet is to increase the potential energy of the system if the angle is different from the above values by increasing the repulsion or attraction between j and k atoms depending on θ_{jik} being greater than or lesser than the required angle. Since water is not a symmetrically tetrahedral molecule, the target angle θ^o_{jik} for the HOH triplet is set at 100° and not 104° to compensate for the effect of the pair potential. The values of the parameters at for the three body potential is given in table II.

III) Computational procedure:

Molecular dynamics simulations were carried out using a fifth order Nordseick Gear predictor corrector algorithm using the above potential to model the interactions between various atom. As explained in the previous section, the Wolf summation was used to handle the long range Madelung summations. A 6.4nm x 6.4nm x 4.2 nm box of glass was first prepared by a melt quench procedure starting at 6000K(30000 steps) and

brought to 300K(60000 steps) by holding at temperatures of 4000K, 3000K,2000K (100000 steps each) and 1000K(40000 steps) with NVE conditions. Each time step equaled 1 femtosecond when simulating glass. This piece of bulk glass contained 11664 atoms and was equilibrated at 298K with a hydrostatic pressure of 1 atm. From the final NPT run, the lowest pressure configuration was selected and used to make a surface glass by performing a NVT simulation for 50000 time steps (1 fs per time step) at 298K with the bottom half of the glass atoms being frozen and adding 12A of vacuum to the top of the glass. This effected the removal of periodic boundary conditions in the Z direction and the formation of surface like structure at the top of the glass. The number of defects and structure of the glass was comparable to earlier results obtained using BMH potentials which were close to experimental results.

For the production runs of simulating the surface interacting with water, a monolayer of water was added on top of the glass surface by placing 169 water molecules in a square pattern. The 169 water molecules correspond to a density of 4 water molecules per nm^2. The rationale behind this number was to fit in a maximum of 8 silanols per nm^2 on the basis of 2 silanols for every water molecule.

With this as the starting configuration, we performed molecular dynamics for 35 picoseconds with a greater number of saves in the initial 5 picoseconds to observe the reaction mechanisms. While emphasis was laid on maintaining the temperature at 298K, after the 30 picoseconds run following the initial 5 picoseconds, we also continued the simulations at 998K obtain a more exhaustive view of the reaction mechanisms. Thus, the increased temperature run is used to look at mechanisms where the kinetic barriers for the reactions to occur at 298K prohibitive. In both the runs involving water, the time step was

0.1fs to accommodate the fast diffusion of light hydrogen. Hence, the production runs of 35 ps was done with 350000 steps of MD calculations.

IV) Silicic acid and water interaction

The correct Si-H interaction parameters were calculated based on the interaction of silicic acid with a single water molecule. The structure of the silicic acid was also designed to confirm with quantum mechanical calculations by choosing an appropriate value for the Si-H repulsion. The minimum energy configurations were identified and are shown in figure 1. The net energy of the most stable single acceptor double donor configuration was found to be 10.31kcal/mol at 1K. This and the stable structures, as well as the structure of the silicic acid molecule were found to be consistent with the results from quantum mechanical calculations [32, 33].

V) Results of surface – vapor interactions.

The arrangement of the initial configuration is described under computational procedure. That the surface of the glass that comes in contact with the water would be oxygen terminating has been observed earlier and was found to be the case here also. The structure of the glass that we obtained with the new potential compared well with experimental results as well as structures obtained with BMH – type potentials. [34] Since the emphasis in this work is on observing the defect species and coordination numbers of the silicon and oxygen atoms, the initial structure of the glass has been depicted in terms of the coordination numbers of silicon and oxygen as a function of the z coordinate as shown in fig 2. For the purpose of analysis, the entire glass was sectioned into slabs of dimension 6.4A x 6.4A x 1A along the z dimension and the number of silicons and oxygens in the slabs, of different coordinations are shown in the graph. In all

of the graphs showing the coordination, the units of y-axis are the number of species in each slab and the x-axis is the z-coordinate of the top of the slab. As can be seen there is a much higher concentration of defective species (3 coordinated Si and 1 coordinated O) at the surface indicated by the spikes at high values. As mentioned earlier, the higher number of oxygens at the top most slab shows that the surface is oxygen terminating. The final NVT relaxation of the glass for 50000 steps allowed for the relaxation of the fractured surface and ensured that there were no 2 or lower coordinated silicons at the surface.

Figures 3 a, b, c and d show one of the observed mechanisms where silanols are formed at under coordinated species without breakage of any of the siloxanes. The single water molecule gets close enough to one of the dangling non-bridging oxygens (fig 3a) of the surface and gives up a proton to the oxygen. This results in the formation of a silanol and a hydroxyl group(.fig 3b). The free hydroxyl ion does not seem to be stable and is almost immediately captured by a neighboring 3 coordinated silicon (fig 3c) and the end result is the formation of 2 silanols (fig 3d). This is the seems to be the predominant mechanism of silanol formation in the observed system.

Figures 4 a,b,c and d show another possible mechanism for silanol formation. 4a shows the initial configuration of a water molecule getting close to a 3 coordinated silicon. In 4b, the water molecule itself is captured by the silicon (indicated by the green arrow) and this results in the formation of an $SiOH_2$. The $SiOH_2$, in this case, has a short lifetime because of the over coordination of the oxygen and it soon dissociates a proton as shown by the red arrow in 4c to a neighboring non-bridging oxygen. Notice that the under coordinated silicon to which the NBO is attached also tries to form a stretched

bond with the neighboring bridging oxygen. However, this bond is also unstable and soon dissociates and eventually that silicon ends up as $Si(OH)_2$.

A possible reason for mechanism described in fig 3 to be predominant could be that the driving force for the reaction being determined by the concentration of dangling surface oxygens which get to face the incoming water molecules first. The second described mechanism is dependant on the concentration of defective silicons, which, though almost equal in number to the defective oxygens as seen in fig 2, are present below the surface oxygens.

While the mechanisms described in figures 3 and 4 depicted the formation of silanols without breaking the siloxane bond, there were also silanols forming by breaking of siloxane. But this occurred only once at the low temperature and once at 998K. A common feature in both the siloxane breaking mechanisms seemed to be the formation of a 5 coordinated silicon which subsequently broke off from one of the bridging oxygens. These two events are depicted in fig 5 and 6. Combined Classical-Quantum simulations at the silica surface and on 2 member chains of silica have also shown such reactions and the requirement of the formation of a 5-membered silica has been inferred from these studies [35] [36].

A direct effect of the reactions as demonstrated by the above mechanisms is that the structure of water at the surface is relaxed and the defect sites are “repaired” with respect to coordination. This dissociative adsorption [37]effect can be observed in the concentration profiles presented in fig 7. As was expected based on previous results of simulation[37], no dissolution of silicon or $Si(OH)_4$ was observed even at high temperature. This shows the number of non-defective oxygens and silicons as a

function of the z coordinate of the volume element containing the atom. The concentration of under coordinated species are so low (of the order of 1-5 per volume element), that they have not been shown in the graph. One can also notice that the concentration of correctly coordinated oxygens and silicons has increased at the surface. This is due to the additional bonds formed with hydrogens and oxygens respectively of the water molecule. The brown line in the graph shows the concentration of silanols (these were included in the final count of the number of 2 coordinated oxygens indicated by the black line) and it indicates silanol formation even at a depth of 38Å inside the glass. This shows that silanols are formed in not just the top surface, but also deeper beneath the surface of the glass. Evidence that the silanols can form at the inner layers is also seen in the concentration profile of molecular water which also penetrates up to the 37Å inside the glass. Given that under coordinated atoms in the dry glass are found till at 45Å, this indicates that the penetration of water amounts to a total of about 8Å after 35ps.

Diffusion studies of water diffusion on silica surfaces have been explained as a first order reaction that reaches equilibrium and a constant SiOH concentration at longer times [8] [38]. This does look apparent in the current simulations because of the strong dependence of the SiOH concentration on the concentration of remaining H_2O as seen in fig 8. The final silanol concentration obtained was 3.91/nm^2(this number includes adsorbed H_2O and Si_2OH each of which potentially could form a silanol based on the observed mechanisms), which is comparable to experimentally observed values[25] as well as those obtained by MD simulation techniques[18]. In contrast to previous results obtained by this group, there was no significant change in the distribution of rings in the

glass sample. This could be attributed to the fact that there were no excess small membered rings at the surface. It has been previously observed that the small membered rings are reactive sites and are attacked by water[39]. However, there was an increase in the total number of ringed structures with the greatest increase being in the number of 4-membered rings. The distribution of 4-membered rings in the wet and dry glass surfaces is depicted in fig 9 and this trend is seen in higher and lower membered rings also.

VI) Proton transfer.

The graphics of the simulation revealed the presence of the occasional hydronium ion at the glass surface. It is know that proton transfers in silica[40] and other glasses[41] occur by a hopping mechanism involving a suitable proton donor like the hydronium and that the presence of molecular water facilitates this proton transfer [42] [43]. Hence, we looked at the details of the role that the hydronium plays on the glass surface. Fig 10(a-h) shows the details of this proton transfer over 4 molecular distances. The first picture shows just the presence of 3 molecules of water over the silica surface with an under coordinated silicon and oxygen. The subsequent figures show how the water molecule is first adsorbed onto the under coordinated silicon and then subsequently transfers a proton to neighboring water molecule and eventually creates another silanol from an under coordinated oxygen atom. As can be seen, it is not necessary for all the transferring water molecules to be bound to the glass surface. Evidence of similar mechanisms has also been shown with ab-initio and quantum-classical calculations. In most cases where opportunities for exchange of protons existed as in the presence of neighboring water molecules, silanols or under coordinated oxygens, the lifetime of the hydronium ions was less than 100fs with an average of around 55fs. However, we did

observe some stable hydroniums that lasted for greater than 300fs, though none of these long lasting hydroniums were observed after the first 6ps. This indicates that a majority of proton transfers occur only in the initial period when under coordinated atoms are still available. Evidence of proton transfers along the shorter timescales is seen through quantum mechanical calculations also[14].

VII) Conclusion.

Molecular dynamics studies of interaction between silica surfaces and water vapor revealed some of the mechanisms of the interactions. The water was dissociable and interactions between water molecule and silica was parameterized based on water-silicic acid interactions. The effect of the presence of water on the surface was to repair most of the under coordinated species at the surface. Since there was little change in the ring structure, it could be concluded that small amounts of water in the form of vapor at the surface does not lead to a significant disruption in the silicon network. Penetration of water and formation of silanols was observed to about 8A inside the glass surface. The hopping mechanism of proton transfer through the formation of the occasional hydronium was also observed. Mechanism hitherto observed only through quantum calculations over 100’s of atoms, have been successfully simulated using a simple pair and three body classical molecular dynamic approach performed on over 10000 atoms. The current potentials were thus found suitable to study molecular mechanisms in water silica interactions.

Table Ia: parameters of the two body potential.

Species	A_{rep} (J)	ξ (Å)	ξ_r (Å)	C_6 (J-Å^6)
O-H	2.283×10^{-16}	24	f(T, P)	-
O-O	4.250×10^{-17}	24	0.610	4.226×10^{-18}
Si-O	2.67×10^{-16}	24	0.373	7.00×10^{-18}
Si-Si	7.00×10^{-17}	24	0.640	-
Si-H	5.00×10^{-16}	24	0.350	3.80×10^{-18}
H-H	-	24	-	-

Table Ib: Charges on species at 298K

Species/multiple	q/e	q^d/e
O	-.904	+.226
Si	+1.808	-.452
H	+.452	-.113

Table Ic: Three body parameters :

Species	λ (ergs)	$r^0_{\alpha\beta}$ (Å)	γ (Å)	θ°_{HOH}
O-Si-O	1 x 10-11	2.8	2.0	120
Si-O-Si	15 x 10-11	3.0	2.8	141
H-O-H	30×10^{-11}	1.6	1.3	100

Table Ic: The A-matrix of equation 12 columns A(:,0)-A(:,2)

0.655726502	$-1.04442689 \times 10^{-2}$	$8.31892416 \times 10^{-5}$
3.403472×10^{-4}	-3.986929×10^{-6}	1.742261×10^{-8}
-4.057853×10^{-8}	4.677537×10^{-10}	$-2.007873 \times 10^{-12}$
1.657262×10^{-12}	$-1.838785 \times 10^{-14}$	7.549619×10^{-17}

Table Id: The A-matrix of equation 12 columns A(:,3)- A(:,6)

$-3.07929142 \times 10^{-7}$	$5.44770929 \times 10^{-10}$	$-3.73609493 \times 10^{-13}$
$-3.364186 \times 10^{-11}$	2.419996×10^{-14}	0
3.800411×10^{-15}	$-2.672717 \times 10^{-18}$	0
$-1.355453 \times 10^{-19}$	8.939302×10^{-23}	0

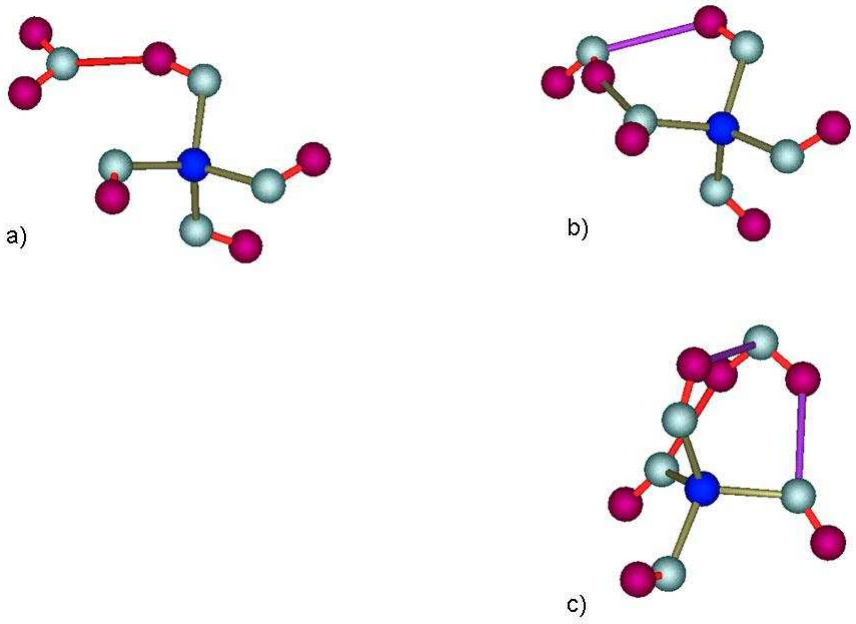

Fig 1 – Stable acid-water configurations. (a) and (b) were observed at 10K and 50K and at 298K while (c) was observed only at 1K. The hydrogen bonded O-H distances in all the above figures is under 2.4Å.

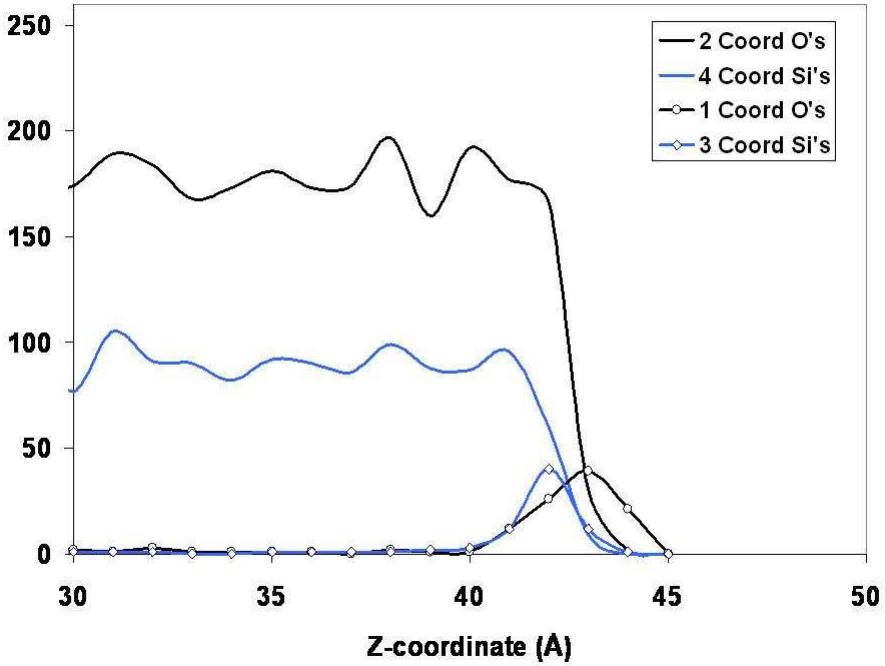

Fig 2 – Coordination profile of the dry surface. There is a high concentration of defective coordinated species at the surface.

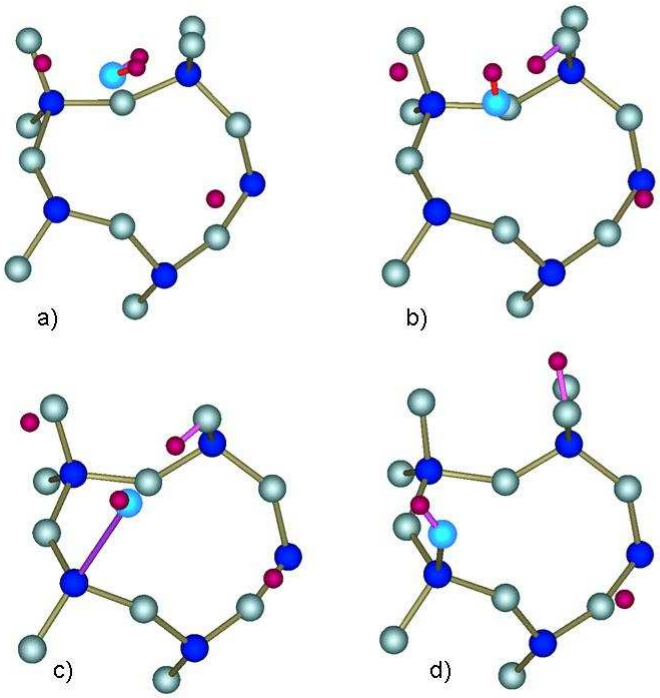

Fig 3 – Silanol formation – This was the predominant mechanism of silanol formation.

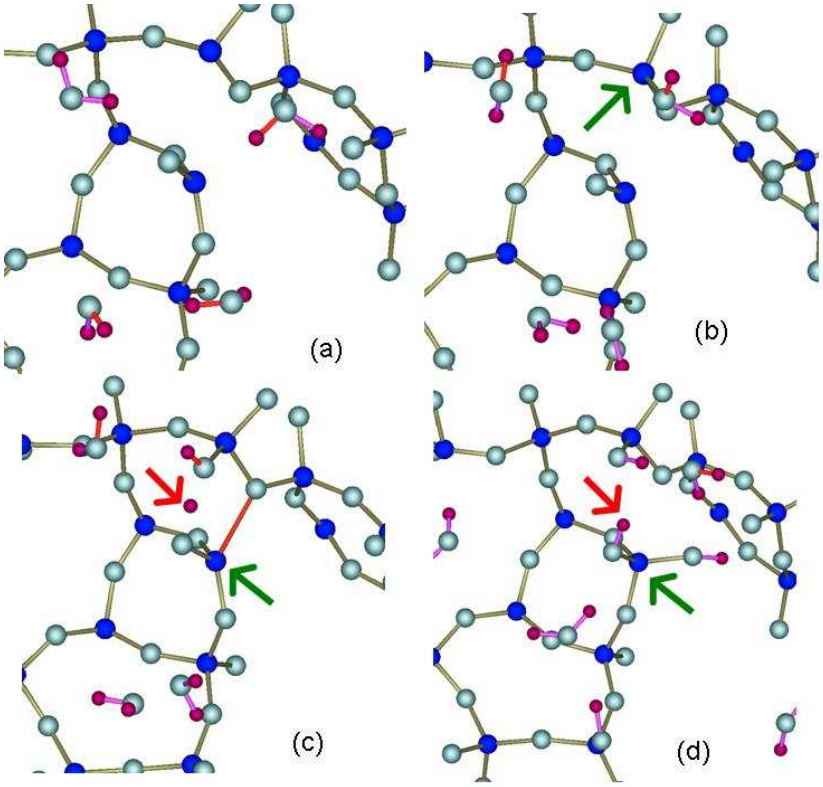

Fig 4 – Silanol formation – Another mechanism of silanol formation through dissociation of adsorbed surface water. Note that the free water molecule is adsorbed onto a surface 3 coordinated silicon and then dissociates a water molecule.

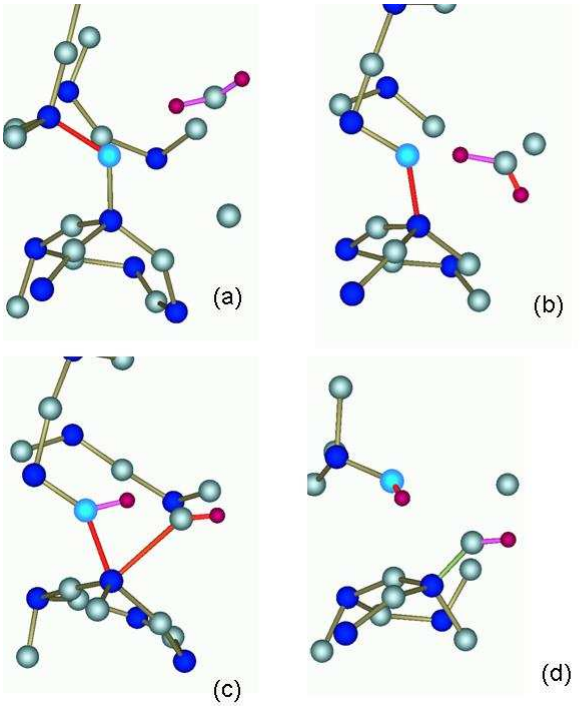

Fig 5 – Siloxane break – high temperature.

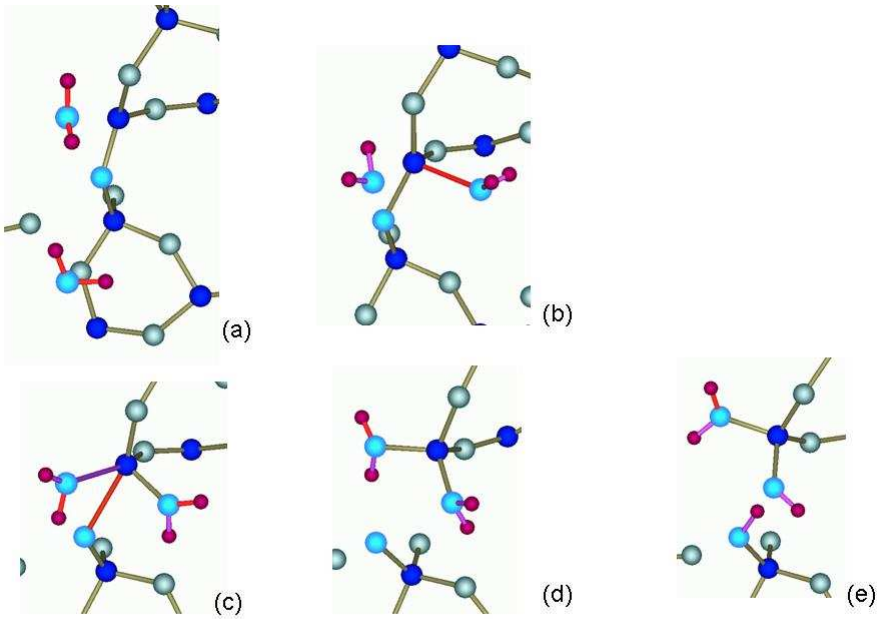

Fig 6 – Siloxane break – low temperature.

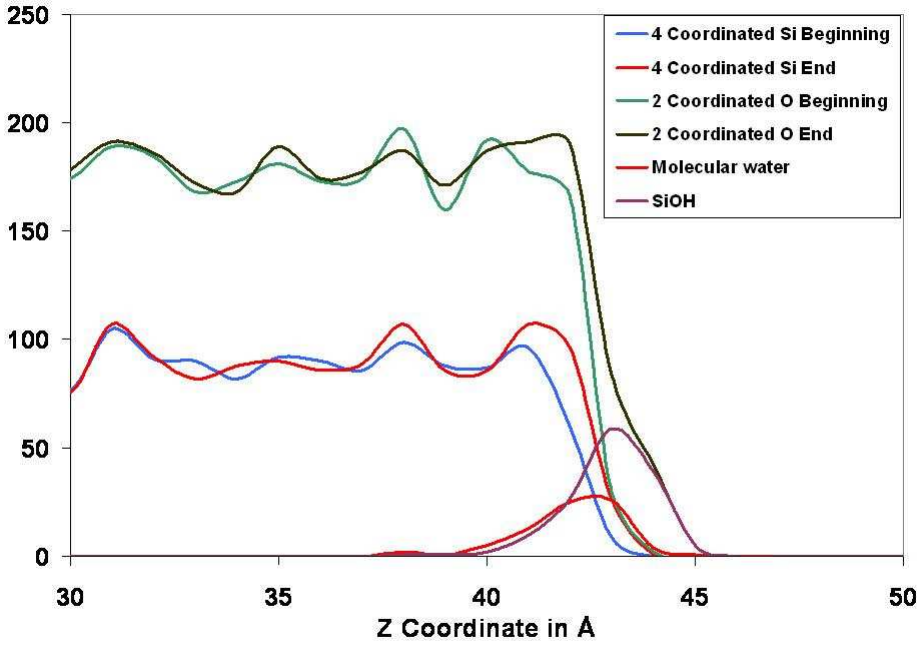

Fig 7 – Comparison of coordination profile and concentration of species.

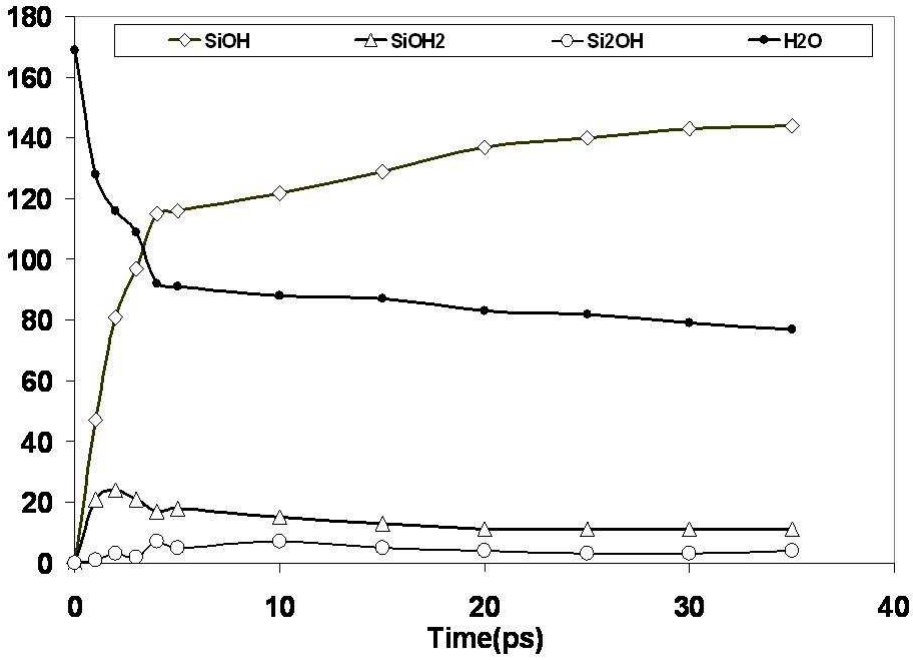

Fig 8 – Kinetics of Species formation.

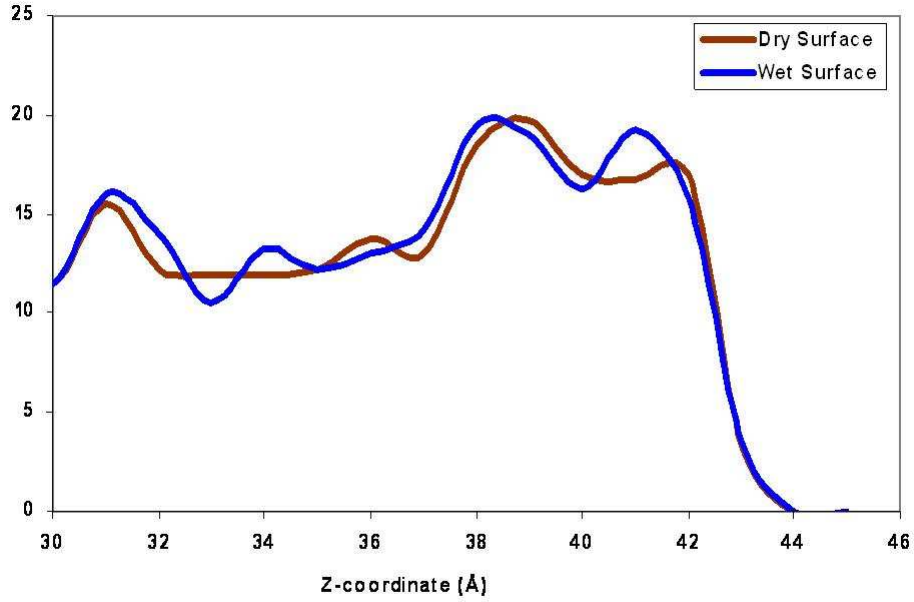

Fig 9 – Concentration profile of 4-membered rings.

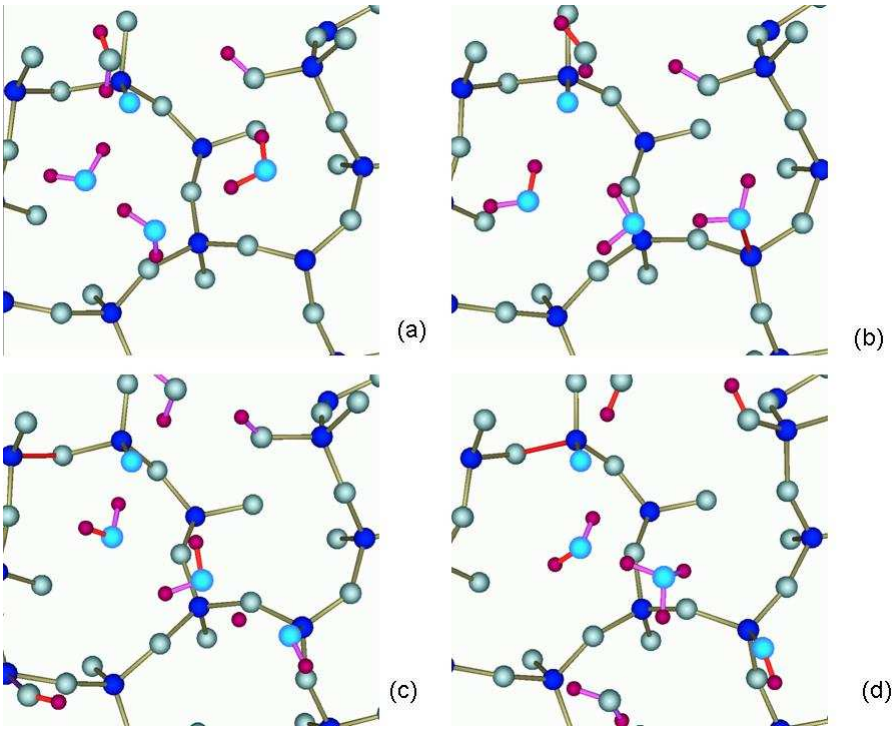

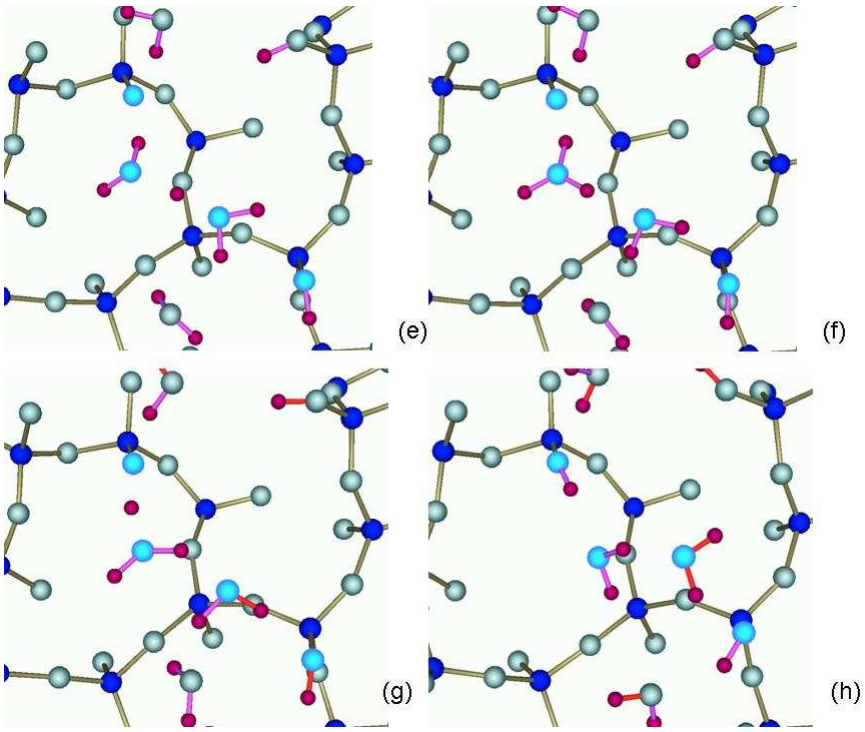

Fig 10 – Proton transfer with the aid of hydronium ion.

References

1. Iler, R.K., *The Chemistry of Silica*. The Chemistry of Silica. 1979, New York: John Wiley and Sons.
2. Franks, F., *Introduction-Water, The Unique Chemical.* Water-A comprehensive treatise. Vol. 1. 1972: Plenum Press. 20.
3. Kell, G.S., *Thermodynamic and Transport Properties of Fluid Water*, in *Water-A comprehensive treatise*, F. Franks, Editor. 1972, Plenum press: New York.
4. Tong, Q.-Y. and U. Gosele, *Semiconductor Wafer Bonding: Science and Technology*. 1999, New York: J. Wiley.
5. Scherer, G.W. *Internal Stress and cracking in stone and masonry*. in *16th European Conference - Fracture*. 2006. Greece: To be published in proceedings.
6. Garofalini, S.H., *Molecular Dynamics Computer Simulations of Silica Surface Structure and Adsorption of Water Molecules.* J. Non-Cryst. Solids, 1990. **120**: p. 1-12.
7. Berger, S. and Tomozawa, *Water diffusion into a silica glass optical fiber.* J. Non-Cryst. Sol., 2003. **324**: p. 256-263.
8. Doremus, R.H., *Diffusion of water in silica glass.* J. Mater. Res., 1995. **10**(9): p. 2379-2389.
9. Sauer, J., C. Morgeneyer, and K.-P. Schroder, *Transferable Analytical Potential Based of Nonempirical Quantum Chemical Calculations (QPEN) for Water-Silica Interactions.* J. Phys. Chem., 1984. **88**(25): p. 6375-6383.
10. Sauer, J., *Molecular Structure of Orthosilicic Acid and Importance of (p-d)pi Bonding. An Ab Initio Molecular Orbital Study.* Chem. Phys. Lett., 1983. **97**(3): p. 275-278.
11. Sauer, J., *Molecular Models in ab Initio Studies of Solids and Surfaces: From Ionic Crystals and Semiconductors to Catalysts.* Chem. Rev., 1989. **89**: p. 199-255.
12. Sauer, J., *Molecular Structure of Orthosilicic Acid, Silanol, and H_3SiOH-AlH_3 Complex: Models of Surface Hydroxyls in Silica and Zeolites.* J. Phys. Chem., 1987. **91**(9): p. 2315-2319.
13. Bolis, V., C. Busco, and P. Ugliengo, *Thermodynamic study of water adsorption in high silica zeolites.* J. Phys. Chem., 2006. **B 110**: p. 14849-14859.
14. Ma, Y., A.S. Foster, and R.M. Nieminen, *Reactions and clustering of water with silica surface.* J. Chem. Phys, 2005. **122**: p. 144709-(1-9).
15. Mischler, C., et al., *Water adsorption on amorphous silica surfaces: a Car-Parrinello simulation study.* J. Phys.: Cond. Mat., 2005. **17**: p. 4005-4013.
16. Demontis, P., G. Stara, and G.B. Suffritti, *Behaviour of water in hydrophobic zeolite silicate at different temperatures. A molecular dynamics study.* J. Phys. Chem., 2003. **B 107**: p. 4426-4436.
17. Puibasset, J. and R.J.M. Pellenq, *A comparision of water adsorption on ordered and disordered silica substrates.* Phys. Chem. Chem. Phys., 2004. **6**: p. 1933-1937.
18. Du, J.C. and A.N. Cormack, *Molecular dynamics simulation of the structure and hydroxylation of silica glass surfaces.* J. Am. Ceram. Soc, 2005. **88**.

19. Garofalini, S.H., E.B. Webb, and D.A. Litton, *Molecular Dynamics Simulations of Enhanced Reactivity of Silica Surfaces to Moisture*, in *Semiconductor Wafer Bonding: Science, Technology, and Applications*, U. Gosele, et al., Editors. 1998, The Electrochemical Society: Pennington, NJ. p. 37-45.
20. Garofalini, S.H., *Applicability of the Molecular Dynamics Technique to Simulate the Vitreous Silica Surface*, in *Structure and Bonding in Non-Crystalline Solids*, G.E. Walrafen and A.G. Revesz, Editors. 1986, Plenum: New York. p. 1-12.
21. Feuston, B.F. and S.H. Garofalini, *Oligomerization in Silica Sols.* J. Phys. Chem., 1990. **94**(13): p. 5351-5356.
22. Feuston, B.F. and S.H. Garofalini, *Onset of Polymerization in Silica Sols.* Chem. Phys. Lett., 1990. **170**: p. 264-270.
23. Martin, G. and S.H. Garofalini, *Sol-Gel Polymerization: Analysis of Molecular Mechanisms and the Effect of Hydrogen.* J. Non-Cryst. Sol., 1994. **171**: p. 68-79.
24. Bunker, B., et al., *Kinetics of Dissociative Chemisorption on Strained Edge-Shared Surface Defects on Dehydroxylated Silica.* Surf. Sci., 1989. **222**: p. 95-118.
25. Zhuravlev, L.T., *Concentration of Hydroxyl Groups on the Surface of Amorphous Silica.* Langmuir, 1987. **3**: p. 316-318.
26. Maciel, G.E. and D.W. Sindorf, *Silicon-29 Nuclear Magnetic Resonance Study of the Surface of Silica Gel by Cross Polarization and Magic-Angle Spinning.* J. Am. Chem. Soc., 1980. **102**: p. 7606-7607.
27. Brinker, C.J., et al., *Surface Structure and Chemistry of High Surface Area Silica Gels.* J. Non-Cryst. Solids, 1990. **120**: p. 26-33.
28. Lasaga, A.C., *Atomic treatment of mineral-water surface reactions*, in *Mineral-Water Interface Geochemistry*, M.F. Hochella and A.F. White, Editors. 1990, Mineralogical Society of America: Washington, D. C. p. 17-85.
29. Geisinger, K.L., G.V. Gibbs, and A. Navrotsky, *A Molecular Orbital Study of Bond Length and Angle Variations in Frameowork Structures.* Phys. Chem. Minerals, 1985. **11**: p. 266-283.
30. Guillot, B., *A reappraisal of what we have learnt during three decades of computer simulations on water.* Journal of Molecular Liquids, 2002. **101**: p. 219-260.
31. Mahadevan, T.S. and S.H. Garofalini, *Dissociative water potential for molecular dynamics simulations.* J. Phys. Chem, 2007. **In press**.
32. Pelmenschikov, A.G., G. Morosi, and A. Gamba, *Quantum Chemical Molecular Models of Oxides. 3. The Mechanism of Water Interaction with the Terminal OH Group of Silica.* J. Phys. Chem., 1992. **96**: p. 7422-7424.
33. Rustad, J.R. and B. Hay, *A molecular dynamics study of solvated orthosilicic acid and orthosilicate anoin using parameterized potentials.* Geochimica et Cosmochimica Acta, 1995. **59**(7): p. 1251-1257.
34. Garofalini, S.H., *Defect Species in Vitreous Silica - A Molecular Dynamics Simulation.* J. Non-Crys. Sol., 1984. **63**: p. 337-345.
35. Cao, C., et al., *Fracture, water dissociation, and proton conduction in SiO2 nanochains.* J. Chem. Phys., 2007. **126**: p. 211101-211103.
36. Du, M.-H., A. Kolchin, and H.-P. Cheng, *Hydrolysis of a two membered silica ring on the amorphous silica surface.* J. Chem. Phys, 2004. **120**(2): p. 1044-1054.

37. Du, Z.M. and N.H. de Leeuw, *Molecular dynamics simulations of hydration, dissolution and nucleation processes at the alpha quartz (0001) surface in liquid water.* Dalton Trans., 2006. **22**: p. 2623-2634.
38. Guissani, Y. and B. Guillot, *Transport of rare gases and molecular water in fused silica by molecular dynamics simulation.* Mol. Phys., 1998. **95**(2): p. 151-161.
39. Feuston, B.P. and S.H. Garofalini, *Water-Induced Relaxation of the Vitreous Silica Surface.* J. Appl. Phys., 1990. **68**: p. 4830-4836.
40. Nogami, M. and Y. Abe, *Evidence of water-cooperative proton conduction in silica glass.* Phys. Rev. B, 1997. **55**(18): p. 12108-12112.
41. Nogami, M., et al., *High proton conductivity in Porous P2O5-SiO2 Glasses.* J. Phys. Chem., 1999. **103**: p. 9468-9472.
42. Nogami, M., R. Nagao, and C. Wong, *Proton Conduction in Porous Silica Glasses with High water content.* J. Phys. Chem., 1998. **102**: p. 5772-5775.
43. Daiko, Y., T. Kasuga, and M. Nogami, *Pore size effect on proton transfer in sol-gel porous silica glasses.* Microporous and Mesoporous Materials, 2004. **69**: p. 149-155.

MANUSCRIPT III: Water confined in silica nano-layers : a Molecular Dynamics study.

Water confined in silica nano-layers : a Molecular Dynamics study.

T.S.Mahadevan and S.H.Garofalini

Abstract: Structural and dynamic changes to the properties of water confined by silica nano slabs was analyzed by simulating the above system using Molecular Dynamics. Previous research had revealed the importance of using inter atomic potentials that allowed for dissociation of water and reaction to occur at the water-silica interface. We validate the results obtained by comparison with quantum computations and experimental analysis. Dissociation of water and formation of silanols was noticed at the interface due to the presence of glass. The density profiles of the system were studied to reveal a peak in the silanol concentration at the interface and diffusion of water into the glass. Diffusion of molecular species at the interface was compared with that of bulk liquid and liquid in the interior of the water film. Changes to water structure at the interface was analyzed using radial distribution functions. The effect of temperature on the concentration profiles and structure at the interface was also studied by performing simulations at 7 different temperatures. Based on previous MD results of structure of bulk water, we observe the changes in the hydrogen bonded structure of confined water with temperature is and compare these to temperature and pressure induced changes seen in bulk water.

(I) Introduction:

In recent times it is well known and expected that the properties of most materials change drastically in the nano size regimes and materials exhibit novel properties when confined to small sizes. Water is no exception to this, and since water has been one of the

most studied and documented chemicals[1], it is worthwhile to investigate the change in properties of water when confined in nano sized pores. Many technological applications involve water in constrained geometries like hydrophilic wafer bonding[2], interactions between drugs and bio-molecules[3], de-pollution, corrosion and structural deterioration[4] and catalysis studies. While experimental studies provide results of phenomena in the macro scale[5, 6], understanding of molecular mechanisms in such constrained ambience requires the building of computational models which, while producing results that are consistent with macroscopic experimental results, should also be capable of providing intuitive knowledge of the molecular mechanisms and reactions.

Based on the interactions substrates can be classified as either hydrophobic in case of non-interactive or weakly interactive ambience, or hydrophilic in case of interactive environments. Several studies of hydrophobic interfaces show changes in the orientation of water molecules and structural and phase differences from the bulk[7-9], [10].

This work reports the molecular dynamics studies of water interacting with silica in a constrained slab geometry, which is a hydrophilic under the given circumstances. Several works in literature exist describing such interactions in various geometries and this includes both experimental and simulations.[6-8, 11-15]. In summary, some of the common experimental results for water constrained in silica pores are :

(a) Depression in crystallization temperature depending on pore geometries. The crystallization is noted to appear in the bulk phase and not at the surface of the substrate[6].

(b) Lowering of the frequency spectrum with respect to bulk water[6].

(c) Enhanced hydrogen bonding with reduction in temperature[6].

(d) Formation of defective forms of cubic ice in pores with diameters greater than 30nm[6].

(e) Hysteresis in ice nucleation and melting[6].

(f) Accumulation of water at the interface.[16-19]

There are also some varied results about the changes in diffusion coefficients in constrained environments[20].

Some important aspects that need to be addressed in the study of water interacting with hydrophilic silica are the formation of silanols and the diffusion of water into the substrates. Computational studies of water silica interactions focusing on silicon wafer bonding, formation of siloxanes and silanols and mechanisms of oligomerization of silicic acid has been investigated earlier by this group [17, 21, 22]. These simulations used atomic water models where the water molecules were capable of dissociation and reaction with the silica surface based on a fixed charge coulomb term and a short range interaction based on BMH potentials. Earlier results by this group have indicated the relaxation of the silica surfaces due to the presence of water and the formation of siloxane bonds across a layer of water as would be the case in silicon wafer bonding. The reaction between a water monolayer and a silica surface has also been studied and this indicates the clustering of water molecules on the free surface which is a consequence of the hydrophilic nature of the interactions and the defect seeking capabilities of the water molecules. While these results were informative about the mechanisms of water-silica interactions, a major drawback of the above simulations was that the properties of bulk

water that was used were not very accurate. For example, the BMH potential acts only over a distance of 5.5Å and reproduces only the first neighbor distances of water accurately, while significant structural information is present till the third peak of O-O pair distribution function at around 7Å. Hence, we developed a potential function acts over longer ranges and reproduces the properties of water to a far greater accuracy.

We have established the utility of this potential in studying silica surface interacting with water vapor in our previous work[23]. This works aims at studying the interactions between a film of liquid water 3.5 nm thick, constrained by silica nano-layers using this new potential. We present a brief description of the potential function in section II followed by computational procedure in section III. Sections IV to VIII present the results of the simulations and comments about the results.

(II) Potential function.

The inter atomic potential used in these simulations have been described in an earlier publication by this same authors[24]. In brief, the potential consists of a two and a three body interactions that are represented as function of the distance between atom pairs and triplet configurations.

(a) Two body interactions :

$$U_{tot}(r_{ij}) = U_{electrostatic} + U_{repulsive} + U_{dispersive} \quad (1)$$

where

$$U_{electrostatic}(r_{ij}) = \left[\begin{array}{l} \frac{q_i q_j}{r_{ij}} + \frac{q_i^d q_j}{r_{ij}} \operatorname{erf}(\frac{r_{ij}}{\sqrt{2}\xi}) \\ + \frac{q_i q_j^d}{r_{ij}} \operatorname{erf}(\frac{r_{ij}}{\sqrt{2}\xi}) + \frac{q_i^d q_j^d}{r_{ij}} \operatorname{erf}(\frac{r_{ij}}{2\xi}) \end{array} \right] \operatorname{erfc}(\frac{r_{ij}}{\beta}) \qquad (2)$$

$$U_{rep}(r_{ij}) = A_{rep} \frac{\operatorname{erfc}(r_{ij} / 2\xi_r)}{(r_{ij} / 2\xi_r)} \qquad (3)$$

$$U_{disp}(r_{ij}) = -C_6 / r_{ij}^6 \qquad (4)$$

In the above formulae, the q_i's and q_i^d's are the regular and diffusive charges on the i^{th} atom, r is the distance of separation between the i^{th} and j^{th} atoms, and A_{rep}, ξ, ξ_r, and C_6 are parameters as given in table I. The long range parts of the Madelung terms were handled by a Wolf summation[25] and all the pair interactions were truncated with a spherical cutoff of 1nm. The multiplier $\operatorname{erfc}(r_{ij}/\beta)$ is due to the use of only the real space terms of the Madelung potential. The use of Wolf summation also implies the subtraction of self terms for the electrostatic potential as given by:

$$U_{shift} = \left(\frac{erfc(R_c / \beta)}{2R_c} + \frac{1}{\beta \pi^{1/2}} \right) \sum_{i=1}^{N} q_i^2 \qquad (5)$$

The parameter ξ_r in equation (3) varies with increasing temperature and pressure for the OH interactions to accommodate for the change in OH distances. A detailed description

of the potential equations is given in the earlier paper and it has been found to describe the properties of water accurately in the temperature range under consideration.

(b) Three body potentials :

The three body potential used in the present work is defined by :

$$U_3(r_1, r_2, \theta) = \begin{cases} \lambda \exp\left\{\dfrac{\gamma}{r_1 - r_c} + \dfrac{\gamma}{r_2 - r_c}\right\} \times (\cos\theta - \cos\theta_c)^2 & \text{for } r_1, r_2 < r_c \\ 0 & \text{for } r_1, r_2 \geq r_c \end{cases} \quad (6)$$

where, r_1 and r_2 are the two distances of the 2nd and 3rd atoms from the central (1st) atom and θ is the angle subtended by atoms 2 and 3. The parameters γ, r_c and θ_c for the different three body sets are given in our earlier paper. In short, the three body potential serves to increase the energy with increased deviation from the ideal angle between 2-1-3 atoms and this results in a greater drive for the set of atoms to return to the ideal angle.

(III) Computational Procedure.

Molecular dynamics simulations were carried out using a fifth order Nordesieck-Gear predictor corrector algorithm on a simulation box of approximate dimensions 6.4nm x 6.4 nm x 7.5nm under NPT conditions with a constant pressure of 1 atmosphere in the z direction. The simulations box was comprised of 4851 water molecules sandwiched between 3888 molecules of SiO_2. Initially, prior to attaching the two in a layered configuration, the required glass and water systems were prepared separately. The glass was prepared by a standardized melt quench procedure where silicon and oxygen atoms

in the ratio 1:2 arranged in β-cristobalite structure was melted at an initial temperature of 6000K to attain sufficient diffusion that breaks down the crystalline structure. The starting material was chosen as β-cristobalite as it is close to the density of vitreous silica. This was then cooled to 300K in sequence of temperature 4000K - 3000K - 2000K(100000 time steps each) - 1000K(4000 time steps) - 300K(60000 times steps) with each time step being 1 femto second. The dimensions of the glass cuboid, prepared under NVE conditions, were 6.4nm x 6.4nm x 4.2 nm. This glass cuboid was then equilibrated at 298K under NPT conditions with a hydrostatic pressure of 1atm for 40000 steps and the configuration of glass with pressure closest to 1 atm was taken as the glass sample and it had dimensions of 63.6Å x 63.8Å x 42Å

The water was simulated separately by starting with an initial cubic arrangement of 4851 water molecules at a density of $1x10^{23}$ particles per cc at 298K in a cuboid box of size approximately by less than 6.4nm x 6.4 nm x 3.5nm and was run for 500000 time steps at 0.1 fs per time step.

The glass and water systems were then combined by adding water on top of the glass system with a separation of 2.5Å. This gave a system of approximate dimensions 6.4nm x 6.4 nm x 3.5nm with *v*-SiO_2 in the bottom and water on top. For later analysis, this system was further modified by removing the bottom 21A of glass adding it to the top of water. While the simulation results would remain the same in both cases because of periodic boundary conditions in all the three dimensions, this gives the added convenience of having a symmetric distribution of two layers of glass above and below the water molecules. The resulting simulation box is shown schematically in fig 1. This construct models water confined to a slit like glass pore. Care was taken to allow a 2.5A

gap between the water and glass in the top layer also. The above system was run for 400000 time steps at 0.1fs per time step at five temperatures of 283K, 293K, 298K, 313K, 323K, 333K and 348K to allow for equilibration and stabilizing the density. The index number referring to the atoms were preserved all through the simulation so as to facilitate ease of analysis. Thus, atom numbers 1 to 11664 were SiO_2 atoms and atoms numbered 11665 to 26217 were always water atoms.

(IV) Glass structure and properties.

The initial structure of the glass was measured based on the pair correlation function between Si-O, Si-Si and O-O atom pairs. This gives a reasonable compliance to previous simulation results by this group[26] and by others[27, 28]. The use of a three body potential resulted in the regulation of Si-O-Si and O-Si-O angle to ~146^o and 109^o respectively. The vibrational spectrum of the glass showed the required Si-O stretch peak[29] at ~1100cm^{-1} while the low frequency peaks had all been convoluted possibly because of librations. The glass had expanded by about 0.05% over the temperature of 283K-348K which is higher than the expansion of real glass. The large difference from experimental values in case of expansion is still negligible because of the much higher expansion data for the glass-water system and because of the fluctuations in density in this temperature range and length scales resulting in inaccurate values for densities of glass. Figure 2 shows the pair distribution functions of the different pairs of atoms in glass.

(V) Silanol / Hydronium formation.

Table I gives the silanol concentrations in glass after 102ps. These numbers are comparable to what has been observed experimentally for fully hydrated silica surfaces. [30] The thermal activation energy for silanol increase can be obtained from the slope of the plot between ln(SiOH concentration) and 1/T. In the present case, this gives an energy of ~0.93kcal/mol. DFT [31] and CPMD[32] methods have revealed activation energies for formation of silanols on pristine silica surface as 11Kcal/mol-40Kcal/mol and that the reaction is exothermic. This implies that the number of silanols should decrease with increasing temperature. However, the conditions that we have simulated are drastically different and the reactions here involve chemisorption, dissociation of water and formation of silanols. The mechanisms of silanol formation are similar to our earlier results and based on the increase in silanol concentration with increase in temperature, we are led to believe that the reaction is endothermic.

(VI) Concentration profiles of various species.

The concentration profile of various species in the hydrated slit is shown in figure 3. Since we have modeled the water to have interactions with the glass surface, we do observe significant penetration of water into the glass. The diffusion of water into the irregularities and channels at the surface has been discussed in our earlier work[23] and is observed here also. While we do observe a slight increase in the concentration of water molecules at the interface, it is much lower than he layering like behavior observed in case of hydrophobic interfaces or interactions without chemical interactions. In case of non interacting or hydrophobic interfaces, the concentration profile should[9] [33]indicate layers of water resembling the peaks in O-O pair distribution of water and is

indeed observed in simulations [7] and experiments [34] Double layers of water, not similar to O-O pair distribution function is also observed in simulations of water in cylindrical Vycor™ glass pores[19] – however, these simulations do not allow for dissociation of water molecule or the formation of silanols. Since our potential allows for the reaction between water and silica and for diffusion of water into silica, the peaks at the interface are less prominent. That allowing for diffusion at the interface reduces the peak has been evidenced [8] and the small peaks at the interface are a result of the lowering of diffusion coefficient of water in silica as compared to the self diffusion coefficient of bulk water.

The distribution of silanols is clearly maximum at the surface of the glass and we also observe that the ratio of reacted oxygens to hydrogens is closest to 1 at the maximum. This value for the ratio of reacted hydogens to reacted waters on either side of the maximum, indicating the presence of adsorbed water molecules at the surface as well as below the surface resulting in a higher number for reacted hydrogens as compared to the reacted oxygens. This also indicates that the surface OH bonds have the oxygen and hydrogen in almost the same monolayer plane parallel to the glass surface. This is expected because, during the formation of silanols by dissociation of water, the water molecules dissociate only when close to an under coordinated silicon and a dangling oxygen. This mechanism is explained in our previous work [23]. Since the glass surface is oxygen terminated, the under coordinated silicons are found beneath the oxygen terminating surface. Also, the three body potentials help maintain the SiOH angles also to around 117^{o}. Given the mechanism of silanol formation, it can thus be seen that the dissociated hydrogens attach to the dangling oxygen from below the surface, resulting in

the OH of silanols being in planes that are at acute angles to the surface rather than projecting perpendicularly in to the water.

With increasing temperatures, the increased concentration of water molecules becomes less prominent at the interface becoming comparable to the normal density fluctuation in the central part. This trend is similar to how the O-O pair distribution function changes with temperature and thus correlates to the lowering of density at high temperatures.

Distinction has been made in between marking the oxygens of adsorbed water molecules and the oxygens of those water molecules that have penetrated the glass surface but have not adsorbed on to silicon atoms. Based on the ratio of dissociated and adsorbed oxygens to the free water oxygens, it was determined that a only about 50% of the water molecules that diffuse into the surface are adsorbed onto glass atoms and the rest remain as free water molecules. This was true over the entire temperature range considered. The distinction between the different oxygens is important because the structure of the free water molecules is very different from the adsorbed water molecules.

(VII) Structure of water in the confined space.

Structural modifications to the silica network in the presence of water has been studied by the authors in an earlier work. In this work we try to understand the modifications in the structure of water. The O-O pair distribution function provides ample information about the local arrangement of water molecules and the significance of the various peaks has been explained by Cho et al [35]. In short, water molecules form stable hydrogen bonded clusters with a central water molecules hydrogen bonded to four

other surrounding water molecules resulting in a tetrahedron. The structure of silica is also similar as it forms SiO_4 clusters with a central silicon and 4 oxygens forming a corner shared tetrahedron.

Figure 5 shows the pair distribution function of oxygen atoms (OO-pdf) in bulk water and a comparison of this with the OO-pdf's of various sections of the glass-water system for the 298K sample. NMR studies have revealed the structure of confined water ([20] and references therein) and the proper way to interpret the experimental results. Since, in MD simulations, marking and counting atoms of different species is much easier than in experiment, we have been able to study the OO-pdf and OH-pdf in different thin sections of the sample. Based on the concentration profiles, reference points were chosen at the sample interface and far away from interface and the pair distribution functions were measured for sections of sample that were 3Å thick. For ease of comparison, all the pdf values were normalized with respect to the densities of the section. The 3Å sections were chosen starting at 20Å, 21Å, 22Å, 23Å, 26Å and 35Å in z corresponding to 0, 1Å, 2Å, 3Å, 6Å and 15Å from the interface. In case of 298K data, the values were averaged with pdf data from the corresponding sections at the opposite (high-z) interface also.

The prominent structural modification seemed to be the increase in the number of O-O (which are indicative of molecular positions) neighbors at under 4Å distance which is a behavior observed in water at high temperatures[24] as well as high pressures [36]. The O-O neighbors at 4.5Å which form the "non-H-bonded" second shell neighbors to the oxygen at the center of the tetrahedral cage changing to hydrogen bonded neighbors at 3.4Å at higher pressures is a phenomenon used as a premise in explaining the various

anomalous properties of water by Cho et. al. A similar phenomenon is observed here also in that the second O-O peak at 4Å disappears and there is a rise in the number of neighbors at closer distances. There is some redistribution of the 4.5Å peak over longer distances also as we can see that the third peak which is at around 7A for bulk water is also shifted to shorter distances for the layer closest to the interface. We also observe that the first O-O peak is observably lower in the section closest to the indicating that some of the first neighbors also have migrated to farther distances. This behavior is contrary to the what happens at higher pressure where the first peak increases with increasing pressure and is more akin to behavior of O-O pdf with increasing temperatures [37]. The difference between temperature and pressure effects in water is explained in [38]. Thus, the reduction in the first peak could be a result of some of hydrogen bonded, first neighbor water molecules being shifted to farther distance by bending or breaking of hydrogen bonds in the presence of the corner sharing tetrahedral structure of glass. These shifted water molecules accumulate near the original tetrahedral cage resulting in the shoulder at around 3.3Å, and possibly resulting from the absence of second shell neighbors at 4.5Å which causes the disappearance and redistribution of O-O peak at that distance. As we move away from the interface, this phenomenon is reversed and the O-O pdf starts resembling that of bulk water.

The O-H pdf for bulk and the different sections is shown figure 6 and also compares well with experimental results in [20]. One prominent difference between the bulk water structure and any of the sections in the water-glass film is the reduction in the intensity at around 1.75Å which is the hydrogen bonding distance. The curve is also shifted to lower distances in the 2.4-3.2Å and 1.8-2.4Å range suggesting that some of the

hydrogen bonds that were at the shorter distances have moved to the longer distances. These long hydrogen bonded pairs seem to manifest as a distinct shoulder in experimental results [20] and the change in hydrogen bonded structures is also observed in apolar environments [8]. The effect of disappearance of the second shell at 4.5Å in the O-O pdf is also felt in the O-H pdf's at 4.5Å which is reduced in the sections close to the interface. Hydronium formation at the water-silica interface was reported in our previous work[23] and we did observe some hydroniums at the interface. However, the numbers were not significant enough to make an impact on the structure of water.

Comparison of the O-O and O-H pdf's of various sections in the system was done for the 348K run also and the graphs are in figures 7 and 8. Increasing temperature in bulk water has the effect of reducing the second shell neighbors at 4.5Å, increasing the first minima of the O-O pdf and decreasing the first maxima. Again, this has been explained as being caused by redistribution of the second shell neighbors to form a high density shell closer to the first shell neighbors of the water tetrahedron without a major distortion [38] to the first tetrahedral shell. This effect is noticed in our simulations of bulk water at different temperatures [24] as well as in the present case. The increased temperature has lowered the second peak, but the presence of the confining environment at the interface has effected the second peak to an even greater extent and we notice little change in the intensity of the curve in the 4.5Å region for the interface section with increasing temperature. Accumulation of molecular neighbors at around the 3.4Å without the disappearance of the 4.5Å peak, similar to the temperature effect has also observed in simulations of water confined in cylindrical pores[39], mesoporous Vycor™ glass[40] [41] and zeolite silicates[42] and has been explained as distortion of hydrogen bond

network. Thus, the structural differences between confined water at the interface and in the interior of the water film reduces with increasing temperature as has been experimentally observed [43] as an increased thermal expansion coefficient of confined water. Experimental studies by NMR spectroscopy and dielectric measurements also indicate the presence of complex disordered phases in interfaces in mesoporous silica and Vycor™ glass[6, 12, 15]. The existence of a different phase of water at the interface with different equations of state has also been observed in other simulations[44], [7] and, as seen in the current results, the region of water closest to the interface, including penetrated water seem to indicate a different phase behavior from bulk water. This super cooled phase of water has a structure similar to low density water at high temperatures.

(VIII) Water diffusion in bulk and at interface.

Experimental studies and simulations reveal slower vibrational dynamics of confined water which has been explained as due to the trapping of water molecules in cages caused by increasing density or pressure[13], [16], [45], [20], [11], [3] and resulting in increased relaxation times. It has also been shown that confined water has a higher diffusion rate than bulk ice[6]. Spohr et. al have [19] have indicated the possibility that short time diffusion coefficients in fully hydrated confined water being higher than that of bulk water.

In the present case, we measure the self diffusion coefficient, D of water based on the mean square diffusion of oxygen atoms that are associated with free water molecules only. The distinction between free water and attached water was that the free water molecules were at least 2.1Å away from any silicon. This ensured that neither the structure, nor the diffusion coefficients were severely modified by attached silanols or

adsorbed water. Since 3 dimensional diffusion was being considered, we chose 6Å sections starting at 20Å, 21Å, 22Å, 23Å, 26Å and 35Å distances in z, corresponding to 0, 1Å, 2Å, 3Å, 6Å and 15Å from the interface to measure mean square diffusion. Figure 8 shows the mean square diffusion of the different layers. While we do not observe the explicit flattening of the MSD curve indicating the onset of as seen elsewhere[45], possibly because we are considering larger sections of water to calculate the three dimensional diffusion. However, we do observe that the MSD curve of the section closest to the interface flattens at longer times indicating the slowing of diffusion of the molecules into the sample. The self diffusion coefficient was calculated as the slope of the MSD curve after the onset of steady state indicated by a constant slope region of the MSD curve. A plot of the diffusion coefficients at different temperatures and different sections of the film is given in figure 9. Clearly we observe that the diffusion coefficient is an order of magnitude lower in the section closest to the interface at all the temperatures and this is consistent with other simulations[19]. There are significant inaccuracies in the values of D because the number of diffusing atoms decreases with increasing time and atoms that escape the section are not accounted for once they leave the section. This results in greater inaccuracies at higher temperature but we do observe the trend of diffusion to be in the right direction and the values being reasonably consistent with experiments.

(IX) Conclusion.

MD simulation of hydrated slits in vitreous silica shows significant reactions between water and silica resulting in formation of silanols at the interface. Water molecules also penetrate into the silica layers to the extent of about 10Å causing the

formation of sub surface silanols. Observation of the structure of water at different sections near the interface shows that, near the interface, water forms a structure that has features similar to both high pressure as well as high temperature water. This section of water also has a diffusion coefficient much lower than that of bulk water or even water at the interior of the film. Based on the intensity and shape of the first peak of O-O pdf, we can conclude that water molecules in this section of water have a lower density of first neighbor shell than bulk water, which is akin to the density modification in higher temperature water. Another characteristic observed in the structure of this layer was the disappearance of the second shell of neighbors seen in bulk water. As expected, the structure of water in the interior of the film bears a closer resemblance to that of bulk water. This interfacial region of water, thus is seen to exhibit properties different from that of bulk water and thus can be classified as separate phase of water with a lower order as compared to bulk water. Presence of this slow moving, intermediate layer results in a slight accumulation of water at the interface. Sections of water closer to the interior of the film undergo a gradual transformation to bulk water, indicating that the transformation is akin to glass transitions. Since the glassy phase of water is present only closer to the interface, for larger pores or slits, the contribution to average properties of water by this phase is expected to reduce thus explaining many of the anomalous properties of water confined to restricted geometries.

Table 1: Silanol and adsorbed water density after 9ps.

Temperature	$SiOH/nm^2$	Si_2OH/nm^2	$SiOH_2/nm^2$
283	4.80	0.58	0.42
293	4.97	0.58	0.37
298	4.95	0.57	0.38
313	5.23	0.66	0.18
323	5.20	0.57	0.18
333	5.06	0.69	0.25
348	5.22	0.73	0.17

Fig1: Schematic arrangement and dimensions of system**.**

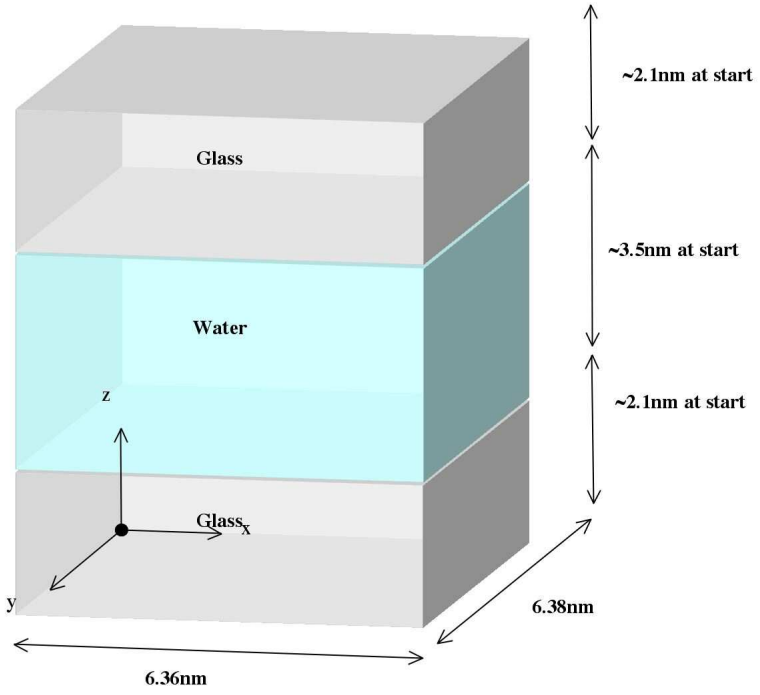

Fig 2: Pair distribution functions of O-O,Si-O and Si-Si for the glass. The number of first neighbours were 4 each for Si-Si and Si-O pairs and 6 for O-O pairs.

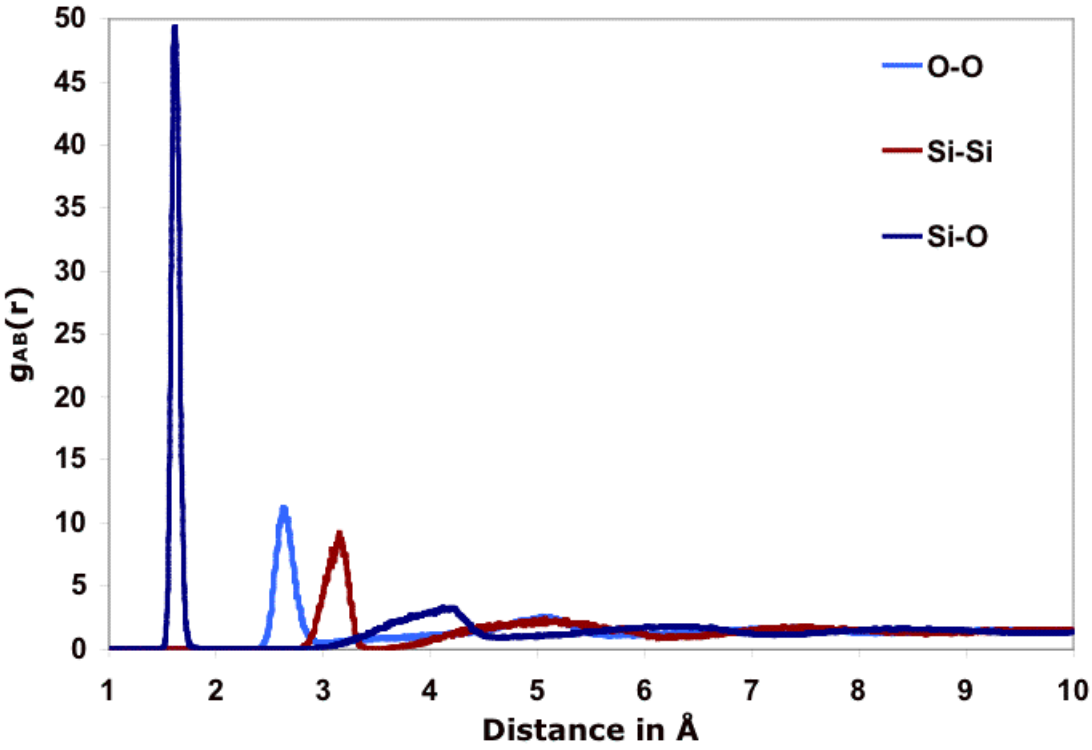

Fig3a: Concentration profiles at 298K

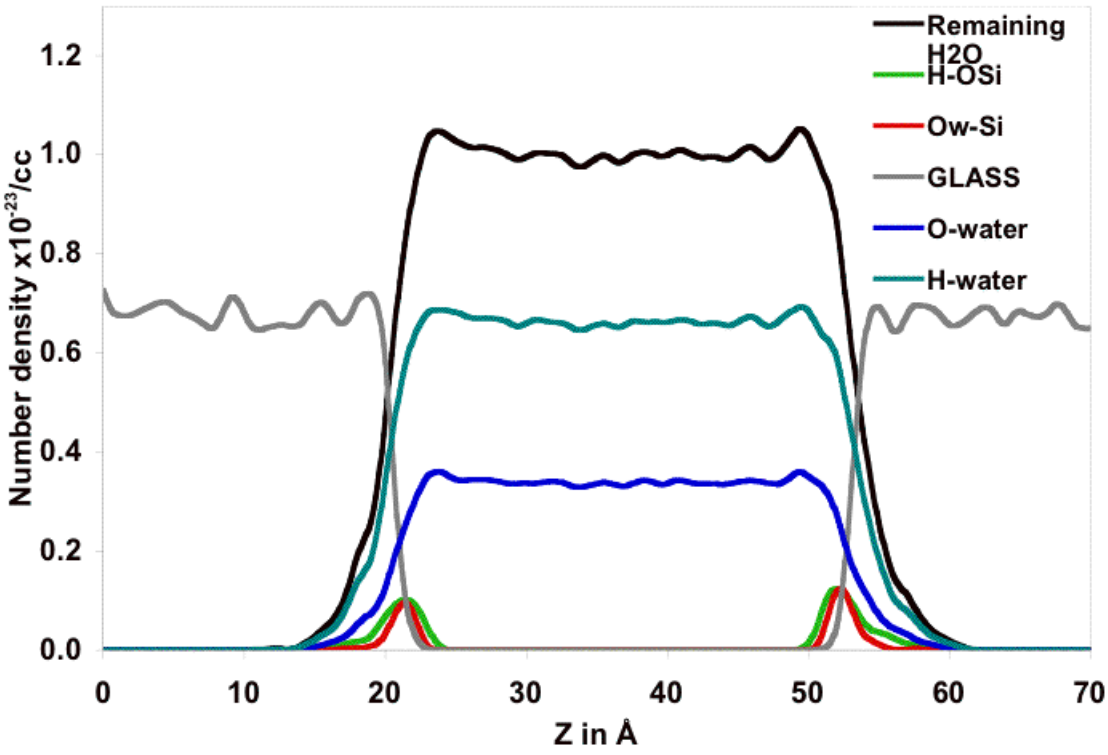

Fig 3b: Concentration profiles at 348K. The density has lowered and there is less difference between the interface and interior of the water.

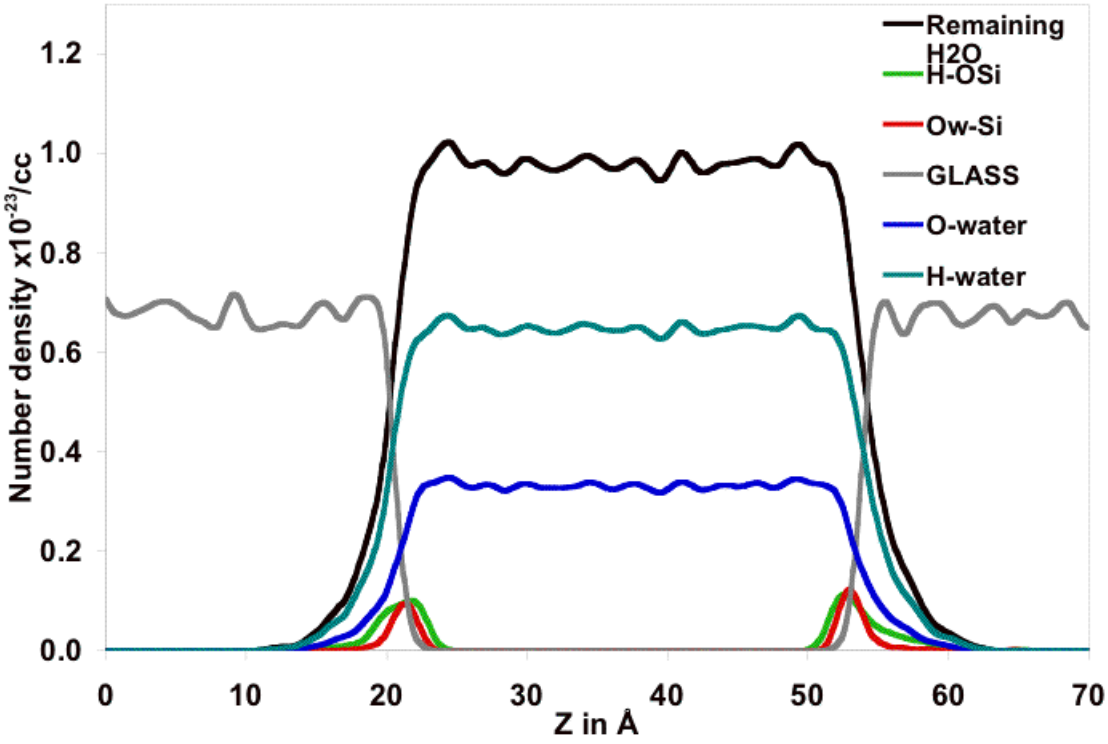

Fig4: O-O pdf at 298K Comparision of various layers.

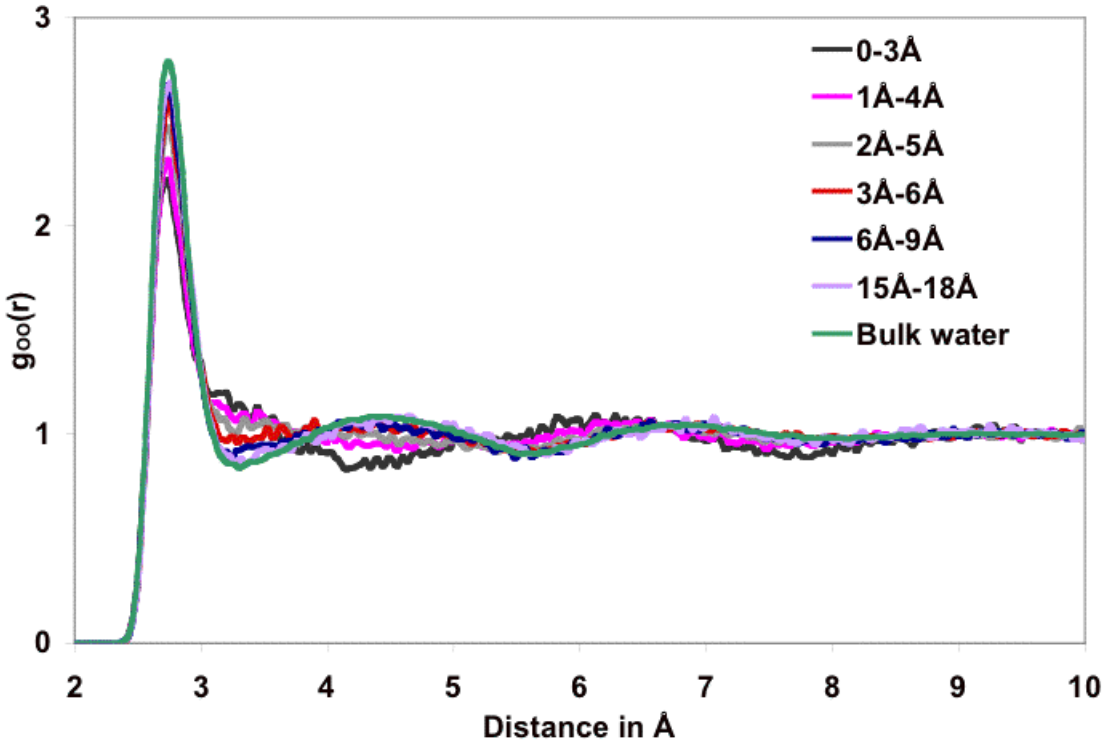

Fig5: O-H pdf at 298K

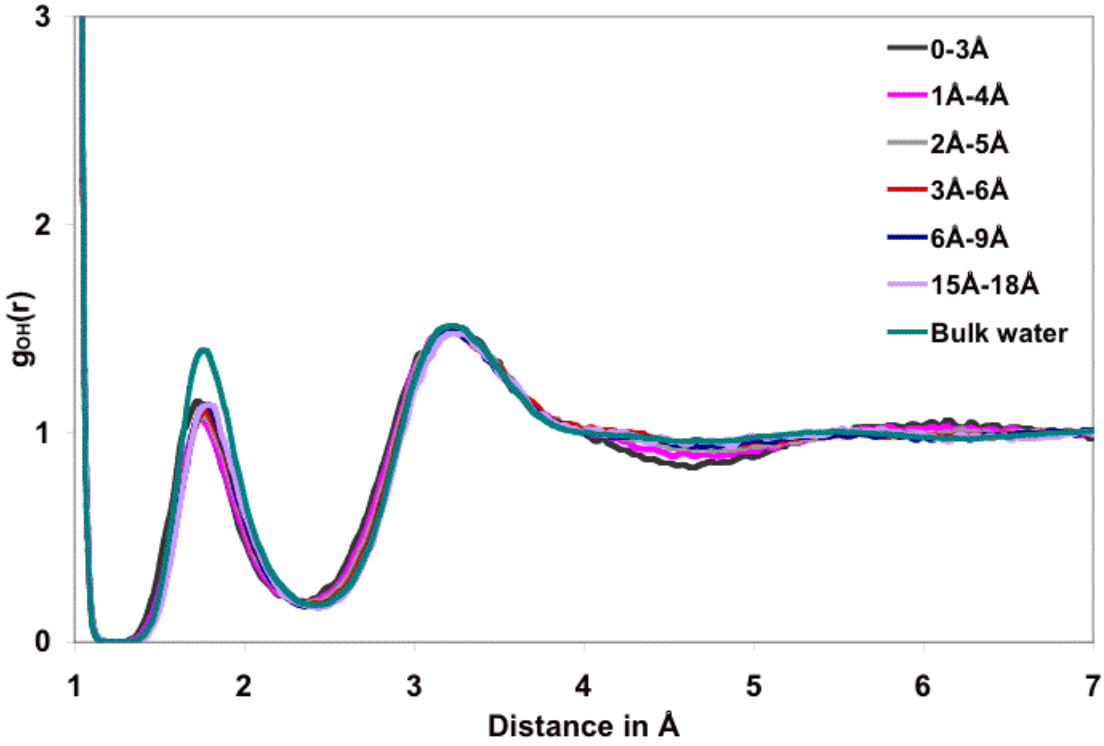

Fig6: O-O pdf at 348K.

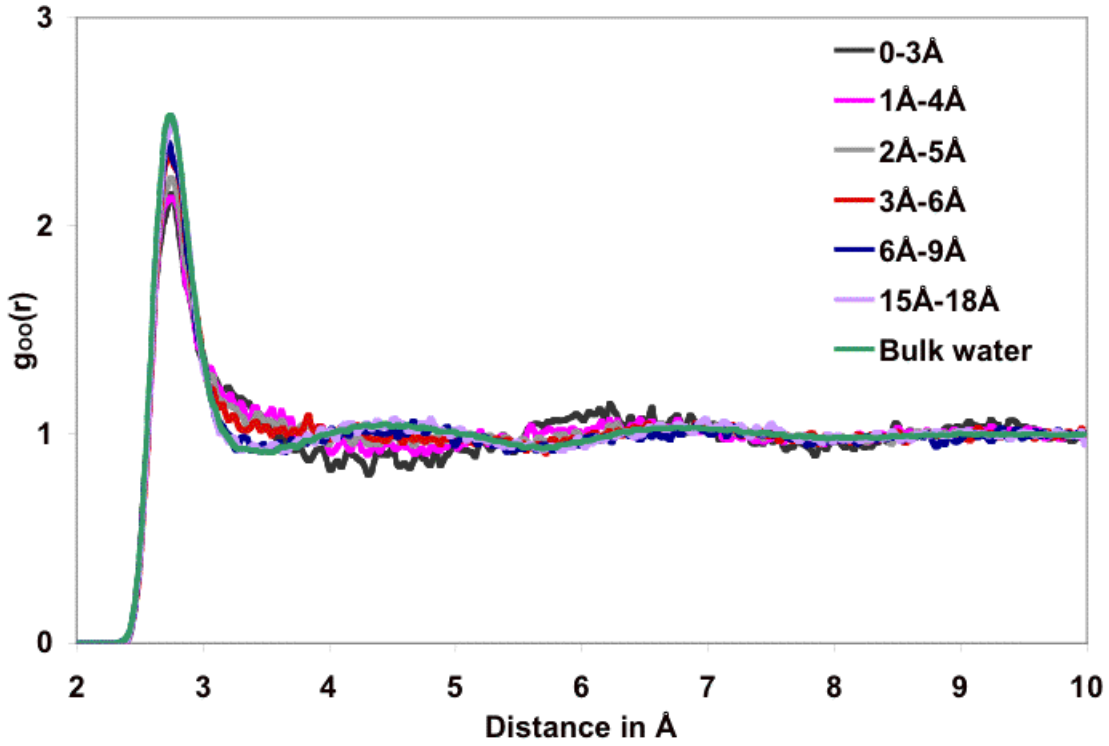

Fig7: O-H pdf at 348K

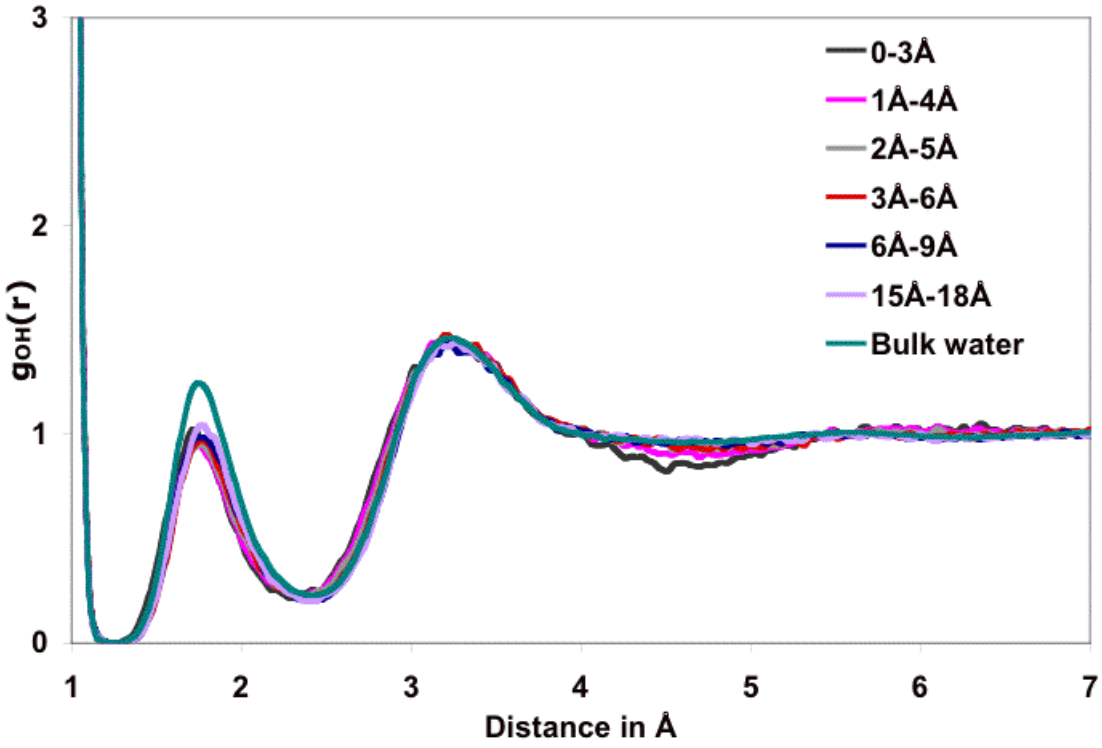

Fig 8: MSD curve at 298K

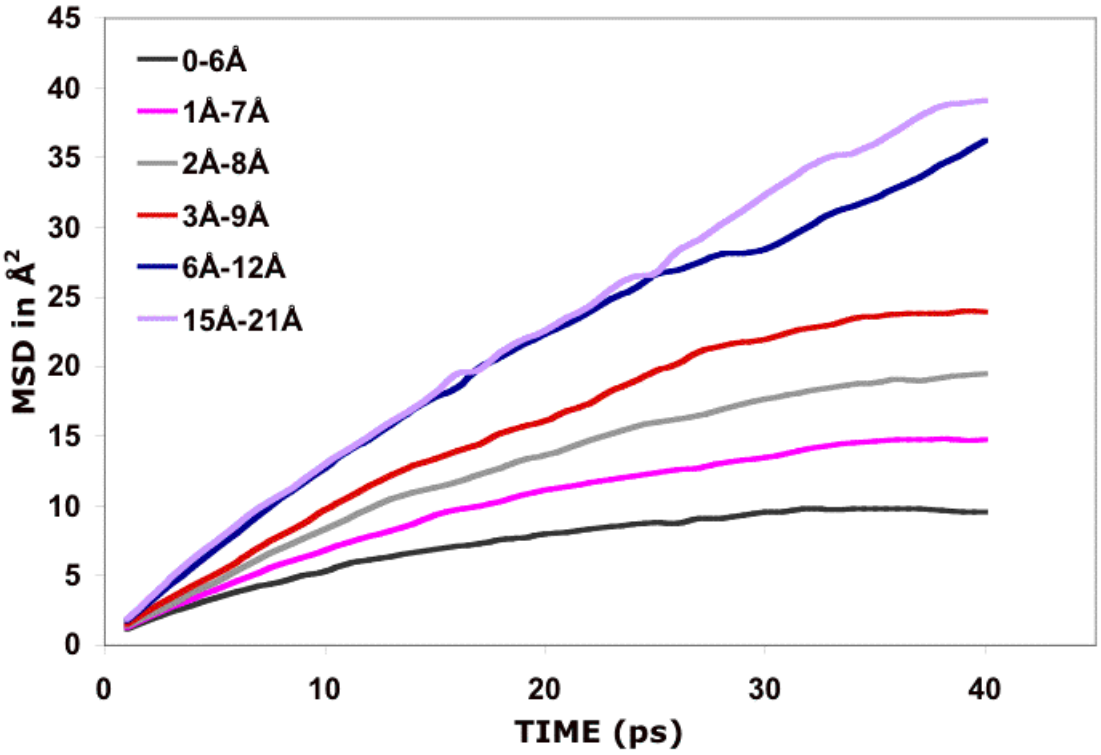

Fig 9: graph of D vs T.

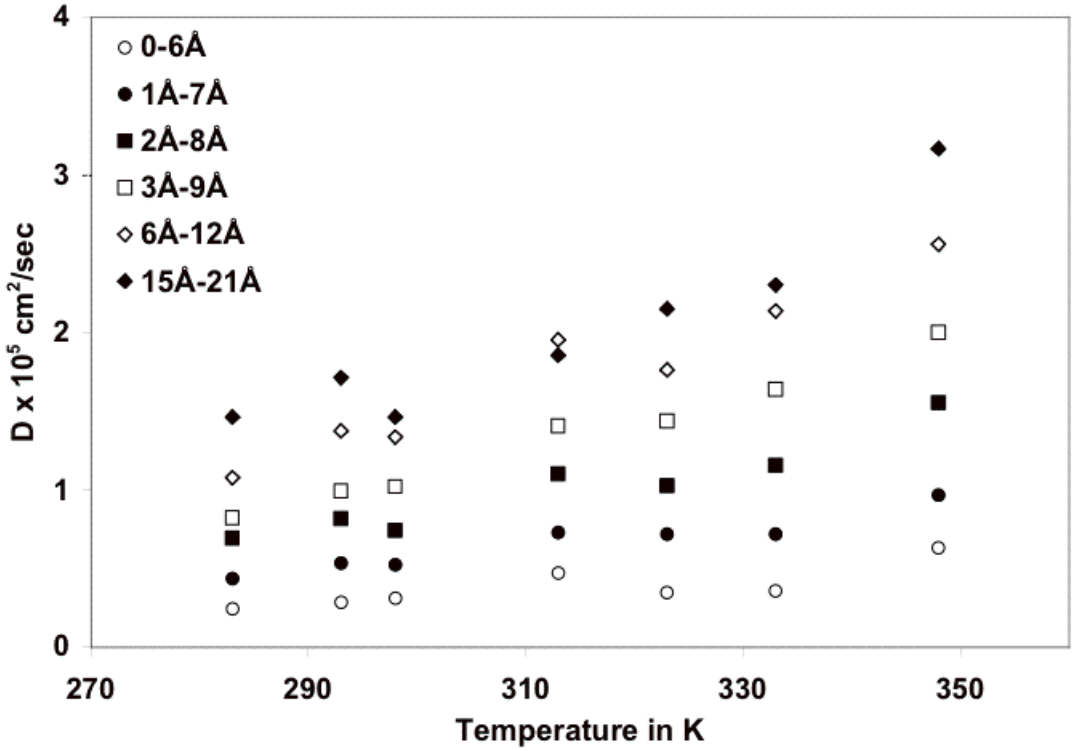

References:

1. Guillot, B., *A Reappraisal of what we have learnt during three decades of computer simulations on water.* J. Mol. Liq, 2002. 101: p. 219-260.
2. Tong, Q.-Y., *Wafer Bonding for integrated materials.* Mat. Sci & Engg, 2001. B87: p. 323-328.
3. Bhattacharya, K. and B. Bagchi, *Slow dynamics of constrained water in complex geometries.* J. Phys. Chem A, 2000. 104: p. 10603-10613.
4. Gonzalez, I.J.G. and G.W. Scherer, *Effect of swelling inhibitors on the swelling and stress relaxation of clay bearing stones.* Environmental Geology, 2004. 46: p. 364-377.
5. Klein, J., et al., *Fluidity of water and of hydrated ions confined between solid surfaces to molecularly thin films.* J. Phys. Cond. Mat, 2004. 16: p. S5437-S5448.
6. Webber, B. and J. Dore, *Structural and dynamic studies of water in mesoporous silicas using neutron scattering and nuclear magnetic resonance.* J. Phys. Cond. Mat, 2004. 16: p. S5449-S5470.
7. Brovchenko, I., A. Geiger, and A. Oleinikova, *Water in nanopores: II. The liquid-vapour phase transition near hydrophobic surfaces.* Journal of Physics: Condensed Matter, 2004. 16: p. S5345-S5370.
8. Jedlovszky, P., *The hydrogen bonding structure of water in the vicinity of apolar interfaces: a computer simulation study.* J. Phys. Cond. Mat, 2004. 16: p. S5389-S5402.
9. Zangi, R., *Water confined to a slab geometry: a review of recent computer simulation studies.* J. Phys. Cond. Mat, 2004. 16: p. S5371-S5388.
10. Scatena, L.F., M.G. Brown, and G.L. Richmond, *Water at hydrophobic surface: Weak hydrogen bonding and strong orientation effects.* Science, 2001. 292: p. 908-912.
11. Crupi, V., D. Majolino, and V. Venuti, *Diffusional and vibrational dynamics of water in NaA zeolites by neutron and Fourier transformed infrared spectroscopy.* J. Phys. Cond. Mat, 2004. 16: p. S5316-S5297.
12. Hiejima, Y. and M. Yao, *Phase Behaviour of water confined in Vycor™ glass at high temperatures and pressures.* J. Phys. Cond. Mat, 2004. 16: p. 7903-7908.
13. Liu, L., et al., *Slow dynamics of supercooled water confined in nanoporous silica materials.* J. Phys. Cond. Mat, 2004. 16: p. S5403-S5436.
14. Puibasser, J. and R.J.-M. Pellenq, *A grand canonical Monte Carlo simulation study of water adsorption on Vycor™-like hydrophilic mesoporous silica at different temperatres.* Journal of Physics: Condensed Matter, 2004. 16: p. S5329-S5343.
15. Swenson, J., *The glass transition and fragility of supercooled confined water.* J. Phys. Cond. Mat, 2004. 16: p. S5317-S5327.
16. Crupi, V., et al., *Dynamical Response and H-bond effects in confined liquid water.* J. Mol. Liq, 1999. 80: p. 133-147.
17. Feuston, B.P. and S.H. Garofalini, *Water-induced relaxation of the vitreous silica surface.* J. Appl. Phys, 1990. 68(9): p. 4830-4835.
18. Hartnig, C., et al., *Modifications of the hydrogen bond network of liquid water in a cylindrical SiO_2 pore.* J. Mol. Liq, 2000. 85: p. 127-137.

19. Spohr, E. and C. Hartnig, *Water in porous glasses. A computer simulation study.* J. Mol. Liq, 1999. 80: p. 165-178.
20. Ricci, M.A., et al., *Water in confined geometries: experiments and simulations.* J. Phys. Condensed Matter, 2000. 12: p. A345-A350.
21. Garofalini, S.H. and G. Martin, *Molecular Simulations of the polymerization of silicic acid molecules and network formation.* J. Chem. Phys., 1994. 98(4): p. 1311-1316.
22. Litton, D.A. and S.H. Garofalini, *Modeling of hydrophilic wafer bonding by molecular dynamics simulations.* J. Appl. Phys, 2001. 89(11): p. 6013-6023.
23. Garofalini, S.H. and T.S. Mahadevan, *Molecular dynamics simulations of water adsorption onto silica surfaces using a dissociate water potential.*???, 2007. ???(???).
24. Mahadevan, T.S. and S.H. Garofalini, *Dissociative water potential for molecular dynamics simulations.* J. Phys. Chem, 2007. 111: p. 8919-8927.
25. Wolf, D., et al., *Exact method for the simulation of Coulombic systems by spherically truncated, pairwise r^{-1} summation.* J. Chem. Phys., 1999. 110(17): p. 8254-8282.
26. Feuston, B.P. and S.H. Garofalini, *Empirical Three-Body Potential for Vitreous Silica.* J. Chem. Phys., 1988. 89(9): p. 5818-5824.
27. Van Ginhoven, R.M., H. Jonsson, and L.R. Corrales, *Silica glass structure generation for ab initio calculations using small samples of amorphous silica.* Phys. Rev. B, 2005. 71.
28. Vashishta, P., et al., *Interaction potential for SiO2: A molecular-dynamics study of structural correlations.* Phys. Rev. B, 1990. 41: p. 12197-12209.
29. Garofalini, S.H., *Molecular dunamics simulation of the frequency spectrum of amorphous silica.* J. Chem. Phys., 1982. 76(6): p. 3189-3192.
30. Zhuravlev, L.T., *Concentration of Hydroxyl Groups on the Surface of Amorphous Silicas.* Langmuir, 1987. 3: p. 316-318.
31. Van Ginhoven, R.M., et al., *Cleavage and Recovery of Molecular Water in Silica.* J. Phys. Chem B, 2005. 109: p. 10936-10945.
32. Mischler, C., et al., *Water adsorption on amorphous silica surfaces: a Car-Parrinello simulation study.* J. Phys. Cond. Mat, 2005. 17: p. 4005-4013.
33. Truskett, T.M., P.G. Debendetti, and S. Torquato, *Thermodynamic implications of confinement for a waterlike fluid.* J. Chem. Physics, 2001. 114(5): p. 2401-2417.
34. Antognozzi, M., A.D.L. Humphris, and M.J. Miles, *Observation of molecular layering in a confined water film and study of the layers viscoelastic properties.* Applied Physics letters, 2001. 78(3): p. 300-302.
35. Cho, C.H., S. Singh, and G.W. Robinson, *Understanding all of waters' anomalies with a nonlocal potential.* J. Chem. Phys., 1997. 107(19): p. 7979-7987.
36. Okhulkov, A., Y.N. Demianets, and Y.E. Gorbaty, *x-ray scattering in liquid water at pressures of up to 7.7 kbar: Test of a fluctuation model.* J. Chem. Phys., 1993. 100(2): p. 1578-1588.
37. Guillot, B. and Y. Guissani, *How to build a better pair potential for water.* J. Chem. Phys., 2001. 114: p. 6720-6733.
38. Urquidi, J., et al., *Origin of temperature and pressure effects on the radial distribution function of water.* Phys. Rev. Letters, 1999. 83(12): p. 2348-2350.

39. Gallo, P., M.A. Ricci, and M. Rovere, *Layer analysis of the structure of water confined in Vycor™ glass.* J. Chem. Phys., 2002. 116(1): p. 342-346.
40. Puibasset, J. and R.J.-M. Pellenq, *A grand canonical Monte Carlo simulation study of water adsorption on Vycor™-like hydrophilic mesoporous silica at different temperatres.* J. Phys. Cond. Mat, 2004. 16: p. S5329-S5343.
41. Puibasset, J. and R.J.-M. Pellenq, *A comparison of water adsorption of n ordered and disordered silica substrates.* Phys. Chem. Chem. Phys, 2004. 6: p. 1933-1937.
42. Demontis, P., G. Stara, and G.B. Suffritti, *Behaviour of water in hydrophobic zeolite silicate at different temperatures. A molecular dynamics study.* J. Phys. Chem B, 2003. 107: p. 4426-4436.
43. Derjaguin, B.V., V.V. Karasev, and E.N. Khromova, *Letters to the editors: Thermal expansion of water in fine pores.* J. Colloid & Interface Sci., 1986. 109(2): p. 586-587.
44. Brovchenko, I., A. Geiger, and A. Oleinikova, *Water in nanopores. I. Coexistance curve from Gibbs ensemble Monte Carlo simulations.* J. Chem. Phys., 2004. 120(4): p. 1958-1972.
45. Gallo, P., et al., *Non-exponential kinetic behaviour of confined water.* Europhys. Lett., 2000. 49(2): p. 183-188.

CURRICULUM VITA

THIRUVILLAMALAI SUNDARESHWARAN MAHADEVAN

Aug 1991 – May 1995	B.Tech Metallurgical engineering, Institute of Technology – Banaras Hindu University Varanasi – 221005, India.
Sep 2000 – Jan 2008	Ph.D, Materials Science and Engineering, Rutgers University, Piscataway, NJ -08854
Sep 1995 – Aug 2000	Development Engineer Larsen and Toubro Limited., (EWAC Alloys) Mumbai – 400080, India.

Publications (partial list):

T.S.Mahadevan and S.H.Garofalini – "Dissociative water potential for Molecular Dynamics simulations", J. Phys. Chem B 111(30) 2007 p8919-8927

T.S.Mahadevan and S.H.Garofalini, – "Dissociative chemisorption of water onto silica surfaces and formation of hydronium ions" J. Phys. Chem., Accepted

T.S.Mahadevan and S.H.Garofalini – "Molecular Dynamics study of water films confined to silica nano-layers", Under Review.